Flow Analysis of the Arctic Ocean (the Kara Sea and the Barents Sea) by a Hybrid Box Model

Akira WADA* and Minoru OCHIAI*

Abstract : The objective of this report is to discuss the characteristics of flows in the Arctic Ocean Seas (the Kara and the Barents) in connection with marine contamination. In recent years, research has been underway to clarify the fate of radioactive wastes dumped into the Arctic Ocean (especially, the Kara Sea and the Barents Sea). These sea areas are very narrow, shallow and located close to land. To analyze the diffusion of radionuclides and carry out exposure dose assessment by determining the circulation of seawater in these areas, it is necessary to identify the flow characteristics of the seas. As the first step of research, the mechanism of flows in the Barents Sea and the Kara Sea in the Arctic Ocean was investigated (Local model). Using the observation data (water temperature and salinity), the flow was analyzed using a hybrid box model, taking into account river flows and density structures in the seas. The results thus obtained agreed with the observed features in many aspects.

Keywords : *Arctic Ocean, Flow analysis, Kara Sea, Barents Sea, Hybrid box model, Local Model*

1. Introduction

Recently, there has been considerable interest in the dumping of radioactive wastes into the Arctic Ocean (especially, the Kara Sea and the Barents Sea) by the former Soviet Union. These seas are narrow, shallow and close to land (see Fig. 1). To assess the impact of such dumping, it is necessary to establish a safety assessment method that permits the prediction of not only regional but also global－scale effects.

To analyze the diffusion of radionuclides and make an exposure dose assessment by determining the circulation of seawater in these areas, it will be necessary to identify the flow characteristics of the seas. However, little research has been conducted insofar as these sea areas are concerned. Moreover, these seas are largely ice－covered in winter, thus available winter oceanographic data are limited. In this research, the authors used existing salinity and water temperature data and information such as meteorological and oceanographical data

provided by IAEA.

Representatives of both IAEA and Seven Member states (Danish/Norwegian group, Japan, The Netherlands, The Russian Federation, Switzerland, United Kingdom and United States of America) were involved in the modeling, coordinated within the framework of the IAEA's International Arctic Assessment Project (IASAP). The model and assessment exercises included contributions to all the important aspects required for radiological assessment studies (WADA *et al.*, 1997).

This paper centers on flow modeling and its analysis, which is of major significance to assessment exercises. Using these observation data (water temperature and salinity), the water－mass characteristics of the Arctic Ocean were examined with reference to the known data, and the results thus obtained were compared with the results of flow analysis to investigate the present condition of flows in these sea areas.

2. Method of study

What impact will the actual dumping of radioactive waste into the Arctic Ocean have in

---

* Nihon University, College of Industrial Technology, 1–2–1, Izumi, Narashino, Chiba 275–8575
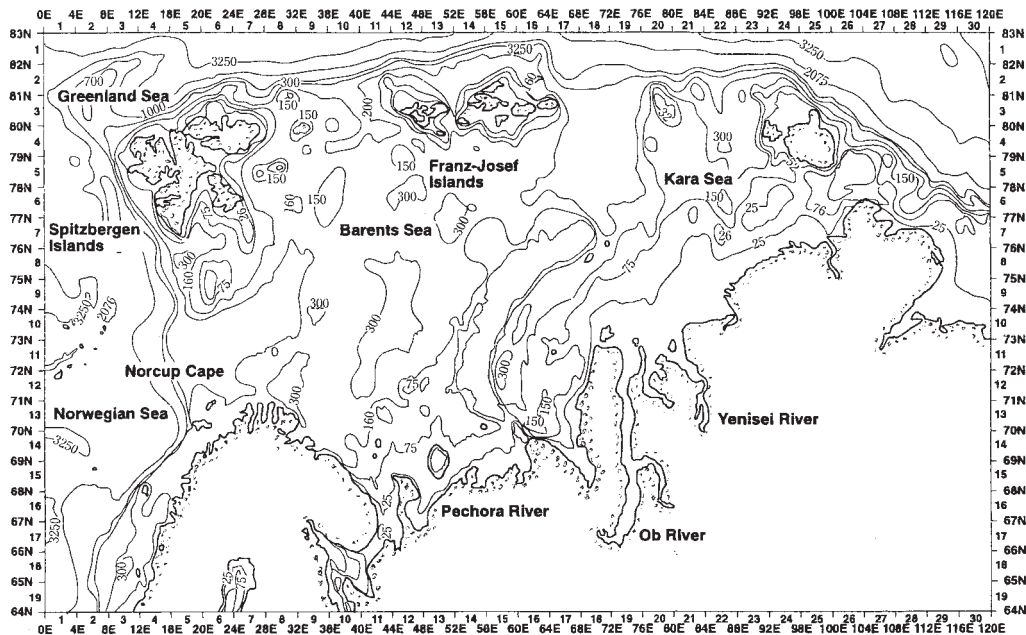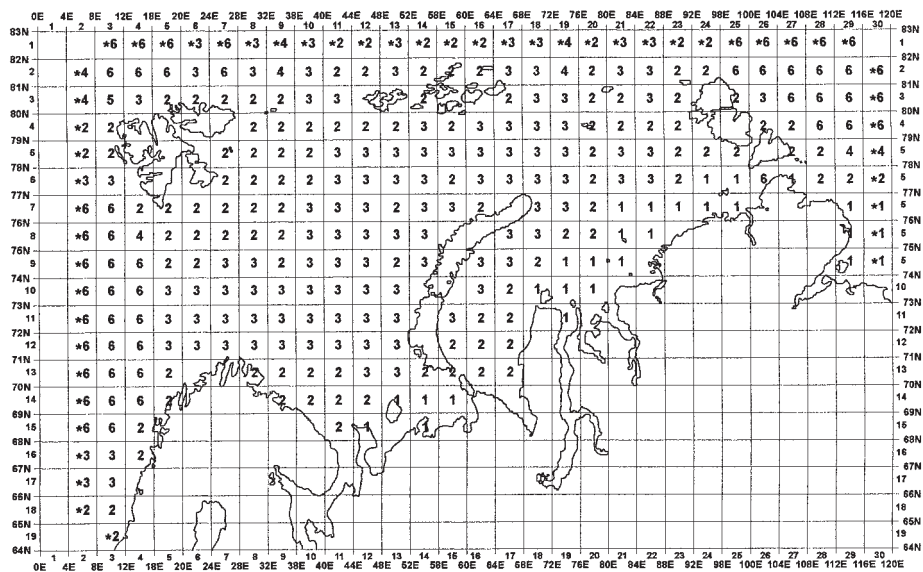
Fig. 1. The Barents Sea and the Kara Sea.

Fig. 2. Grids of the model and the number of vertical layers.

the future? As a first step to solve this question, the authors investigate the flows in the Barents Sea and the Kara Sea based on observed water temperature and salinity distributions in these seas (local scale). Based on data obtained by NOAA's observations (LEVITUS, 1982), water temperature and salinity in the range of 64°–85° N and 0°–120° E were obtained and graphically represented at intervals of 0.1 ℃ and 0.1psu respectively, and were used to examine the oceanographical characteristics of these seas. The horizontal box size was
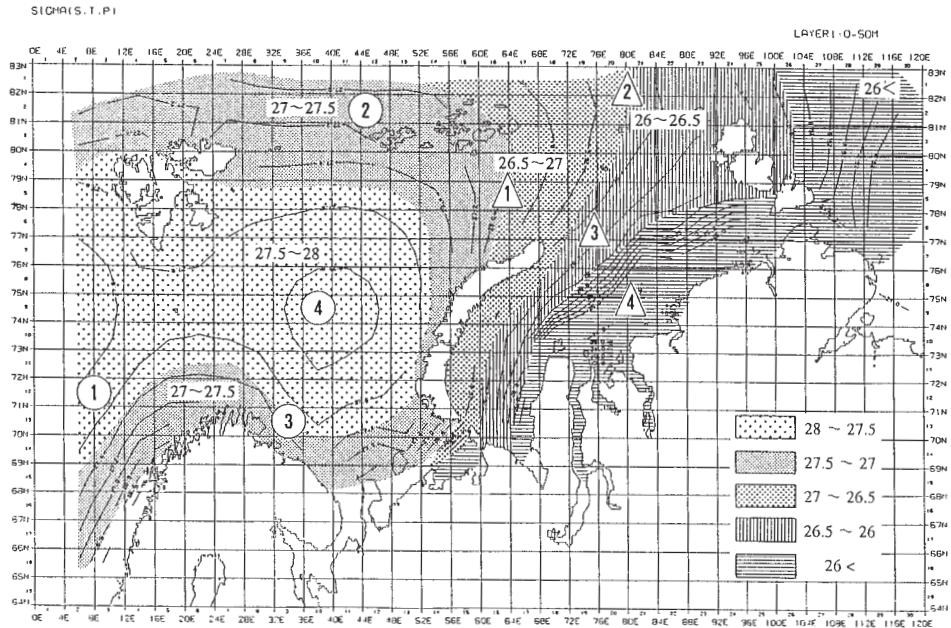
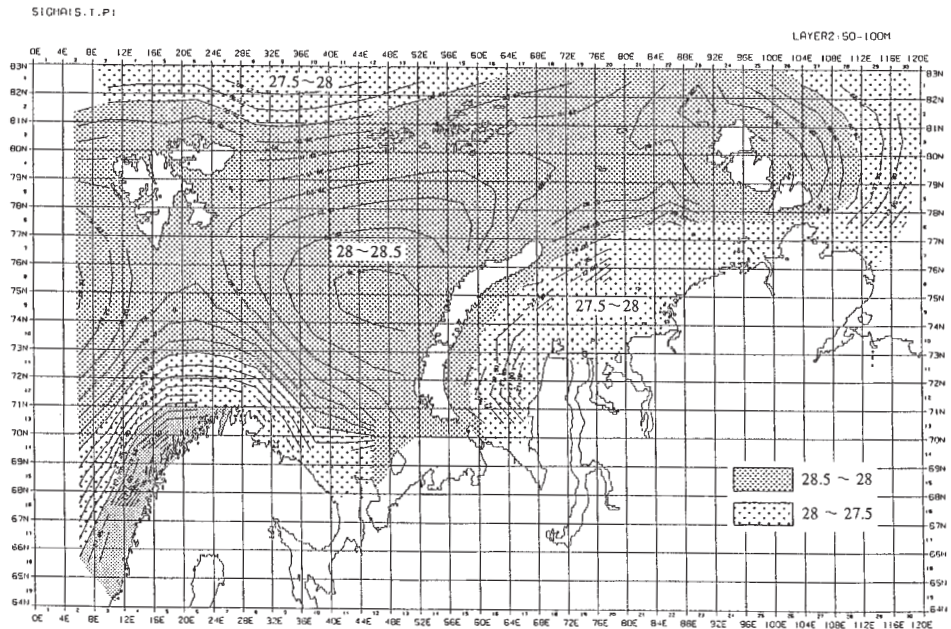Fig. 3. (1) Density distribution σ_t (0–50m layer, warm weather season).

Fig. 3. (2) Density distribution σ_t (50–100m layer, warm weather season).

$4° \times 1°$, and each box was vertically divided into 6 layers (0~50m, 50~100m, 100~200m, 200~500m, 500~900m and 900~2500m).

Figure 2 shows the grids of the model and the number of vertical layers.

3. Oceanographic description of Arctic seawater

Density structure

Barents Sea

The Barents Sea has an area of 1.42×10^6km^2 and volume of 3×10^5km^3. It is largely open to the Norwegian Sea in the west and the central Arctic basin to the north. The average depth is 230m, with a maximum depth of 500m near Bear Island. The position of the Barents Sea between the Atlantic and Arctic Oceans gives it a key role to play in the transport of substances.

The Norwegian Atlantic Current which is a warm current, enters from the western side of North Cape. Then, the current is divided into two major branches. One flows eastward (coastal current system) and the other flows into the northern central area. Cold Arctic water enters from the north between Spitsbergen and Franz-Josef Land, as well as from the north between Franz-Josef Land and Novaya Zemlya (see Fig. 1). The water circulation in the Barents Sea is generally counter-clockwise (Harms, 1992).

The Barents Sea undergoes stratification in spring and mixing in winter. This sea area is high in biological production. Salinity is 32~35 psu.

Based on the temperature and salinity distribution, density distribution maps for the layers of 0–50m and 50–100m are illustrated in Figs. 3 (1) and (2), respectively.

The density of seawater is highest in the central part of the Barents Sea and in the sea area where the Atlantic water, southwest of Spitsbergen flows north along the continental shelf, showing σ_t value of about 28. In the northernmost and southernmost parts of the Barents Sea, the density of seawater is about 0.5 lower in σ_t due to the effects of relatively light Arctic surface−layer water and coastal water, respectively.

In order to examine characteristics of water masses in the Barents and Kara Seas, T−S

diagrams for each calculation box in Fig. 2 are drawn in Figs. 4 (1) and (2), respectively.

Based on the T−S diagram, surface water of the Barents Sea may be classified into four water masses as follows:

① The Atlantic water with higher temperature and higher salinity,

② The Arctic surface water with lower temperature and lower salinity,

③ The coastal water with higher temperature and lower salinity, and

④ The Barents Sea water mass that is mixture of the Atlantic water and the Arctic surface water.

By Fig. 4 (1) it can be recognized that the coastal water mixes only with the Atlantic water. The Arctic surface water first becomes more saline and then mixed with the Atlantic water, forming the Barents Sea water mass.

The density maps of Figs. 3 (1) and (2) correspond with classification of the 4 water masses, which are identified by the number in circle.

Kara Sea

The Kara Sea is 8.8×10^5km^2 in area and 9.8×10^4km^3 in volume. It is rather shallow; its mean water depth is 120m. However, deep valleys exist, namely, the Novaya Zemlya Trough (300~400m) east of Novaya Zemlya, and a trough (600m) north of Novaya Zemlya. In this sea area, there are inflows of river water amounting to 1,500km^3 annually, mainly from the Ob and Yenisey. These fresh water inflows cause a northward flow, forming eddies which are then branched into a northeastward−flowing current along the continent and a southwestward−flowing current along the coast of Novaya Zemlya.

River water inflows are conspicuous in summer, and decrease remarkably in winter. Figure 5 (IAEA,1998) shows monthly changes in major river water runoffs. The structure of water masses in the Kara Sea is dominated by water inflows from the Arctic Ocean and the Barents Sea as well as by river water inflows.

As was done for the Barents Sea, density distribution maps for each layer, based on the vertical distribution map of temperature and salinity for the Kara Sea, are shown in Figs. 3
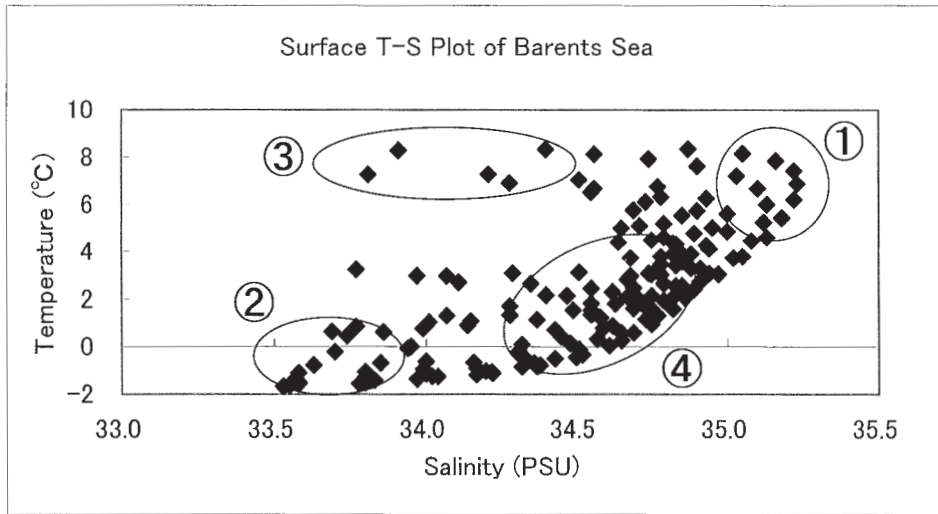
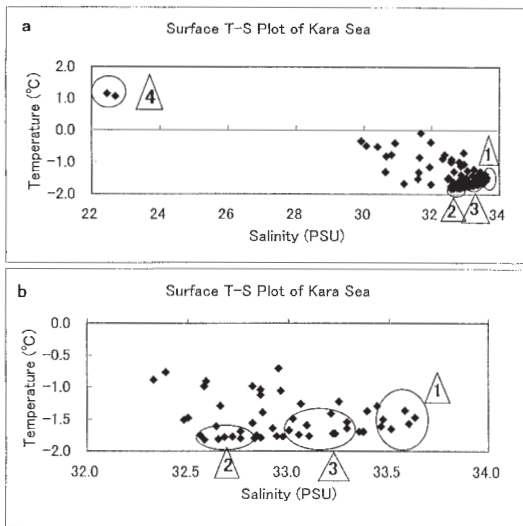Fig. 4. （1）　Surface T-S diagram of the Barents Sea.

Fig. 4. （2）　Surface T-S diagram of the Kara Sea.

（1）and （2）. T－S diagrams were drawn also for the Kara Sea.

Fig. 4 （2）a shows total surface T－S plot of the Kara Sea, while Fig. 4 （2）b is an enlarged map of the part of salinity 32.0–34.0. From these figures, four water masses could be recognized:

⚠ The water mass characterized by higher temperature, derived from the Barents Sea,

⚠ The Arctic surface water with lower temperature and lower salinity,

⚠ The Kara Sea water mass, a mixture of the Kara Sea water and the Arctic surface water, and

⚠ The coastal water with lower salinity.

These water masses of the Kara Sea are denoted with the number in triangle in Fig. 3 （1）. Salinity is 32psu offshore and 10psu near the mouths of the Ob and Yenisey river, as shown in Fig. 6.

The Barents seawater, having high density, reaches the Kara Sea with its density reduced as it advances eastward. The density of seawater in the central part of the Kara Sea becomes about 1–1.5 lower in σ_t in comparison with the Barents Sea.

The low－density water in the Kara Sea is formed by Arctic surface water entering from the north and a vast amount of fresh water entering from both the Ob river and the Yenisey river. Over the continental coast of the Kara Sea, a front is formed with density σ_t falling below 26.

Flow characteristics

LOENG et al. （1991）point out that the three major water masses, namely, coastal water, Atlantic water and Arctic water, are related to ocean current systems. According to Fig. 7 （LOENG et al. 1991）, which shows the distribution of water masses in the Barents Sea, correspondence to the density distribution shown in
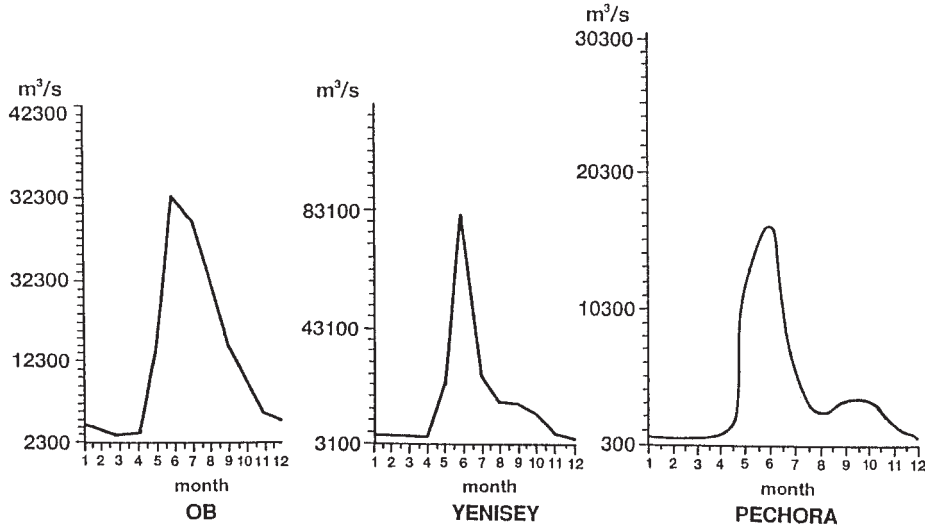
Fig. 5. Average annual cycle of river discharge to the Kara Sea and the Barents Sea (IAEA, 1998).

Fig. 3 is good.

Freezing continues for more than half of the year in this regions. The effect of wind on the flow has never been calculated. GJEVIK and STRAUME (1989) numerically calculated the tides in the North Sea, the Norwegian, Greenland and Barents Seas, and the Arctic Ocean. They concluded that in these sea areas the effect of tides is small, with the exception of coastal areas.

4. Method of flow analysis

A careful consideration must be used in the selection of an appropriate flow analysis technique for the regions having a large inflow of river water from the inland part, high − temperature and high − salinity Atlantic water masses from the western sea areas, low − temperature and high − salinity Arctic seawater from the north, large water depths and complicated topography, as seen in the Arctic Ocean.

To analyze the concentration of radionuclides extending as long as several 100 years following the flow analysis, the conservation of mass not only in each calculation box but also as a whole system must hold. That is to say, it is necessary for the following equation to hold;

$$\sum_{iB,iC} (W_{iB,iC} \ \rho_{iC} - W_{iC,iB} \ \rho_{iC}) + (\text{river inflow}) +$$

$$\text{precipitation}) - (\text{evaporation}) = 0$$

Where, iB: box number in ocean boundary, iC: box number in calculation box, $W_{iB, iC}$: exchange flow rate which enters from box iB to box iC, $W_{iC, iB}$: exchange flow rate which enters from box iC to box iB, ρ_{iC}: density of seawater in calculation box iC, ρ_{iB}: density of seawater in box iB, Σ: sum for all groups (iB, iC) of boundary box and calculation box.

There are two kinds of models to cope with the flow and the dispersion of radionuclides by advection and diffusion, namely compartment or box models and hydrodynamic circulation model.

Compartment or box models provide long time, spatially averaged capabilities, and some uncertainties remain in some key parameters. Hydrodynamic models provide locally resolved, short time − scale results and can only be run for limited time − scales of the order of tens of years. In the hydrodynamic models, the circulation pattern and eddy diffusivities in the model, by trial and error, are adjusted until the observed temperature and salinity distributions can be generated by the model. Moreover, there is a major shortage of quality forcing data for hydrodynamic models applied to the Arctic Ocean.

Temperature and salinity are tracers; they are the easiest of all to measure; we have much better coverage of the ocean for them than
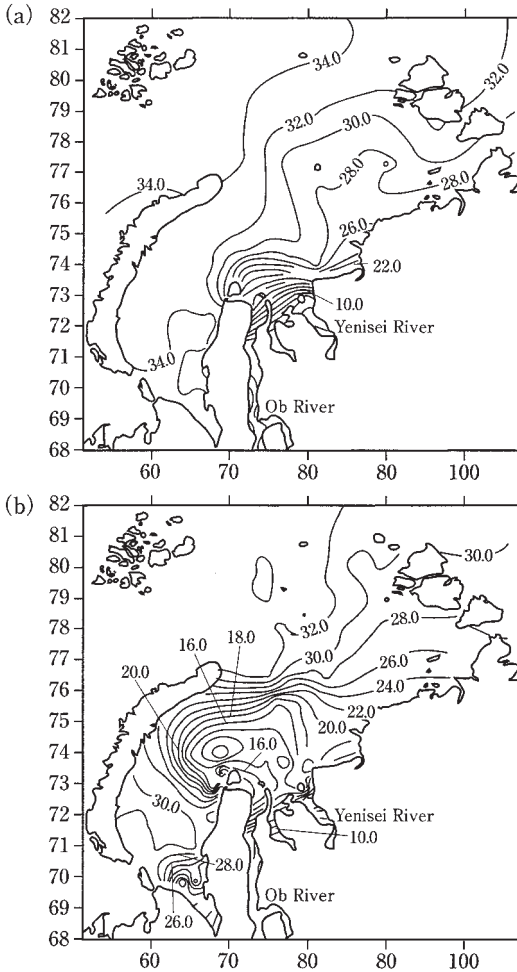
(a)

(b)

Fig. 6. Salinity distribution at the surface from data for (a) winter and (b) summer.

anything else; and their immediate relation to the density field means that they must be the central focus of any effort to understand the flow circulation. In this research, the method of analysis based on the box (compartment) model was selected because it was impossible to clearly determine the flow driving forcing in the sea areas concerned for the hydrodynamic circulation model.

Flow fields can also be generated from the observed temperature and salinity distributions in more objective ways using simplifying assumptions about the general balance of forces in the ocean interior. On the other hand, the calculation of geostrophic velocity has been used for many years in oceanography but has

always suffered from the problem of not knowing what depth independent (barotropic) component of velocity needs to be added to the baroclinic results obtained (the problem of the "level of no motion"). Recently, methods of calculating the barotropic component have been derived (STOMMEL and SCHOTT, (1977); KILLWORTH, (1980)) and methods have been developed using generalized inverse techniques (WUNSCH and Minster (1982), WUNSCH (1996), EMERY and THOMASON (1998)) for calculation the flow.

For radiological assessment purposes, the use of inverse technique is particularly attractive because it does ensure that the model produced will give predictions which are comparable with observed temperature and salinity profiles in the ocean. The model used in this paper is an approach for applying conservation of mass with high accuracy not only in each calculation box also over the whole system. This model has been named a hybrid box model, intermediate one between the box model and the hydrodynamic model, developed by attending the OECD/NEA and IAEA (IASAP) modeling group meetings (IAEA Report 1998). This hybrid box model has been developed to cover the local field (Kara and Barents Seas).

5. Flow analysis by a hybrid box model

In this analysis, the flow which permits reproduction of the observed distributions of water temperature and salinity is mathematically calculated, to subsequently deal with the diffusion of nuclides.

The balance equations of seawater, salinity and heat volumes in each box are used to determine the exchange flow rate between boxes (Fig. 8).

For box i, the following are the conservation equations:

(1) Equation of conservation of seawater mass

$$\sum_{j \neq i} W_{ji}\rho_j - \sum_{j \neq i} W_{ij}\rho_i + \sum R_{ri}\rho_i' P_i - E_i = 0$$

$$[\text{ton/s}] \ (1)$$

Where $W_{ij} \geqq 0$: exchange flow rate from box I to box j [m³/s], ρ_i: density of seawater in box I [ton/m³], obtained by The International Equation of State of Seawater from water temperature and salinity, ρ_r': density of river water in
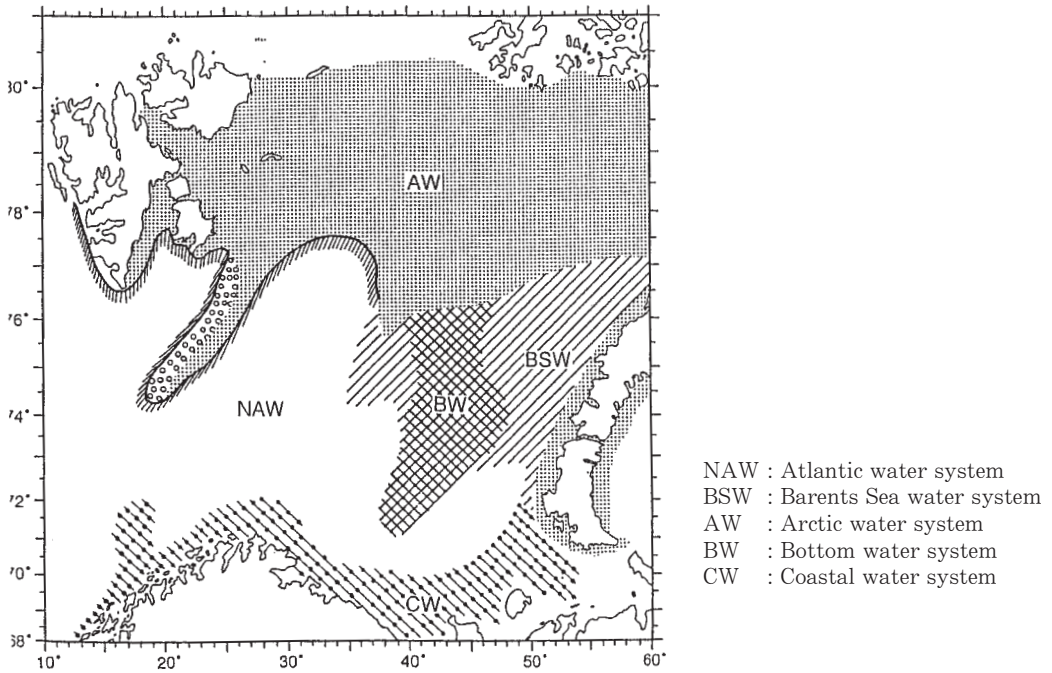
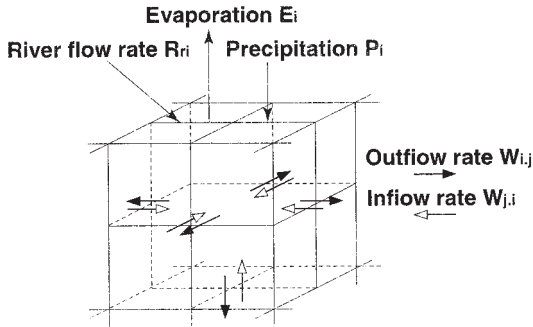Fig. 7. Distribution of water masses in the Barents Sea (LOENG *et al.*, 1991).

NAW : Atlantic water system
BSW : Barents Sea water system
AW   : Arctic water system
BW   : Bottom water system
CW   : Coastal water system

Fig. 8. Outline of the hybrid box model.

river r [ton/m^3]. R_{ri}: inflow of river water from river r to box i (m^3/s). P_i: precipitation into box i [ton/s], E_i: evaporation from box i to the atmosphere [ton/s].

The model was set up so that each exchange is represented by exchange flow rates, one in each direction. These exchange flow rates, which by definition are assumed to be positive, can be interpreted in terms of advection and mixing: to a first approximation, the mixing coefficient is the lesser of the two values and the advection is the difference.

(2) Equation of conservation of salt

$$\sum_{j \neq i} W_{ji}\rho_j S_j - \sum_{j \neq i} W_{ij}\rho_i S_i +$$
$$\sum_r R_{ri}\rho_r{}'(S_i{}' - S_i) = 0 \qquad \text{[ton/s] (2)}$$

S_i: salinity in box i [‰],
$S{}'_i$: salt in river r [‰]

(3) Equation of conservation of heat
$$\sum W_{ji}\rho_j T_j C - \sum W_{ij}\rho_i T_i C + H_i = 0$$
$$\text{[Mcal/s] (3)}$$

T_i: water temperature in box i [℃], H_i: heat entering from the atmosphere into box i [Mcal/s],

C: specific heat of seawater [cal/g ℃], which is presently set at 1.0.

Although we put the terms P_i, E_i in equation (1) and the term H_i in equation (3), we did not use these terms in our calculations due to difficulties in its treatment in the surface layer. It is because the parts of these seas are largely ice－covered year－round. Therefore, the flow was analyzed using a hybrid box model, taking into account river inflows and density structures in the seas.

Table 1. Input condition of river inflow.

River	River flow rates (m³/s)	Water temperature (℃)	Salinity (‰)
Ob	2,425.0		
Yenisey	18,317.0	2.65	15.0
Pechora	4,208.0		

Input conditions of river inflow from the river mouth are shown in Table 1.

Three equations are written in matrix form as;

$$A\,\underline{W} = \boldsymbol{b} \tag{4}$$

Where A is the property matrix containing ρ, ρS and TC, $\underline{W}$ is the vector of exchange flow rates and $\underline{\boldsymbol{b}}$ is the vector of sources and sinks.

These solutions can be expressed as the sum of a particular solution such as the least squares solution which is determined by the sources and sinks, and a series of null space solutions which are independent of the sources and sinks. So far, the least squares solution was considered to be the most useful point since it represents the flow pattern corresponding to the minimum energy in the ocean.[1]

Attempts using a box model have been made to use the observed temperature and salinity distributions in the Atlantic Ocean to derive a flow pattern. In conclusion, this experience with inverse techniques on the large systems such as this research showed that this has been done with the solution containing both negative and positive exchange flow rates. The difficulty in obtaining a positive solution by requiring an exact fit to the observed data is probably due to the existence of temperature and salinity gradients within the model that can only be sustained by a negative exchange flow rate. If these gradients can be removed by revising the original temperature and salinity distributions, then both a positive solution and a good fit to data my be possible.

In this model, the number of exchange flow rates, n, is less than that of equations, m, and solutions of such a problem are easily obtained either by general inverse matrix or by nonlinear programming method without constraints.

However, some of exchange flow rate values thus obtained could be negative, which makes difficult to interpret the solutions as physical phenomena.

The difficulty in finding a solution was that the exchange flow rate must be non-negative (positive or 0) owing to the nature of the model. Therefore, one cannot use a simple linear equation or general inverse matrix representation and has to rely on a non-linear programming method with constraint (non-negative condition). That is to say, one does not require equations (1) to (3) to hold strictly and permits some minimizing errors.

In order to overcome this difficulty, non-negativity constraint was set for the exchange flow rate, $\underline{W}$, $(\underline{W}, \geqq 0)$ and an efficient program was developed based on solution algorithm by mathematical formulation using a non-linear programming. This method is identical with solving a quadratic programming problem so as to minimize the objective function under the condition of non-negative exchange flow rate. That is,

Objective function (square of residual norm): $\| A\,\underline{W} - \underline{\boldsymbol{b}} \|^2 \to$ min., and

Constraint: $W \geqq 0$ $\hspace{1cm}$ (5)

Where A: m×n matrix of coefficients, determined by observation data,

$\hspace{1.2cm}\underline{\boldsymbol{b}}$: m－dimension constant vector determined by boundary conditions,

$\hspace{1.2cm}\underline{W}$: n-dimensional vector of exchange flow rates,

$\hspace{1.2cm}\| \ \|$: Euclidean norm,

$\hspace{1.2cm}$m: number of conservation equations, and

$\hspace{1.2cm}$n: number of exchange flow rates.

If the non-linear programming method with constraint is used, a solution can be obtained and the exchange flow rate thus obtained is non-negative, and errors in equations (1) to (3) are minimum.

---

[1] This technique is frequently employed for solving problems to obtain a fluid movement of which the total energy is restrained to be minimal, where an indefinite number of solutions can exist.

e $= \Sigma_i \{ \alpha_1$(the left side of the equation of conservation of mass (1) in box i)^2
$+ \beta_1$ (the left side of the equation of conservation of salt (2) in box i)^2
$+ \gamma_1$ (the left side of the equation of conservation of heat (3) in box i)$^2 \}$ (6)

Then, e is a function of the exchange flow rates W_{12}, W_{13},... and is the sum of squares of error in the conservation equations.

Exchange flow rates W_{12}, W_{13},... may be obtained under the non-negative condition W_{12}, W_{13},...> 0 to minimize the error function e = e (W_{12}, W_{13},...). This problem is usually called NNLS (Non-Negative Least Squares). Of the three equations of conservation, the unit of the first two equations is [tons/s], and that of the last equation is [Mcal/s].

Adjustment is, therefore, necessary when considering the weight of the three equations. For this adjustment, α_1, β_1 and γ_1 are set as weight constants ($\alpha_1 = 10^9$, $\beta_1 = 10^4$, $\gamma_1 = 1.0$). The values of α_1, β_1 and γ_1 above were decided by taking into consideration the agreement between results of current analysis and observation data of the Pacific Ocean and Tokyo Bay. For solution procedures to obtain the exchange flow rate, W, see Appendix I. Refer to LAWSON and HANSEN (1995) for more details.

Model validation is important. A comparison was made between literature values of water fluxes in the Arctic Ocean and values obtained from the hybrid box models. The validation process for the hybrid model has been severely restricted by the lack of appropriate flow data particularly within the Arctic area.

In the past, flow analyses were conducted in Tokyo Bay under the same input condition such as heat budget process, inflow rate of river waters, temperature and salinity distributions, using both the hybrid box model and 3D hydrodynamic model, thus confirming that there is no major difference in the results of flow circulation pattern obtained by both models (WADA et al., 1996).

On the other hand, the study was conducted focusing the Sea of Japan using the hybrid box model to elucidate the seasonal flow characteristics under the input conditions like inflow of Tsushima Warm Current, temperature and salinity data, heat budget process and inflow of river water from the inland area (TAKAHASHI and WADA, 1999).

The seasonal strengths of the Nearshore Branch of the Tsushima Warm Current, the East Korean Warm Current and the Liman Current were reproduced in the model. The hybrid box model was applied to the safety evaluation in a hypothetical submergence accident onto the seabed in the Pacific Ocean. Agreement was found to be good by comparison of the results of current analysis and the existing knowledge on the ocean currents (WATABE et al, 1996).

6. Results of flow analysis in the local field

Based on the flow velocities obtained from exchange flows in the hybrid box model, particles from each box and river mouth in the Arctic Ocean were tracked and the movement of seawater particles was studied. Particle tracking method is described in Appendix II.

Estimation of Errors

As we search for flows which reproduce the distribution of salinity and temperature in each box, errors in salinity and heat amount can be neglected. As for flow, we calculated error of the conservation equation of seawater for each box. Errors of flow were evaluated both by the absolute error which is the difference of in and outflows and the relative error which is the difference divided by the inflow.

Table 2 shows coordinate in which the maximum error occurs (see Fig. 2), residual errors by the least square method, and the maximum value of relative error (residue/inflow) and coordinates.

Barents Sea

According to the results of tracking (Fig. 9 (1), see Appendix II), the Atlantic water which enters the Barents Sea along the Norwegian Peninsula circulates counterclockwise in the Barents Sea. This flow is in agreement with previously known data (see Figs. 10 (1) and (2)).

The results of tracking shown in Fig.9 (2) indicate that the Norwegian Atlantic current flows in from the west to the north cape. It divides into two main branches. One which flows

Table 2. Errors of conservation equation of seawater,

	Absolute error	Coordinates	Relative error	Coordinates
1stlayer(0–50m)	6×10^{-4}(kton/s)	(20,4)	4×10^{-7}	(17, 13)
2ndlayer(50–100m)	5×10^{-4}(kton/s)	(3,8)	4×10^{-7}	(16, 7)

——— (0～50m)　　——— (50～100m)
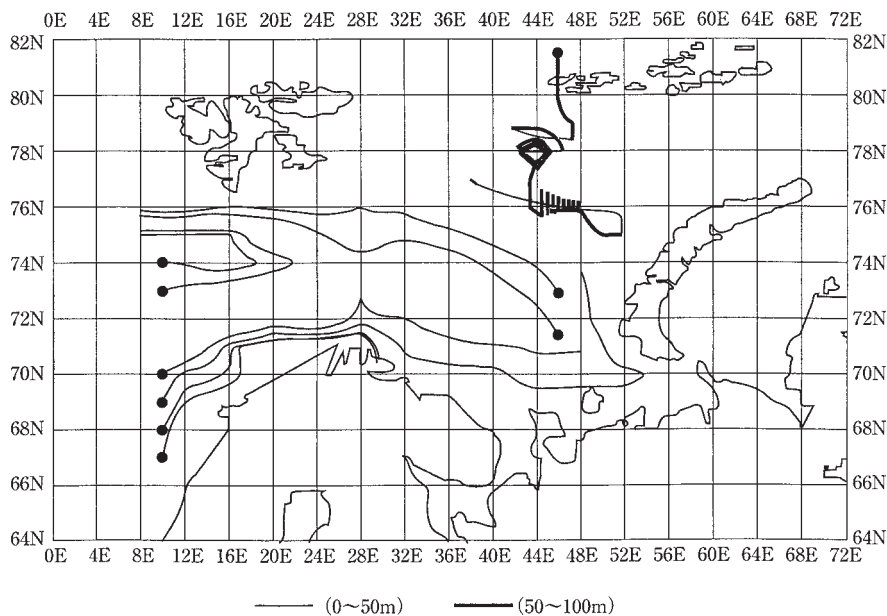
Fig. 9. （1）　Result of tracking（・particle injection point）.
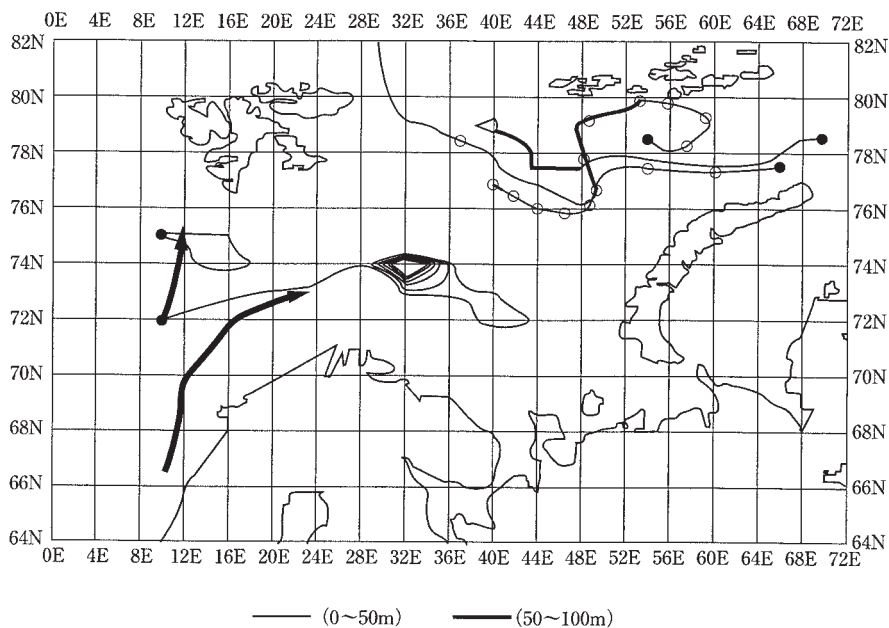

——— (0～50m)　　——— (50～100m)

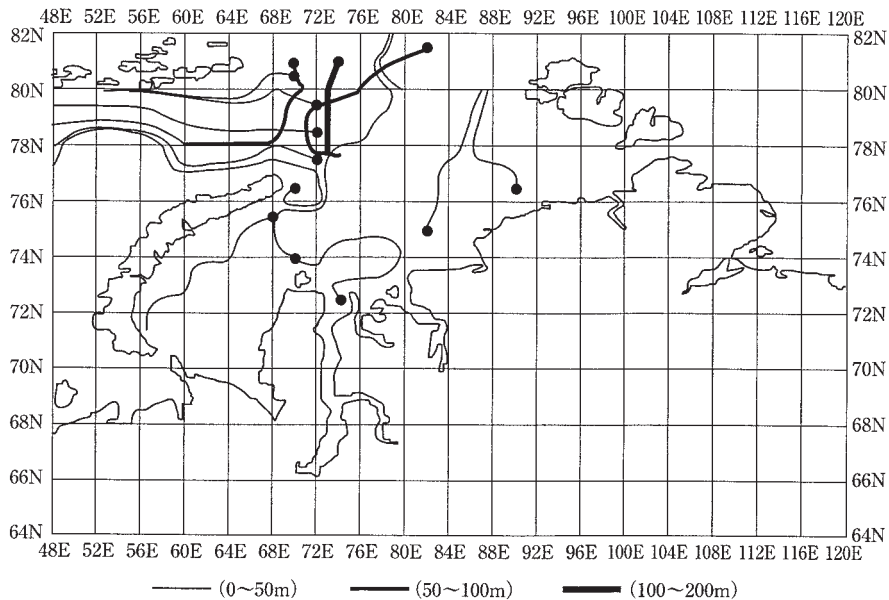Fig. 9. （2）　Result of tracking（・particle injection point）.

Fig. 9. (3) Result of tracking (• particle injection point).

eastward, and another which flows north.

Cold Arctic water enters from the east to the west between Franz-Josef Land and Novaya-Zemlya (Fig. 9 (2)), and from the north between Spitsbergen and Franz-Josef Land shown in Fig. 9 (1). The water circulation in the Barents Sea is generally anticlockwise judging from Figs. 9 and 10.

The current flowing southwestward at the south of Franz-Josef Land divides into two branches at the north of Sentralbanken, one of them being shown to flow southwardly toward Sentralbanken (LOENG, 1989). According to recent observations, however, this flow branch is considered to be rather minor (TANTSJURA, 1959).

As is shown in Fig. 9 (2), water particles enterting from the central part of Atlantic Ocean are recognized to become gyre currents near the front shown in Fig. 10 (2).

Beween Spitsbergen and Franz-Josef Land, there exist path lines both flowing into and flowing out of the Arctic waters (Fig. 9 (1) and (2)).

Kara Sea

Fig. 11 shows schematic flow pattern in the Kara Sea (PAVLOV et al., 1995). The northern

sea area has a current which enters from the central Arctic Ocean along trenches of 80 to 125m deep and current which flows into the Barents Sea between Franz-Josef Land and Novaya Zemlya. The inflow from the central Arctic Sea to the Kara Sea in the second layer (50~100m) and third layer (100~200m) were reproduced successfully by tracking.

The western Kara Sea has the Novozemelskaya Current which flows from northeast to southwest along the east coast of Novaya Zemlya. The results of tracking are shown in Fig. 9 (3). This figure clearly shows that particles advance southward along the east coast of Novaya Zemlya.

The currents flowing north from the river mouths can be observed clearly.

Results and discussion

The results of flow analysis were compared with the migration routes of cod (Haddock and Barents Sea cod) to examine the reproducibility of the results. It is generally considered that Haddock cods live in 4 to 10℃ water. The sea areas which meet these conditions in the Barents Sea are the coastal area and the Atlantic water mass, with high water temperatures. The migration routes observed are shown in

=Atlantic currents.   ⋯▸=Coastal currents.   ‑‑‑▸=Arctic currents.
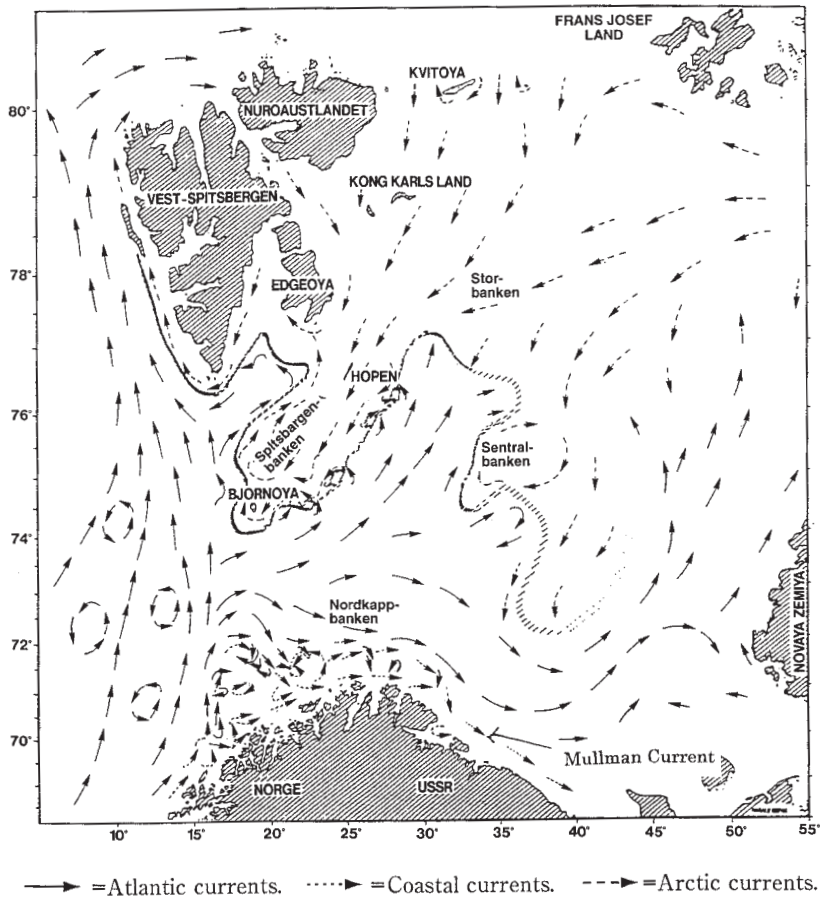
(The hatched line indicates the mean position of the Polar Front)

Fig. 10. (1) Surface -layer flow patterns in the Barents Sea (Loeng *et al.*, 1991).

Fig. 12.

The migration routes of Haddock and Barents Sea cod were compared with the results of flow analysis by the hybrid box model (Fig. 9 (1)). High similarity is recognized. In particular, the route of cods entering the Barents Sea from along the coast of Norway and migrating along the continent agrees with the tracking result. Possibly, Haddock and Barents Sea cod migrate along the Norcup Ocean Current, the Mullman Coastal Current, or the Mullman ocean current. Comparison of the model's current field with the observed surface velocity map indicate that the basic circulation pattern in the Barents Sea and the Kara Sea is captured by the model.

We also calculated the surface dynamic height from the density field and compare the result with that obtained by the particle tracks shown in Figs. 9 (1), (2) and (3). The geostrophic calculation method assumes that there is a level or depth of no motion. Level of no motion may be assumed if the currents have been measured at some depths by current meters. As we have obtained the density field from water temperature and salinity data, we calculate the flow pattern from the surface dynamic heights.

Figure 13 shows the dynamic topography at the surface layer (25m deep) of the Barents and Kara Seas in which the level of no motion is assumed to be 75m deep.
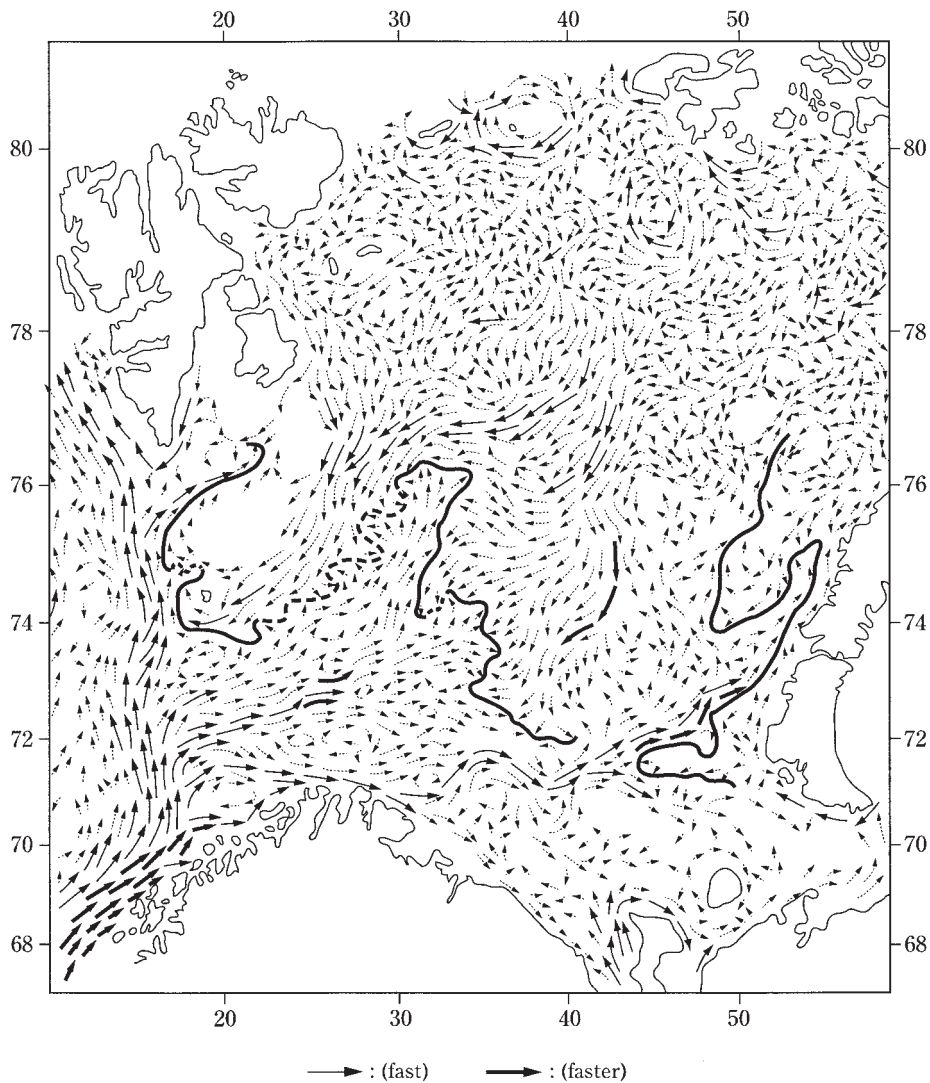
Fig. 10. (2)   Scheme of the water circulation at the surface of the Barents Sea
(Tantsjura, 1959).

Following characteristics of the streamlines can be noticed:

• There exists a current which flows from east to west along the coast of the Barents Sea.

• The current turns anti-clockwise in the eastern part of the Barents Sea and flows westerly in the north of Spitzbergen Island.

• In the area between Spitzbergen Island and Novaya Zemlya, there exists a region of anti-clockwise circulation.

• In the Kara Sea, the coastal current becomes easterly under the influence of the westerly current along the coast of the Barents Sea. Consequently, a large-scale anti-clockwise circulation becomes noticeable in the region comprising the Barents and Kara Seas.

When Fig. 12 and Fig. 9 (1) and (2), which show results of the particle track, are compared, the anti−clockwise current in the Barents Sea is similar in the both cases, although
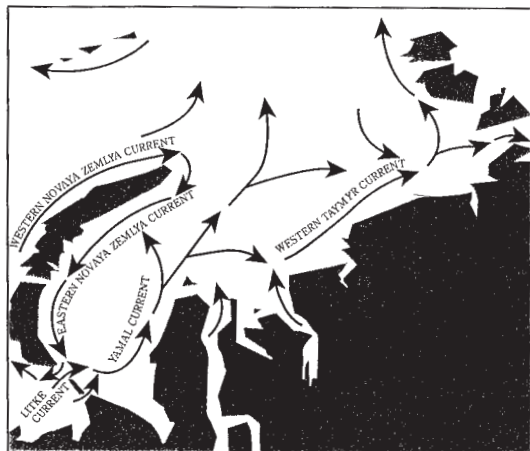
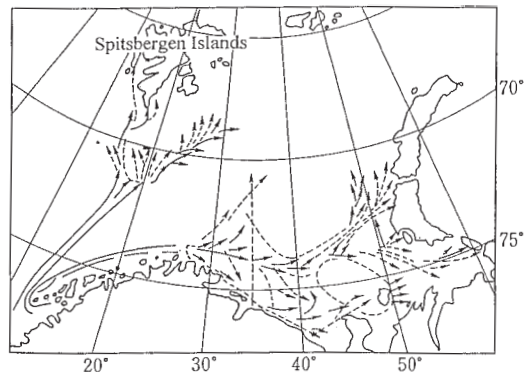Fig. 11. Schematic flow pattern in the Kara Sea (PAVLOV *et al.*, 1995).

Fig. 12. Routes of the eastward migration of cods in the Barents Sea (MASLOV, 1944).
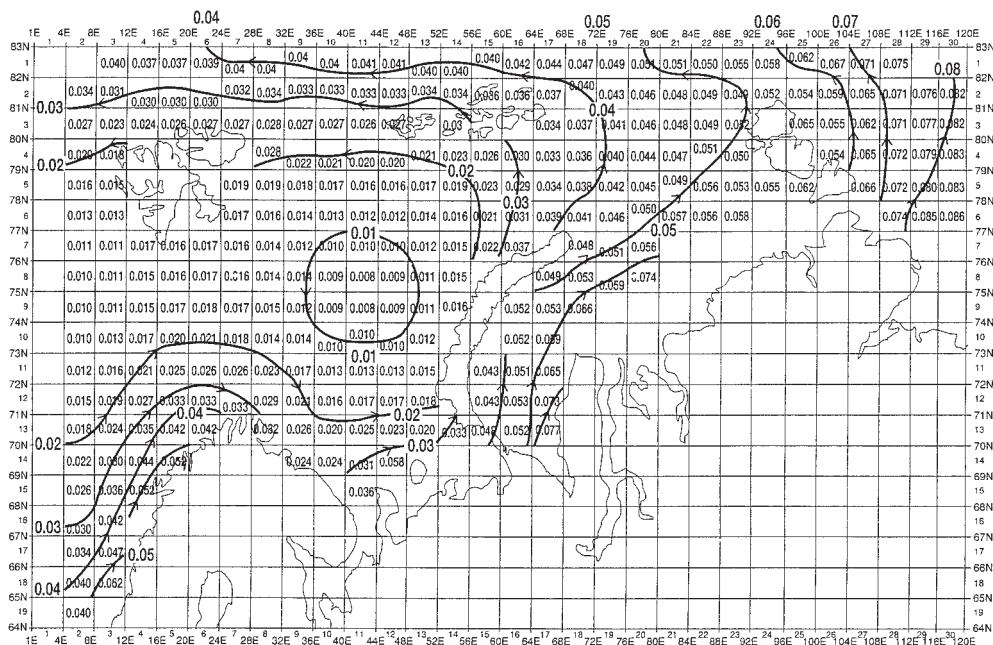———————▶ Migrations of mature cod
·················▶ Migrations of immature cod

Fig. 13. Dynamic depth anomaly in the Barents Sea and Kara Sea (Unit: Dynamic meter×10^{-2}).

the anti−clockwise circulation with a small scale at the center of the Barents Sea can not be seen in the hybrid box model result.

7. Conclusions

Flow analysis was conducted by using observation data (water temperature, salinity) and applying a method for obtaining the exchange flow rate in such a way that the inter−box input and output of salinity, heat and seawater volume was balanced, and as a result,

1) Flows in the Barents Sea are affected by inflows from the neighboring seas (North Atlantic Ocean, Arctic Ocean). Inflow of river water from the Ob, Yenisey, etc. has the largest effect on changes in flows in the

Kara Sea.
2) Flows obtained with the hybrid box model agree with flows based on observed data. For the deep layers, it will be necessary to carry out further studies on the reproducibility of flows because only a small amount of Arctic deep data are available.
3) The tracking of particles was performed with respect to calculated flows. This enabled to obtain a three－dimensional movement of particles with reproducibility of high accuracy.
4) Good agreement is with migration routes of cod.

Acknowledgements

References

EMERY, W. J. and R. E. THOMASON (1998): Data Analysis Methods in Physical Oceanography. Pergamon. Oxford, 634 pp.

GJEVIK, B. and T. STRAUME (1989): Model simulations of the M2 and the K1 tide in the Nordic Seas and the Arctic Ocean. Tellus. **41A**: 73 － 96.

HARMS, I. H. (1992): A numerical study of the barotropic circulation in the Barents and Kara Seas. Continental Shelf Research, **12(9)**: 1043 － 1058.

International Atomic Energy Agency (1998): Radiological Conditions of the Western Kara Sea, Report on the International Arctic Seas Assessment Project (IASAP).

KILLWORTH, P. D. (1980): On the determination of absolute velocities and density gradients in the ocean from a single hydrographic section. Deep Sea Res., **27**, 901–929

LAWSON, C. L. and R. J. HANSEN (1995): Solving Least Squares Problems. siam (Society for Industrial and Applied Mathematics), Philadelphia, Prentice-Hall, INC. 337 pp.

LEVITUS (1982): Climatorogical Atlas of the World Ocean, NOAA Professional Paper 13, National Oceanonic and Atmospheric Administration, U. S. Department of Commerce.

LOENG, H., E. SAKSHAUG, C. C. E. HOPKINS and N. ORITSLAND (1991): Features of the Physical Oceanographic Conditions of the Barents Sea. Polar Research. **10 (1)** : 5–18.

MASLOV, N. A. (1944): The bottom-fishes of the Barents Sea and their fisheries, Trudy PINRO, M.-L. YⅢ: 3–186 (in Russian).

PAVLOV, V. K. and S. L. PFIRMAN (1995): Hydrographic Structure and variability of the Kara Sea:Implications for pollutant distribution. Deep-Sea Res., **42. (6)** : 1369－ 1390.

STOMMEL, H. and SCHOTT, F. (1977): The beta spiral and the determination of the absolute velocity field from hydrographic station data. Deep Sea Res., **24**, 325–329.

TAKAHASHI, Y. and A. WADA (1999): Study on Flow in the Sea of Japan by Box Model. Journal of Hydroscience and Hydraulic Engineering, JSCE. **17** (2): 139–158.

TANTSJURA, A. (1959): About the current of the Barents Sea, Proc. PINRO, **11**, 35–53 (in Russian)

VOLKOV, V. A., O. JOHANNESSEN, V. E. BORODACHEV, G. N. VOINOV, L. H. PETTERSSON, L. P. BODYLEV and A. V. KOURAEV (2002): Polar Seas Oceanography, An integrated case study of the Kara Sea, Chichester, UK, Praxis Publishing, 450pp.

WADA, A., T. TAKANO and T. HOZUMI (1996): Estimation method for Residence Time of Bay Water. Journal of Hydroscience and Hydraulic Engineering, JSCE, **14** (1): 57–66.

WADA, A., Y. KINEHARA and T. TAKANO (1997): Marine contamination in the Arctic Ocean. J. of Global Environmental Engineering. JSCE. **3**: 37–51.

WATABE, N., Y. KOHNO, D. TSUMUNE, T. SAEGUSA and H. OHNUMA (1996): An Environmental Impact Assessment for Sea Transport of High Level Radioactive Waste. RAMTRAN, **7** (2/3):117–127

WUNSCH, C. (1996): The Ocean Circulation Inverse Problem. Cambridge University Press. Cambridge, 442 pp.

WUNSCH and MINSTER (1982): Methods for box

models and ocean circulation tracers: Mathematical programming and non-linear inverse theory, J. Geophys. Res., **87**, 5647–5662.

Appendix I
Solving method for the hybrid box model

Solution of obtaining the exchange flow rates by means of a compartment model is identical with solving a quadratic programming problem so as to minimize the objective function under the condition of non-negativity of exchange flow rate, W. That is,

Objective function (square of residual norm): $\| A W - b \|^2$, and Constraint: $W \geq 0$,

where A:　m n matrix of coefficients, determined by observation data,

b:　m-dimension constant vector determined by boundary conditions,

W:　n-dimension vector of exchange flow rates,

$\| \cdot \|$: Euclidean norm,

m:　number of conservation equations, and

n:　number of exchange flow rates.

Mathematically, this problem is called convex quadratic programming problem or NNLS (Non Negative Least Squares).

Solution processes

Algorithm of the active set method is premised on three points as follows:

1) When all of exchange flow rates are 0, it satisfies the equations and constraint,

2) Solution of quadratic programming problem without constraint can be obtained by the usual least squares method, and

3) Criteria of optimum solution are given by the Kuhn－Tucker's condition that is usually applied in quadratic programming method.

Outline of the algorithm for obtaining optimum solution is summarized as follows:

① First, let all elements of exchange flow rate be 0, and select an element Wq that leads to the optimum solution most closely;

② Solve the quadratic programming problem without constraint, and correct the resulting solution so as to fulfill the non-negativity restraint;

③ Using the corrected solution, solve again

quadratic programming problem without constraint, and correct solution that does not satisfy the non-negativity constraint; and

④ When the non-negativity constraint is fulfilled, select another element of exchange flow rate that has been set to be 0, and repeat the procedures above, thus decreasing one by one the number of elements set to be 0, until the optimum solution is reached.

Appendix II
Particle Tracking Method in Arctic Sea Box Model

1.　Particle Tracking Method Particle tracking is defined here as positioning of a particle from a given initial position in a given flow field after an arbitrary time elapsed. Equations representing a particle tracking movement in the spherical coordinates are:

$$\dot{\lambda} = \frac{u}{r \cos \varphi}$$

$$\dot{\varphi} = \frac{v}{r}$$

$$\dot{r} = w,$$

where u: longitudinal flow rate component (m/s), v: latitudinal flow rate component (m/s), and w: vertical flow rate component, each being function of: longitude,: latitude, and r: vertical coordinate (distance from the geocenter, respectively. The mark " $\cdot$ " denotes the temporal differential.

One of the typical solutions for such equations is the (explicit) Eulerian solution, Δt being the time interval:

$$\lambda^{n+1} = \lambda^n + \Delta t \frac{u(\lambda^n, \varphi^n, r^n)}{r^n \cos \varphi^n}$$

$$\varphi^{n+1} = \varphi^n + \Delta t \frac{v(\lambda^n, \varphi^n, r^n)}{r^n}$$

$$r^{n+1} = r^n + \Delta t w(\lambda^n, \varphi^n, r^n) \qquad (\text{A II} \cdot 2)$$

in which the position at time $n \Delta t$ is approximated as $(\lambda n, \varphi n, rn) \approx (\lambda\ (n \Delta t), \phi\ (n \Delta t), r\ (n \Delta t)$.

In solving the Eq. (A II・2) using a computer, we must decide the flow field

$(\frac{u(\lambda^n, \varphi^n, r^n)}{r^n \cos \varphi^n}, \frac{v(\lambda^n, \varphi^n, r^n)}{r^n}, w^n)$

Since the flow field given by Arctic Sea Box Model is defined only at discrete positions, flow field at an arbitrary position needs to be

obtained by interpolation.

2. Interpolation of Flow Rate

Processes in the particle tracking program "stm. f" are as follows:

1) Dimensions of the left-and right-hand members of Eq. (A Ⅱ・1) are matched, that is to say, the flow field (u, v, w) is transformed into the flow field (u, v, w):

$$\dot{\lambda} = u, \ u = \frac{u}{r \cos \varphi},$$

$$\dot{\varphi} = v, \ v = \frac{v}{r}$$

$$\dot{r} = v, \ w = w, \quad\quad\quad\quad (\text{A Ⅱ・3})$$

in which the dimension of flow rate in the longitude latitudinal equations is angle per unit time.

2) Obtain the flow field (u, v, w) at an arbitrary position by means of multilinear interpolation (three − dimensional bilinear interpolation; see appendix "Basis of Interpolation").

Analysis of Seawater Circulation in the Whole Region of the Arctic Ocean

Akira Wada*, Tairyu Takano** and Minoru Ochiai*

Abstract : Research has been underway to clarify a situation resulting from the dumping of nuclear submarines into the local area (the Barents Sea and the Kara Sea) of the Arctic Ocean by the former Soviet Union. As the first step of research, the flow analysis in the local area (the Barents Sea and the Kara Sea) in the Arctic Ocean was studied. Using the observed data of water temperature and salinity, the flow was analyzed using a hybrid box model. The results obtained agreed with the observed features in many aspects (Wada and Ochiai, 2004). As the second step of research, the entire Arctic Ocean was studied (Regional model). A numerical hybrid box model was developed. The results obtained agreed with the observed features in many respects. Especially, stream flows in the Norwegian Sea, Barents Sea and Kara Sea showed fairly realistic features. The flow field in the surface layer in the central Arctic Ocean agreed with that in previously known data. In the intermediate and deep layers, there was a stream flow that agreed with the known cyclonic circulation. East of Greenland, a stream flow equivalent to the East Greenland Current was recognized.

Keywords : Arctic Ocean, Flow analysis, Hybrid box model, Regional model

1. Introduction

The Arctic Ocean receives warm and saline water from the Atlantic, while cold and fresh water exits the Arctic Ocean with East Greenland Current. The warm inflow of Atlantic water gives the major oceanic heat input for the Arctic Ocean. It influences the sea ice distribution and thickness. The saline water inflow influences the stratification and mixing processes in the interior of the Arctic Ocean. North Atlantic water enters the Arctic Ocean through two main pathways. Part of the Atlantic inflow takes a route through the Barents Sea. The remainder of the Atlantic water enters through Fram Straight as the West Spitzbergen Current (Gerdes & Schauer, 1997).

The most important connection of the Arctic Ocean with the rest of the World Ocean is

*Nihon University, College of Industrial Technology 1–2–1, Izumi, Narashino, Chiba 275–8575, Japan
**Laboratory of Aquatic Science Consultant Coorporation Kami-Ikedai 1–14–1, Ota-ku, Tokyo 145–0064, Japan

through the 2600m deep Fram Strait between Greenland and Svalbard. Shallower openings in the land belting the Arctic Ocean connect it to the Pacific and to the Atlantic through the Bering Strait and the Canada Archipelago, respectively (Figs. 1 and 2).

The Arctic Ocean has an area of $9.2 \times 10^6 \text{km}^2$ with a volume of $1.7 \times 10^7 \text{km}^3$ and it is semi-enclosed by land. Part of it is as deep as 4,000m. There are three major water masses, as described below. (IAEA report IASAP–7, 1998, Coachman and Aagaard, 1981)

i. Arctic surface-layer water: This water mass exists up to a depth of 200m from the surface, and both temperature and salinity undergo remarkable changes depending on the ice cover.

ii. Atlantic water: The warm and salty Atlantic layer extends below the pycnocline down to depths of 800–900m and is characterized by a mid-depth temperature maximum ranging between 0.5℃ and 4℃, and salinity is around 35 psu. This water mass is generated from the North Atlantic waters inflowing through the Fram Strait
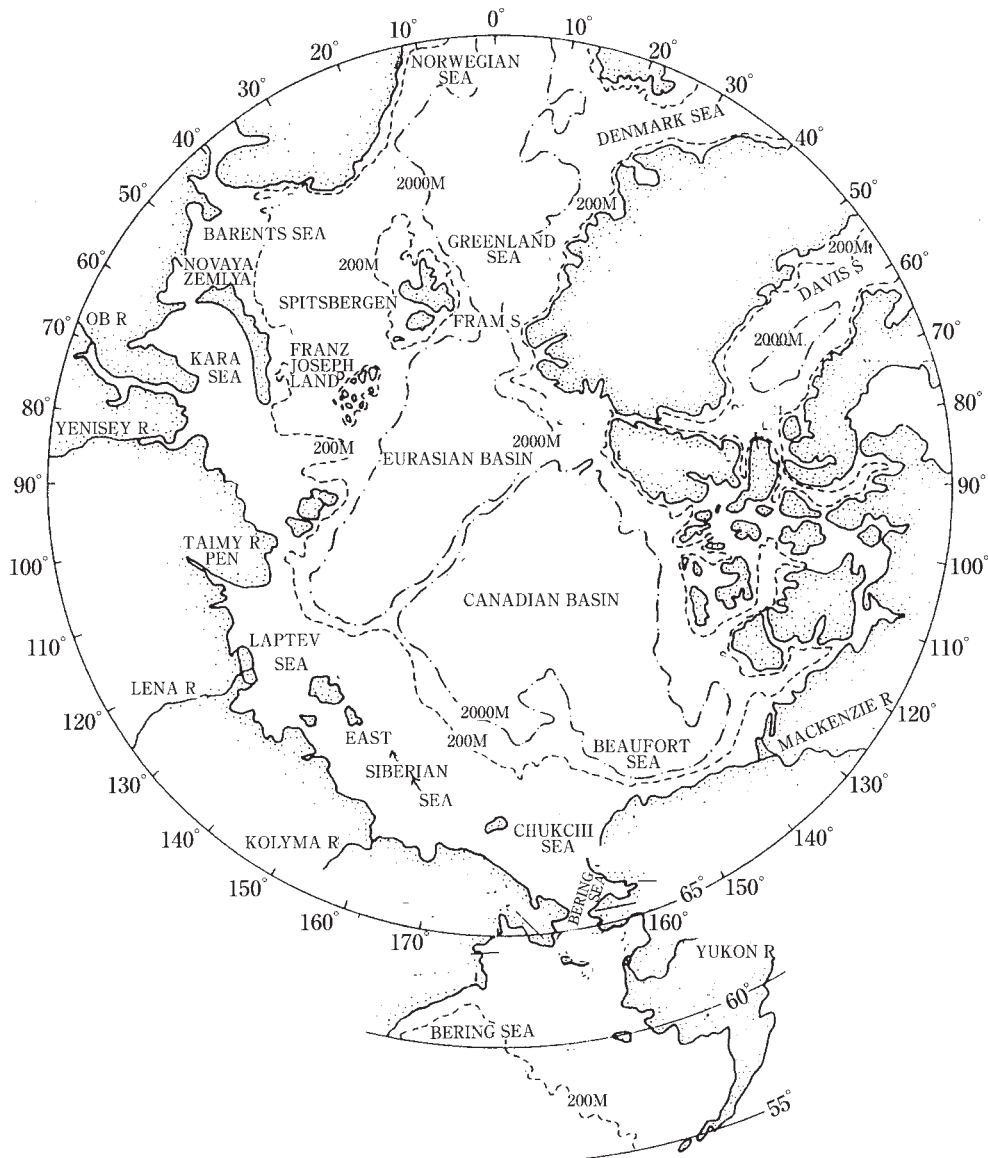
Fig. 1.   Basins of the Arctic Ocean (Smith and Grebmeier, 1990).

and over the Barents and Kara Sea shelves.
iii. Arctic deep-layer water: This water mass,
      extending below the Atlantic layer to the
      bottom of the ocean, has relatively high
      and uniform salinity (34.93 to 34.99 psu)
      and temperature (-0.8°C -0.4°C).

The water of the Arctic Ocean is balanced by
flows which pass through the Bering Strait
and the Norwegian Sea, by precipitation and

river run off and by outflow to the Barents and
Greenland Seas and through the Canadian Arc-
tic archipelago. The relative contributions of
the thermohaline and wind-driven circulation
to the Arctic flow are not yet clear.

The idea of "thermohaline" circulation as-
sumed that water exchange between the Arctic
Ocean and the Greenland and Norwegian Seas
was caused by differences in water temperature

and salinity between these basins. This idea is believed that the Arctic Ocean circulation was mainly thermohaline driven.

In contrast to the "thermohaline" idea, some scientists insisted that the inflow of Atlantic water into the Arctic Basin was caused by wind-forced outflow of surface water to the Greenland Sea. A series of 2-D numerical model results showed that wind were the major factor driving the Arctic Ocean circulation. Recently, 3-D coupled ice-ocean models were presented by some researchers. All of these models were directed to developing new models and describing better observed features of water and ice dynamics. WALSH and CHAPMAN (1996), SERREZE et al. (1992) and other scientists showed that the sea ice drift was done by the action of the atmosphere.

On the other hand, HOLLAND et al. (1996) demonstrated that buoyancy forcing is critical to maintain the mixed-layer circulation. It is considered that both thermohaline and wind-driven forcing are important to the Arctic Ocean's circulation (PROSHUTINSKY and JOHNSON, 1997). At the present stage, there is insufficient information for clearly separating the roles of atmospheric and thermohaline forcing in the Arctic Ocean.

The purpose of this study consists in analyzing flow characteristics of the whole area of Arctic Sea, in order to evaluate environmental effects of dumping radioactive wastes in this sea. For analyzing diffusion of radionuclides in the sea and for evaluating radiation exposure dosage of the inhabitants, it is necessary to know water circulation of the sea area. As the first step of the study, we conducted flow analysis employing the hybrid box model, by dividing specified areas of Barents Sea and Kara Sea into boxes of 4° by 1° horizontally and 6 layers vertically. Obtained results of the analyses proved to be in good agreement with established flow patterns so far reported (WADA and OCHIAI, 2004). In the second stage of the study, we took the whole region of Arctic Sea as an object area, dividing into horizontal boxes as shown in Fig. 2 and 5 layers in the vertical direction. We adopted the hybrid box model as used in the first step. The model used in this paper is an approach for applying conservation of mass with high accuracy not only in each calculation box but also over the whole system. This model is named a hybrid box model, intermediate between the box model and the hydrodynamic model. The method developed in this report has been developed to cover the regional field (Arctic Ocean).

2. Method of analysis

In this research, the method of analysis based on the box (compartment) model was used. The objective of this model is to determine a exchange flow rate that can reproduce the water temperature and salinity observed in each box by creating the equations of preservation for seawater, salinity and heat balance for every box. As the second step following the first step of research, the entire Arctic Ocean was studied, using horizontal boxes of 222×222 km which varied with locations on the spherical coordinate system, which were divided vertically into 5 layers (0–50m, 50–100m, 100–200m, 200–500m and 500–4250m). (Regional model, Fig. 2)

The upper 4 layers in both models (the first and the second steps) have the same layer thickness. The annual mean horizontal and vertical exchange flow rates in a total of 892 compartments were calculated to examine the movement of seawater.

Data used are:

(1) Water temperature and salinity

The data shown in the Climatological Atlas of the World Ocean (Levitus, 1982) relate to annual mean and seasonal mean fields. Of these data, flow analyses were conducted using the annual mean field. It is because flow calculations used in assessing exposure dose rates are based on the results of flow calculations using annual mean data from the viewpoint of the character of assessment.

(2) Topography

Topography is based on the ETOPO5 Data (NOAA, 1988) which are given in 5'grids.

(3) River flow rate (See Fig. 2)

From the mean flow curves shown in the monthly continental flow data (PAVLOV et al., 1993), months corresponding to the seasonal classification of water temperature and salinity are taken out and integrated.

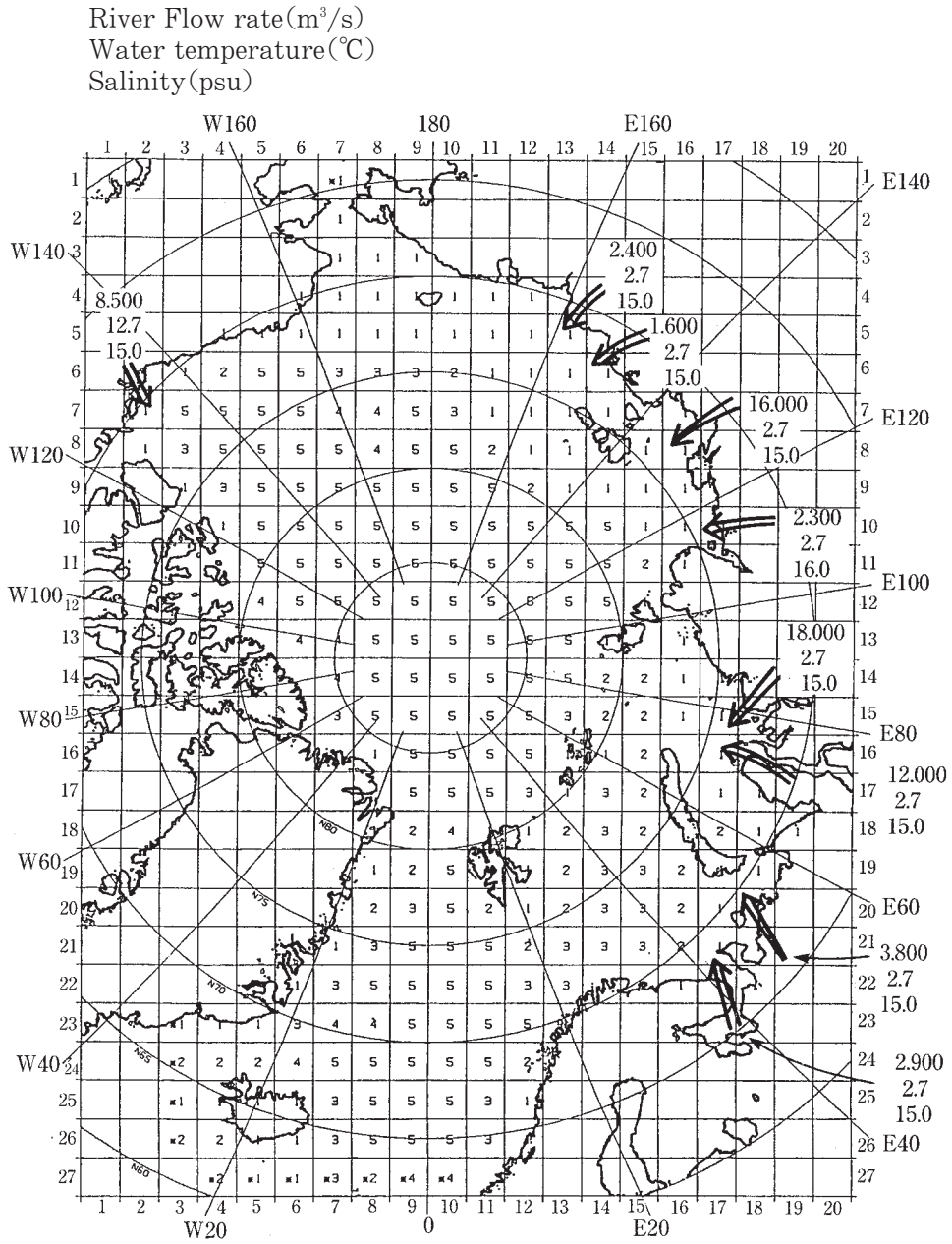River Flow rate(m³/s)
Water temperature(℃)
Salinity(psu)

Fig. 2.　Division of grids, the number of layers and river inflow positions in the Arctic Ocean.

3. Results of flow analysis in the whole Arctic Ocean

Let us now compare the results of flow analyses in the Arctic Ocean with available data (mainly surface flows).

Fig. 3 shows well-known observed flow patterns in the Arctic Ocean (PICKARD and EMERY, 1990). The circulation of the surface waters of the Arctic Ocean is increasingly well understood based on studies of sea-ice drift. The
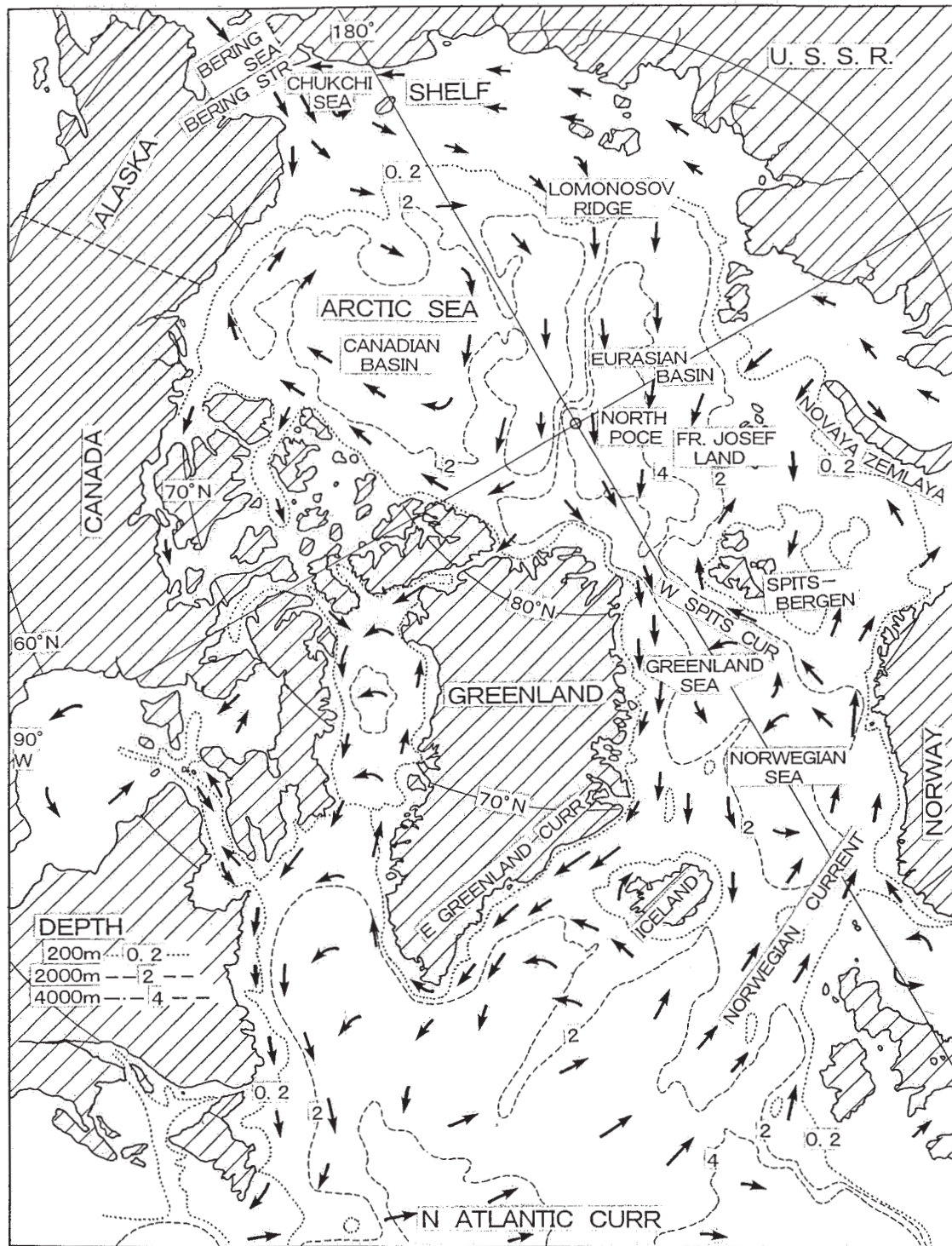
Fig. 3. Observed flow patterns in the Arctic Ocean (PICKARD and EMERY, 1990).
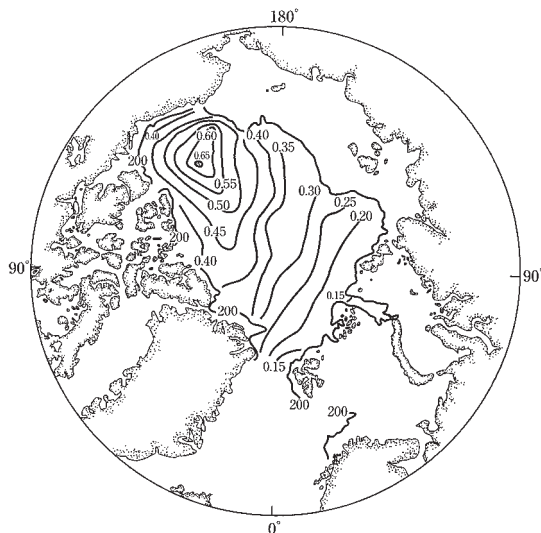
Fig. 4.   Surface currents in the Arctic Ocean (0/1200
      dbar) based on COACHMAN and AAGAARD (1974).

prominent long-term features of the Arctic ice
drift are the anticyclonic Beaufort Gyre occu-
pying most of the Canadian Basin and the
Transpolar Drift Stream flowing from the pole
toward Fram Strait (Figs. 3 and 4). Here, the
authors examine the velocity field at different
depths in the model.

Results are shown in Figs. 5 through Figs. 6
(1), (2) and (3). Fig. 5 shows five lines illus-
trating the vertical behavior of water particles.
Figs. 6 (1), (2) and (3) show horizontal veloc-
ity vectors in each layer. Fig. 7 shows sche-
matic diagram of flows in the vertical direction
along five lines shown in Fig. 5.
(1) Norwegian Sea and Greenland Sea

Fig.8 shows schematic of mean ocean circula-
tion in the Fram Strait portion of the Green-
land Sea (MUENCH et al., 1992, WALKER et al.,
1995). Two main currents exchange water be-
tween the Arctic and the outer ocean through
Fram Strait. The west Spitzbergen Current
(WSC) is a northward-flowing extension of the
Norwegian-Atlantic current. It flows through
Fram Strait off the west coast of Spitzbergen,
carrying warm, relatively salty water into the
Arctic Ocean. The East Greenland Current
(EGC), which lies west of the East Greenland
Polar Front, is the main current out of the Arc-
tic Ocean.

The Fram Strait region appears to be a

region of pronounced recirculation of Atlantic
water, much of it joining the southward-
moving East Greenland Current to flow-back
into Greenland (MUENCH et al., 1992, WALKER
et al., 1995, GASCARD et al., 1995)

According to the results of tracking (WADA
and OCHIAI, 2004), shown in Figs. 6 (1), (2),
(3) and 9, it is illustrated that a seawater parti-
cle in the Norwegian Sea (in the first layer) en-
ters the Barents Sea, where it circulates
anticlockwise, and that it submerges to the sec-
ond layer in the south of Spitzbergen. Then the
particle goes northward in the West
Spitzbergen Current (WSC), and turns to the
south by the East Greenland Current (EGC)
flowing southward. The particle flows further
toward the North Atlantic Ocean, moving to
the third layer. These behaviors of seawater
particle agree with the observed data (WADA
and OCHIAI, 2004, HUNKINS, 1990).

In Fig. 10, a seawater particle deposited at
the surface near the North Pole moves to the
second layer as it passes between Franz-Josef
Land and Novaya Zemlya Island, and abruptly
turns toward the west. As in the case of Fig. 7,
it then moves to the third layer and flows
southward.

Vertical movements of water particles occur
mainly between the first and third layers. Line
(1–1') in Fig. 7 clarifies the behavior of
seawater particles in the vertical direction.

- In the second and third layers (50–200m
  deep), the water mass which has come up
  north from the southern Norwegian Sea
  and part of the water mass which has come
  out of the Barents Sea pass through the
  circulating current zone and enter the Arc-
  tic Ocean from west of Spitzbergen (Figs.
  6 (2) and (3)).
- The North Atlantic water settles in the cir-
  culating current zone southwest of Spitz-
  bergen and enters the Arctic Ocean
  through the middle and deep layers as
  shown in Figs. 6 (1), (2), Fig.7 and Fig. 9,
  thus agreeing closely with the observed
  data as shown in Fig. 8.
- Circulation in the Fram Strait is repre-
  sented schematically in Fig. 8 which are de-
  scribed by GASCARD et al (1995),
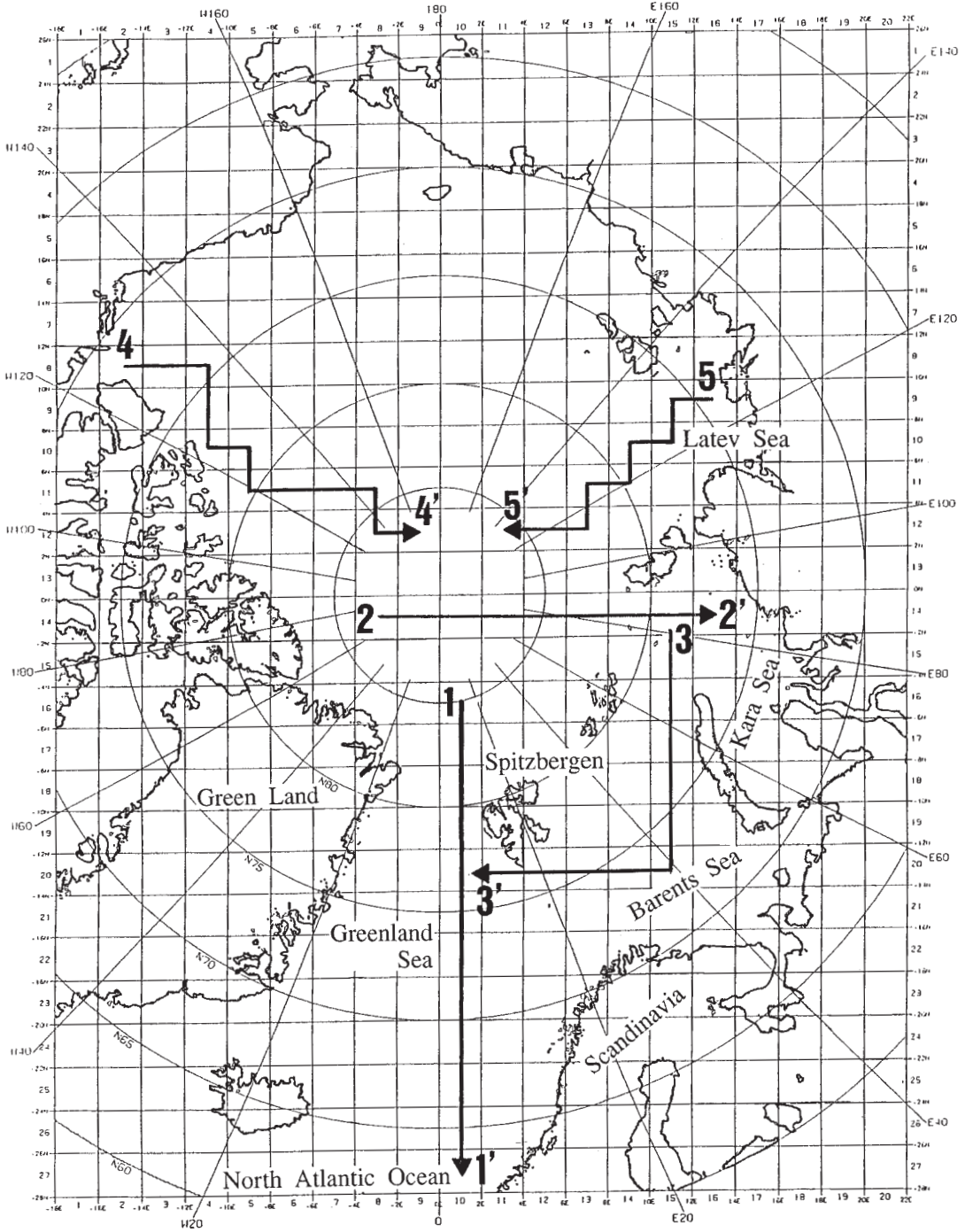 HUNKINS (1990), PAQUETTE et al. (1985),

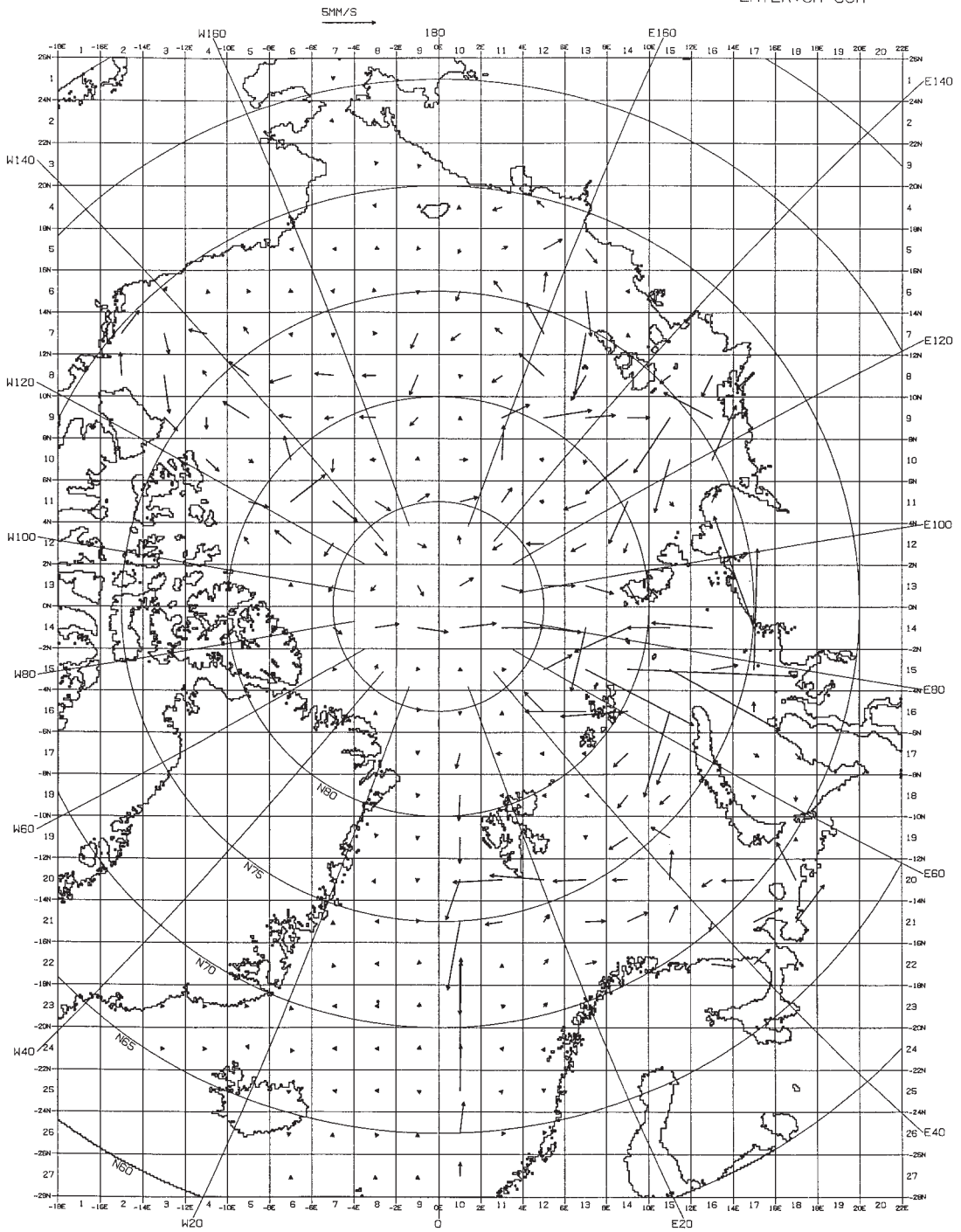Fig. 5.   Five measuring lines for studying the flow patterns.

LAYER:0M-50M

Fig. 6. (1) Velocity vectors in the surface layer (0–50m).

LAYER:50M-100M
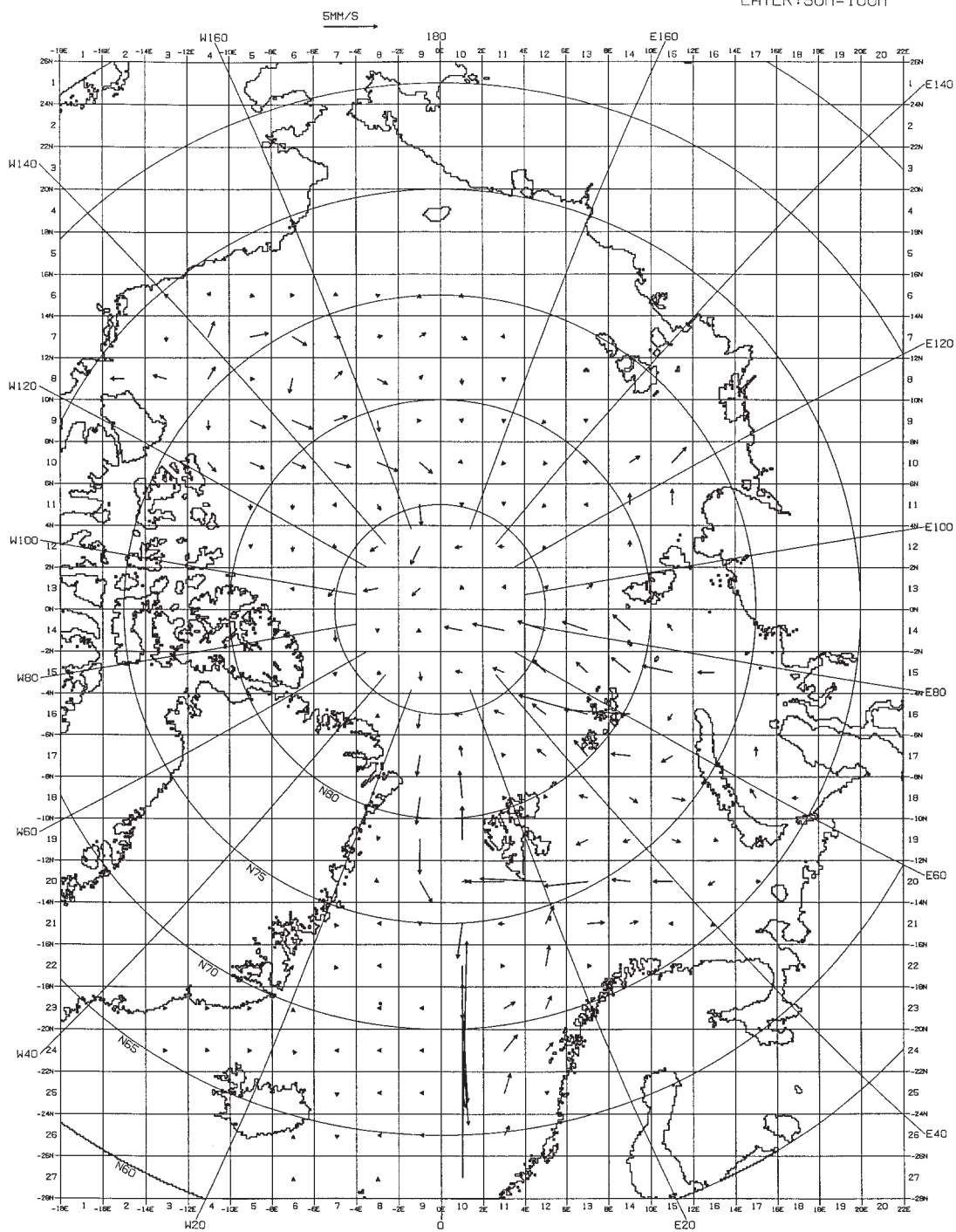
5MM/S

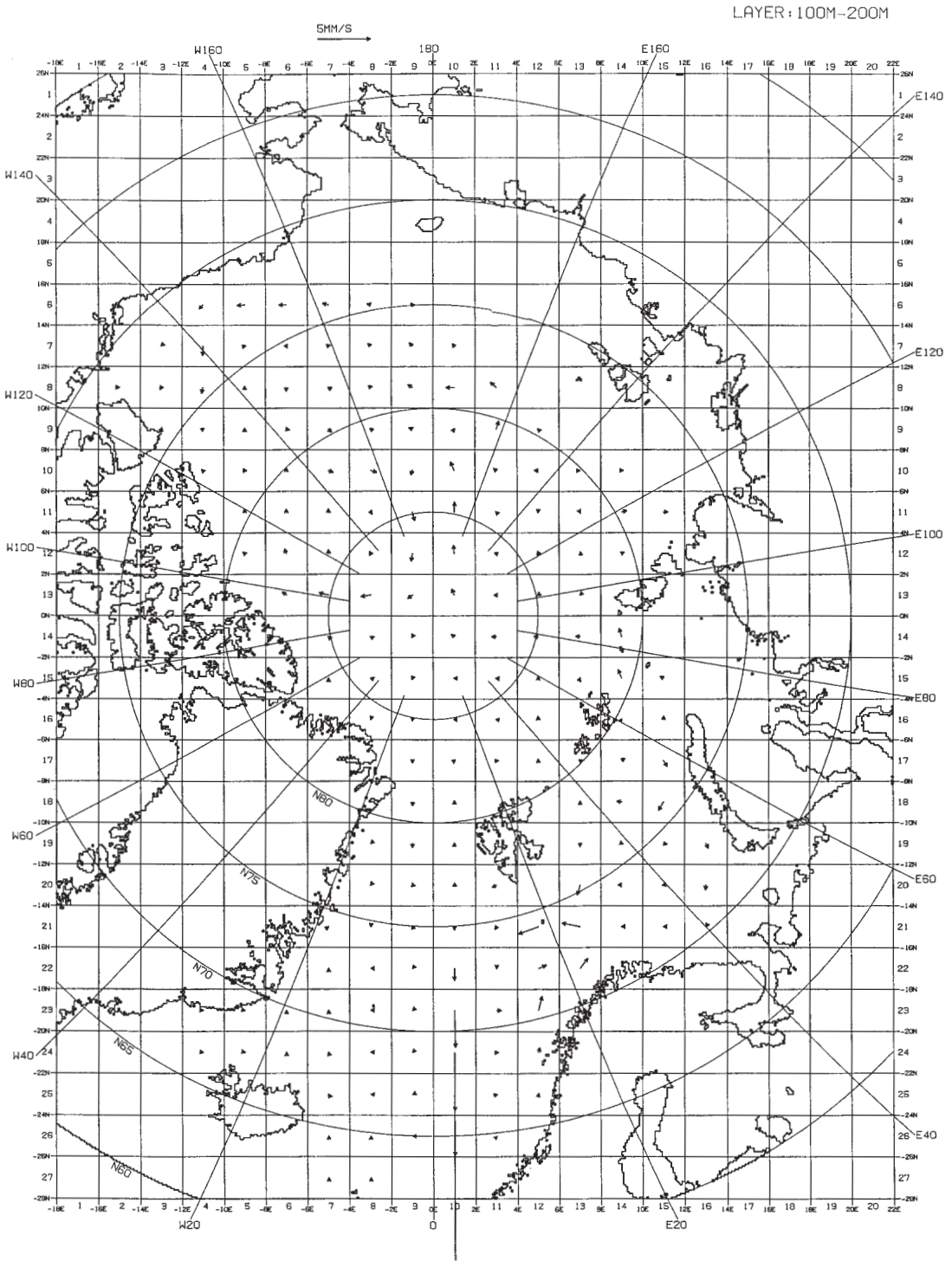Fig. 6. (2) Velocity vectors in the second layer (50–100m).

LAYER：100M−200M

5MM/S

Fig. 6. （3）　Velocity vectors in the third layer （100–200m）.

Line (1—1')

Line (2—2')
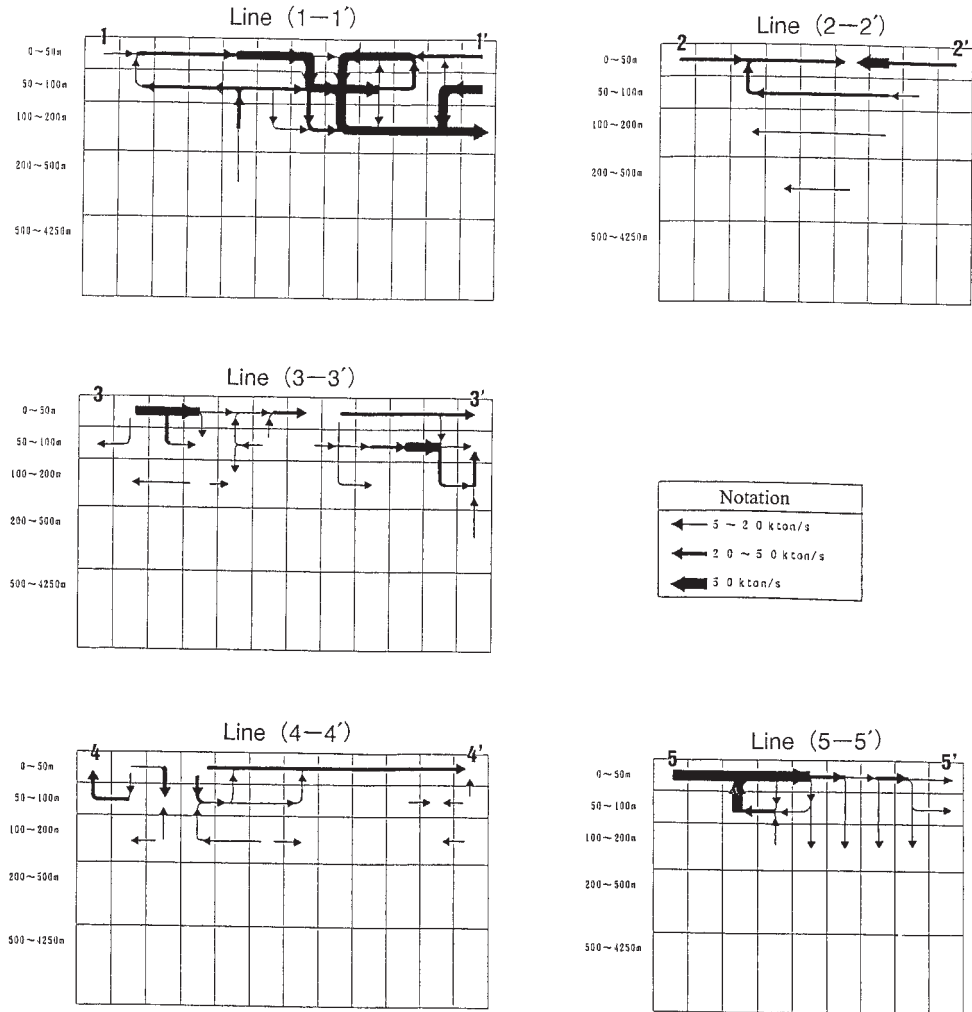
Line (3—3')

Notation

Line (4—4')

Line (5—5')

Fig. 7.   Schematic diagram of vertical flows in the Arctic Ocean.

based on measurement. The model results shown in Figs. 6 (1), (2) and Fig. 9 resembles the situation of Fig. 8.

− The results of analysis given above confirm our assumption that density differences between the fresher Arctic Ocean and the more saline Atlantic Ocean waters are considered to be the primary driving force.

(2) Bering Strait exchange (Figs. 3 and 6 (1))
The northward flow through the shallow and narrow Bering Strait connects the Pacific (Bering Sea) and Arctic (Chukchi Sea) oceans. COACHMAN and AAGAARD (1981) note that the flow through Bering Strait is driven by a mean sea level slope of order 10^{-6} down toward the north, due to an effect related to the lower density of the Pacific relative to the Atlantic.

(3) Barents Sea and Kara Sea (Figs. 6 (1), (2) and 9)

− In the Barents Sea, the water mass which has come out of the Norwegian Sea joins the water mass coming out of the Kara Sea and the water coming out of the Pechora River while circulating counterclockwise in the central part of the Barents Sea, and flows westward to the south of Spitzbergen.
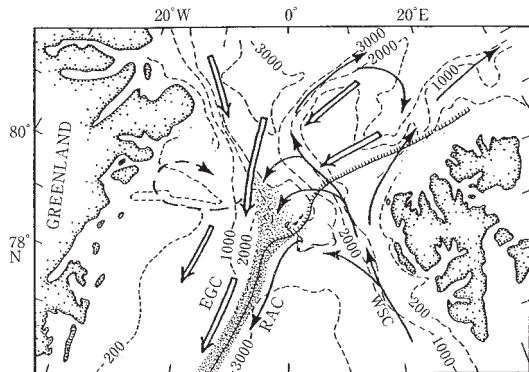
Fig. 8. Schematic of mean ocean circulation in the Fram Strait portion of the Greenland Sea. Hollow arrows depict flow of cold Polar Water, and solid arrows depict flow of warmer Atlantic Water. In areas where both water types occur, the Atlantic Water lies beneath the Polar Water. The hachured line indicates a typical summer ice edge location. The East Greenland Polar Front is indicated by the stippled region.

Major currents are labeled as follows: WSC, West Spitsbergen Current; EGC, East Greenland Current; and RAC, Return Atlantic Current. Dushed lines are isobaths, with depths in meters.

─This current agrees closely with the observed data (Fig. 3, Figs. 8 and 10, WADA and OCHIAI, 2004), though there is some difference in position.

─In the western Kara Sea, the water mass which has come eastward from the polar point joins the water mass from the Kara Sea (fresh water mass from the Yenisey River and Ob River) and flows southward to the Barents Sea.

(4) Arctic Ocean

─In the surface layer of the Arctic Ocean, we tracked the particle injected on the 1st layer near the Laptev Sea.

Result of the particle track is shown in Fig. 10. The particle drifted in a clockwise circulation, gradually moving to the 2nd and 3rd layers. In the Canadian Basin, it entered a small-scale clockwise circulation, and returning to the 1st layer, moved towards the central part of the Arctic Sea.

─In the second and third layers, part of the water mass which has entered from the Norwegian Sea circulates cyclonically in the Arctic Ocean, the opposite direction to

that of the Arctic water above it. It closely agrees with the circulation route (estimated) of the North Atlantic Ocean water in the intermediate and deep layers of the Arctic Ocean (SCHLOSSER et al. 1995, GERDES and SCHAUER 1997).

Due to the paucity of high-quality deep data, the sense of circulation in the deep layers is not well established. AAGAARD and CARMACK (1989) and SMETHIE et al. (1988) deduced from mooring and tracer data a cyclonic flow around the Eurasian basin.

─After circulating in the Arctic Ocean, water enters the Norwegian Sea again from the northeast coast of Greenland, which agrees with the observed data (PICKARD and EMERY 1990).

4. Consistency with the local model (Kara Sea, Barents Sea)

The authors compared the results of flow analyses with the local model (WADA and OCHIAI, 2004) and the results obtained with the regional model. Both models agree that Atlantic Ocean water enters the Barents Sea along the Norwegian Peninsula, circulates counterclockwise in the Barents Sea and enters the Arctic Ocean and Norwegian seas again. Both models reproduce the current which enters from the Arctic Ocean and the current which flows into the Barents Sea between Franz-Josef and Novaya Zemlya. The consistency between the two models is high.

5. Estimation of Errors

As we research for flows which reproduce the distribution of salinity and temperature in each box, errors in salinity and heat amount could be neglected. As for flow, we calculated errors of the conservation equation of seawater for each box. Errors of flow were evaluated both by the absolute error which is the difference of in- and outflows and the relative error which is the difference divided by the inflow. Table 1 shows coordinates in which the maximum error occurs (See Fig. 2), residual errors by the least square method, and the maximum value of relative error (residue/inflow) and coordinates.
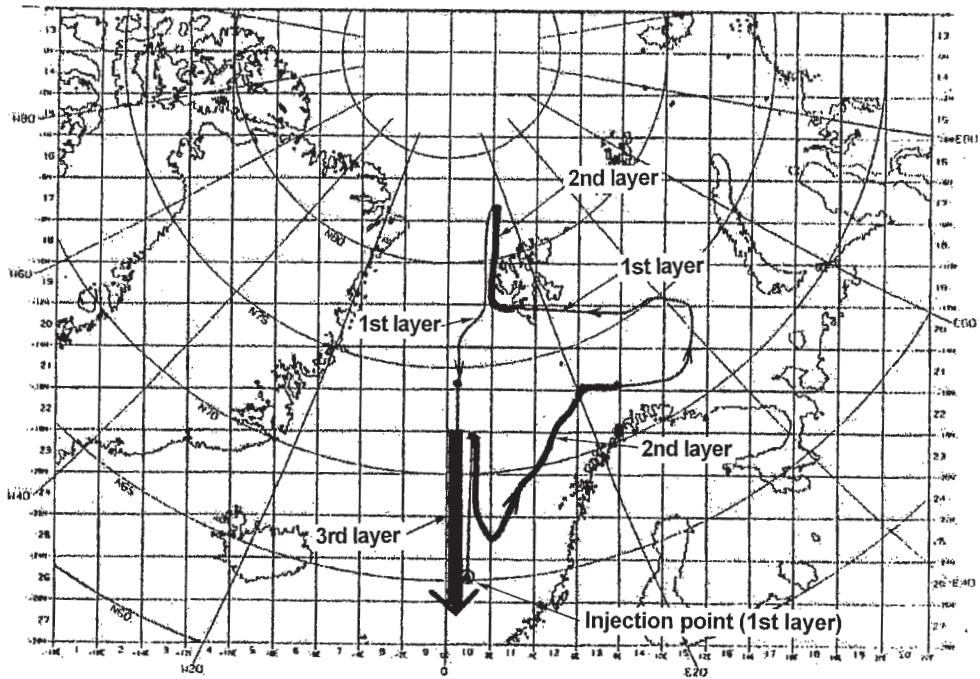
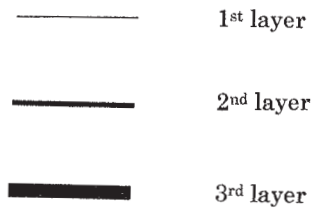Fig. 9. Tracking of seawater particle in the Greenland Sea.

————————— 1ˢᵗ layer

———————— 2ⁿᵈ layer

———————— 3ʳᵈ layer

Table 1. Errors of conservation of seawater volume.

	Coordinates	Absolute error	Relative error
1st layer (0−50m)	(17, 16)	-9×10^{-5} (kton/s)	2×10^{-7}
2nd layer (50−100m)	(10, 20)	6×10^{-5} (kton/s)	2×10^{-7}
3rd layer (100−200m)	(10, 20)	-8×10^{-6} (kton/s)	4×10^{-7}
4th layer (200−500m)	(10, 20)	8×10^{-6} (kton/s)	3×10^{-7}
5th layer (500−900m)	(11, 14)	-8×10^{-6} (kton/s)	1×10^{-7}

The values above indicate the errors of the boxes which showed the largest error in each layer.
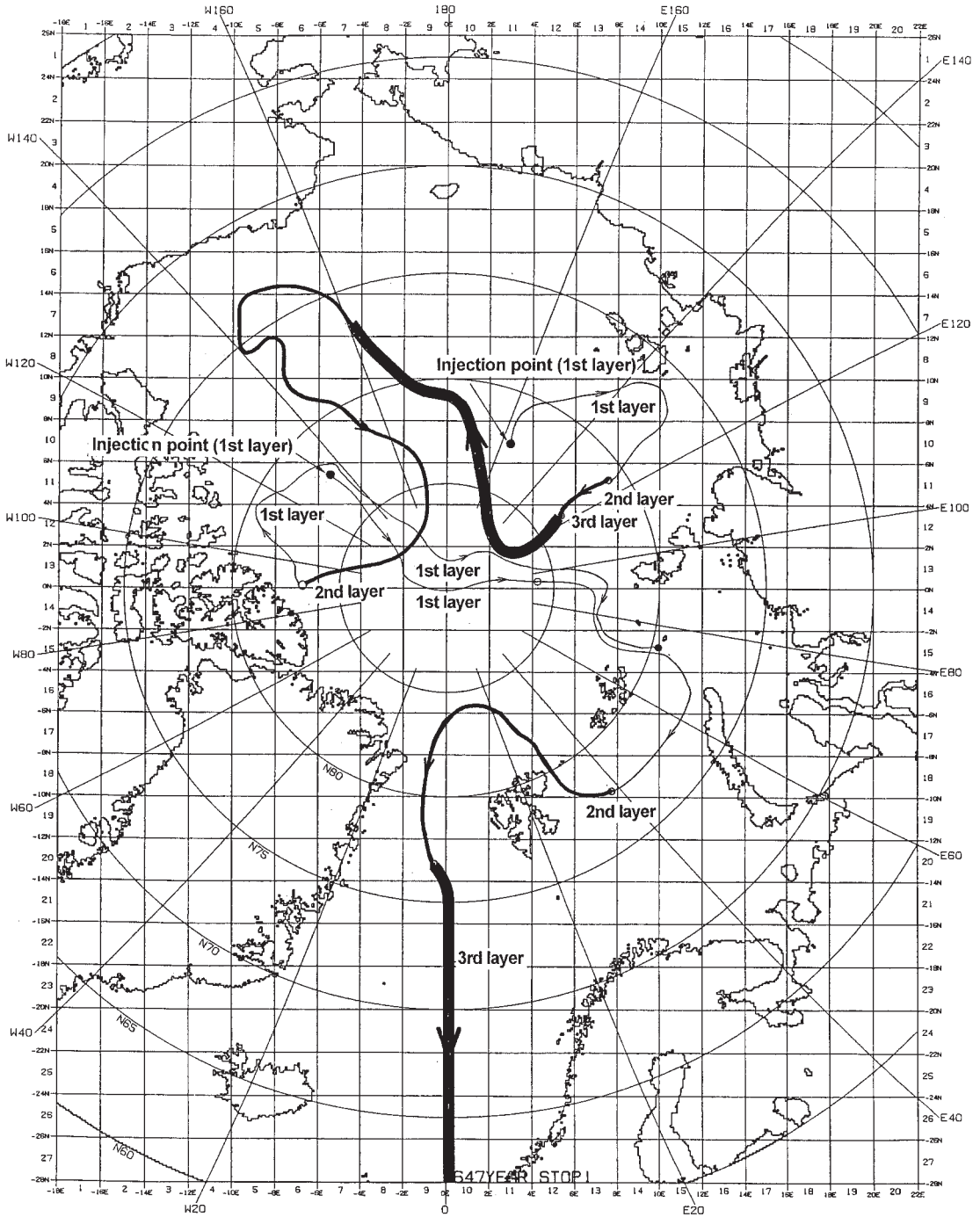
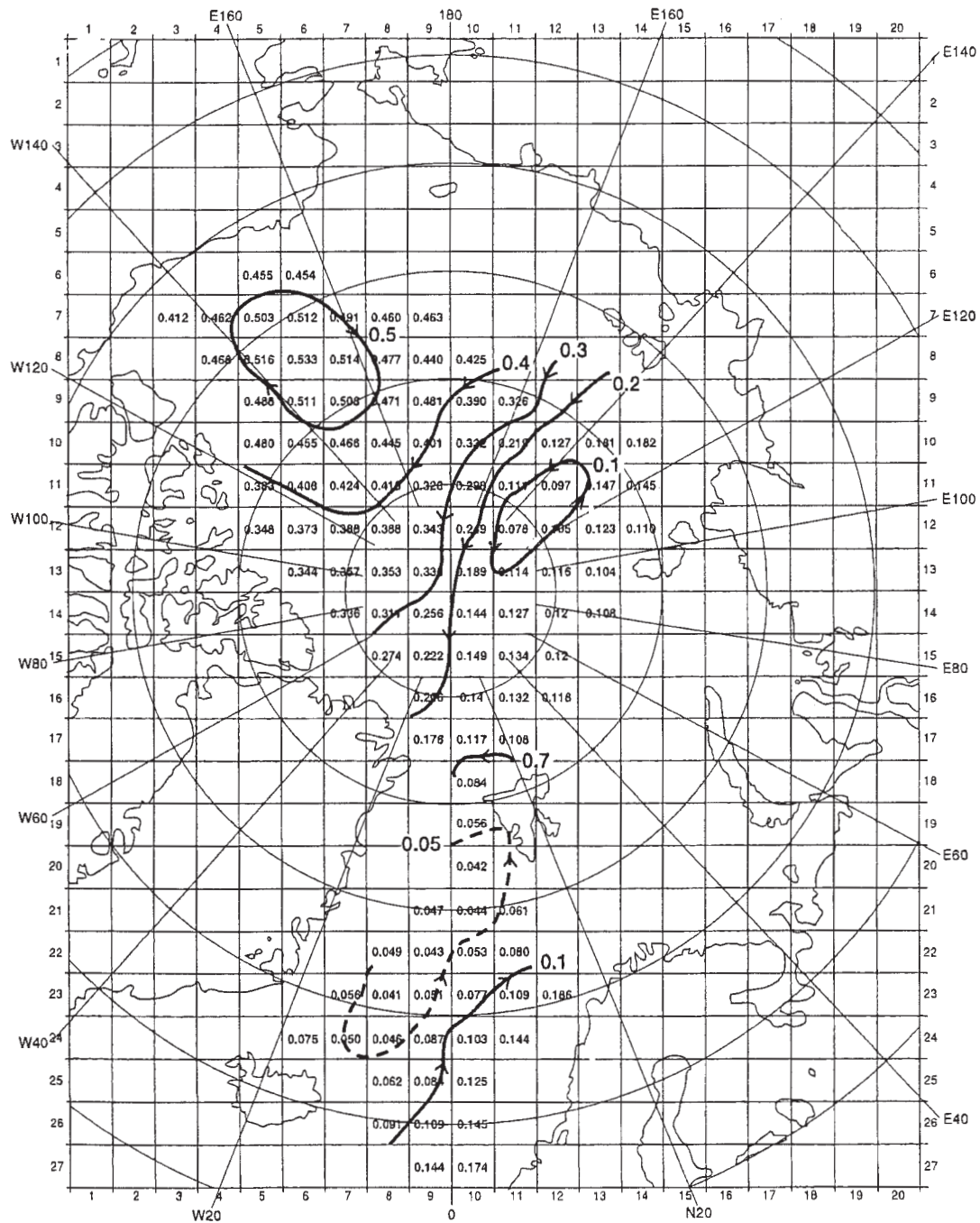Fig. 10.   Tracking of water particle in the whole Arctic Ocean.

Fig. 11. Dynamic depth anomaly in the Arctic Ocean (Unit: Dynamic meter $\times 10^{-2}$).

6. Comparison with geostrophic flow field

In this section, we calculated the surface dynamic height from the density flow in the whole Arctic Sea, and compare the result with that obtained by the hybrid box model which is illustrated in Fig. 6 (1), (2) and (3). In the present calculation, the level of no motion is assumed to be at 350m depth based on the results of the hybrid box model. Fig. 11 shows the obtained dynamic topography. Main features of the calculated result are:

· A clockwise circulating current exists with a center at 150° W, 76° N.

· A small-scale anti-clockwise circulation exists with a center at 140° E, 84° N.

· There exists a current that starts from the coast of Russia and passing through the North Pole, reaches near the coasts of Greenland and Canada.

From comparison of Fig. 10 and Fig. 11, it is noticed that although size of the clockwise circulation in the Canadian Basin is similar in the both cases, direction of the circulation off the Laptiv Sea is opposite. The current from the North Pole to Norwegian Basin is similar in the both cases.

7. Conclusions

A numerical hybrid box model was developed. The results reproduced many of the observed features such as the currents described below.

Particularly, stream flows in the Norwegian Sea, Barents Sea and Kara Sea agree closely with the observed data. The flow field in the surface layer of the Arctic Ocean agrees with the observed data. We could reproduce stream flows such as the West Spitzbergen Current (WSC) and the East Greenland Current (EGC) in the Fram Strait which showed a very complex flow structures.

The method of analysis used in this research was aimed at determining the flow field on the basis of observational data such as water temperature and salinity. Therefore, the importance of this data is unfathomable. Most notably regarding the Arctic Ocean, the availability of oceanographical data is very limited in comparison with other seas, so that further accumulation of data is required.

References

AAGAARD, K. and E. C. CARMACK (1989): The role of sea ice and other fresh water in the Arctic circulation. J. of Geophys. Res., **94** (C10), 14485–14498.

COACHMAN, L. K. and K. AAGAARD (1974): Physical oceanography of Arctic and subarctic seas, in Marine Geology and Oceanography of the Arctic Seas, pp. 1–72, Springer-Verlag, Berlin.

COACHMAN, L. K. and K. AAGAARD (1981): Reevaluation of water-transports in the vicinity of Bering Strait, Oceanography and Resources, Vol. 1, 95–110, Univ. of Washington Press, Seatle.

GASCARD, J. C., C. RICHEZ and C. ROUAULT (1995): New Insight on Large–Scale Oceanography in Fram Strait: The West spitzbergen Current. Coastal and Estuarine Studies, **49**: 131–182, American Geophysical Union.

GERDES, R. and U. SCHAUER (1997): Large–scale circulation and water mass distribution in the Arctic Ocean from model results and observations. J. of Geophys. Res., **102**, 8467–8483.

HOLLAND, D. M. L., L. A. MYSAK and J. M. OBERHUBER (1996): Simulation of the mixed-layer circulation in the Arctic Ocean. J. Geophys, Res., **101**, 1111–1128.

HUNKINS, K. (1990): A review of the physical oceanography of Fram Strait. *In* The physical Oceano=graphy of Sea Straits, I. J. Pratt(ed), Kluwer, 61–94.

International Atomic Energy Agency (1998): Radiological Conditions of the Western Kara Sea, Report on the International Arctic Seas Assessment Project (IASAP).

LEVITUS, S. (1982): Climatological Atlas of the World

Ocean, NOAA Professional Paper 13, National Oceanic and Atmospheric Administration, U. S. Department of Commerce.

MUENCH, R. H., M. G. MCPHEE, C. A. PAULSON and J. H. MORISON (1992): Winter oceanographic conditions in the Fram Strait–Yermak Plateau region, J. Geophys. Res., **97**, (C3): 3469–3484.

NOAA, National Geophysical Data Center (1988): ETOPO5 5-minute gridded elevation data, National Oceanic and Atmospheric Administration.

PAQUETTE, R., R. BOURKE, J. NEWTON and W. PERDUE (1985): The East Greenland Polar Front in autumn. J. of Geophys. Res., **90** (C3): 4866–4882.

PAVLOV, V. K., M. Yu. KULAKOV and V. V. STANOVOY (1993): Oceanographical description of the Kara and Barents Sea, Report to the International Arctic Seas Assessment Program, IAEA working material, Vienna, Contractual Service Agreement between IAEA and V. K. PAVLOV, St. Petersburg.

PICKARD, G. L. and W. J. EMERY (1990): Descriptive Physical Oceanography, An Introduction. 5th Edition, Pergamon. 214–216, 320pp.

PROSHUTINSKY, A. Y. and M. A. JOHNSON (1997): Two circulation regimes of the wind-driven Arctic Ocean, J. Geophys. Res., **102**, 12493–12514.

SCHLOSSER, P., J. H. SWIFT, D. LEWIS and S.L. PFIRMAN (1995): The role of the large-scale Arctic Ocean circulation in the transport of contaminants. Deep–Sea Res., **42** (6): 1341–1367.

SERREZE, M. C., J. A. MASLANIK, R. G. BARRY and T. L. DEMARIA (1992): Winter atmospheric circulation in the Arctic Basin and possible relationships to the Great Salinity Anomaly in the northern North Atrantic, Geophys. Res. Lett., **19** (3), 293–296.

SMETHIE, W. M. Jr, D. W. CHIPMAN, J.H. SWIFT and K. F. KOLTERMANM (1988): Chlorofluoromethanes in the Arctic Mediterranean seas, Deep–Sea Research. **35**, 347–369.

WADA, A. and M. OCHIAI (2004): Flow Analysis of the Arctic Ocean (the Kara Sea and the Barents Sea) by a Hybrid Box Model, La mer, **41**, 137–154.

WALKER O. SMITH, Jr. (1990): Polar Oceanography, Part A, Physical Science, XV, Academic Press, San Diego, 409pp..

WALKER O. SMITH, Jr. and JACQUELINE M. GREBMEIER (1995): Arctic Oceanography: Marginal Ice Zones and Continental Shelves, Coastal and Estuarine Studies, American Geophysical Union, 131–135, 287pp..

WALSH, J. E., and W. L. CHAPMAN (1996): Arctic contribution to upper-ocean variability in the North Atlantic, J. Clim, **3** (12), 1462–1473.

An Observation on the Cyclonic Eddy in the Coastal Side of the Non-large Meander Path of the Kuroshio

Yoshihiko SEKINE[*] and Shunsuke TANAKA[*†]

Abstract : A weak cyclonic eddy exists in the coastal side of the non-large meander path of the Kuroshio south of Japan, while a large cyclonic eddy with a large cold water mass is accompanied by the large meander path of the Kuroshio. The CTD and ADCP observations were carried out in August 1999 and we observed a western part of the cyclonic eddy to the east of Kii Peninsula in non-large meander path of the Kuroshio. Main results of the observation are presented in this paper. It is shown that various horizontal intrusions of the less saline water with different potential density (σ_θ) are occurring in the salinity minimum layer. Less saline water accompanied by the cyclonic eddy in the coastal (northern) side of the main Kuroshio flow is relatively thin and covers a narrow range of σ_θ in the marginal area of the cyclonic eddy. Conversely, in the offshore (southern) side of the main Kuroshio flow, the horizontal intrusion of North Pacific Intermediate Water (NPIW) is thick and covers a wider range of σ_θ. The origin of the less saline water accompanied by the cyclonic eddy on the coastal side of the main Kuroshio flow is discussed.

Keywords : *Cyclonic eddy, Intermediate Oyashio Water, Salinity minimum layer*

1. Introduction

The Kuroshio south of Japan has bimodal path characteristics and a larger cyclonic eddy with a large cold water mass is formed in periods of large meander path (SHOJI, 1972; TAFT, 1972; ISHII *et al.*, 1983), while a weak cyclonic eddy is also observed in periods of non-large meander path. It is well known that the salinity minimum layer also exists on both sides of the main flow of the Kuroshio (e.g., SEKINE *et al.*, 1991; YANG *et al.*, 1993a,b and SENJYU *et al.*, 1998), while salinity in its minimum layer is relatively high in the mean flow of the Kuroshio. Both dominant salinity minimum waters have a potential density (σ_θ) of 26.7–26.9.

YASUDA *et al.* (1996) pointed out that on the eastern side of the Izu Ridge, the North Pacific Intermediate Water (NPIW) of salinity less than 34.1 psu is formed by mixing of the Kuroshio Water and Oyashio Water to the east of 150° E and this spreads southwestward up to 25° N to form a salinity minimum layer in the subtropical circulation. SEKINE *et al.* (2000) showed that the southwestward flow of NPIW is influenced by the topographic effect of the Izu Ridge and a westward shift of NPIW over the Izu Ridge into the Shikoku Basin is confined to the south of 30° N at a depth deeper than 2000 m, which is schematically shown in Fig. 1.

The Intermediate Oyashio Water (IOW) originated from the Oyashio Water (OW) flows southward along the east coast of Honshu and then reaches Sagami Bay (YANG *et al.*, 1993a,b; SENJYU *et al.*, 1998). SEKINE and UCHIYAMA (2002) detected the outflow of IOW from Sagami Bay to the Shikoku Basin through a southeastern channel off the Izu Peninsula. They also showed that a part of IOW to the south of the Boso Peninsula flows southward along the eastern side of the Izu Ridge, then flows into the Shikoku Basin through the gate channel of the main Kuroshio

[*]Institute of Oceanography and Climate, Faculty of Bioresources, Mie University, 1515 Kamihama-chou, Tsu, Mie 514–8507 Japan.
[†]FUJISOFT ABC INC.
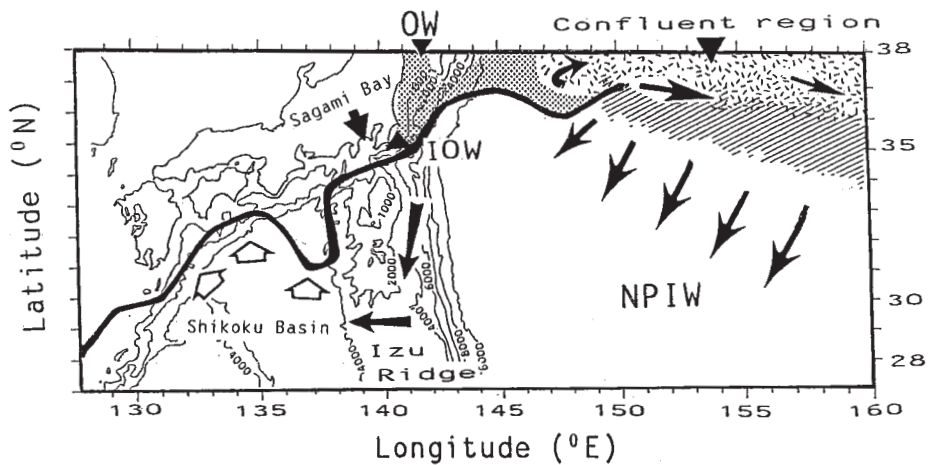4–38, Honmachi Naka-ku Yokohama, 231–0005, Japan

Fig. 1. Schematic view of the flow pattern of the NPIW formed by the mixing between the Kuroshio water and the Oyashio Water (OW) at the area with aslant lines (after, Sᴇᴋɪɴᴇ and Mɪʏᴀᴍᴏᴛᴏ, 2002). The NPIW moves southwestward shown by the slant arrows. Near the Izu Ridge, the NPIW is influenced by the topographic effect of the Izu Ridge (Sᴇᴋɪɴᴇ *et al.*, 2000) and further westward shift is possible to the south of 30° N, where depth of the Izu Ridge exceeds 2000 m. In the Shikoku Basin, the NPIW flows northward shown by the open arrows and essentially exists in the southern offshore side of the main Kuroshio axis. The OW flows along the Japanese Coast and ventilates to form the Intermediate Oyashio Water (IOW). The IOW reaches Sagami Bay, part of which flows out from Sagami Bay.

path over the Izu Ridge between Miyake-jima and Hachijo-jima islands. The schematic view of these results is also shown in Fig. 1.

Together with these observational evidences, it is inferred from Fig. 1 that two waters forming the salinity minimum layer are separated by the main Kuroshio flow. The NPIW is confined to the south of the main axis of the Kuroshio Extension (Rᴇɪᴅ, 1965 and Tᴀʟʟᴇʏ, 1993, Yᴀsᴜᴅᴀ *et al.*, 1996). Recently, Sᴇᴋɪɴᴇ and Mɪʏᴀᴍᴏᴛᴏ (2002) showed a similar tendency on the western side of the Izu Ridge with the exception of the horizontal intrusion across the main Kuroshio axis to the northern coastal area during the decay period of the small meander of the Kuroshio in May 1992.

Based on these observational results, the origin and distribution of the salinity minimum water on the northern coastal side of the Kuroshio main axis in the Shikoku Basin should be examined with particulars. Here it is noted that because no less saline coastal and bay waters have a potential density greater than 26.0 owing to the characteristics of less saline water (e.g., Sᴇᴋɪɴᴇ *et al.*, 1991), they can not be an origin of the salinity minimum water

on the coastal side of Kuroshio. In this context, we could observe a western part of the cyclonic eddy in the coastal side of the main Kuroshio flow during non-large meander path by use of training vessel "Seisui-Maru" of Mie University on 26–31 August 1999. Composite of the satellite imageries of thermal infrared by NOAA 12, 14 and 15 during the observation are shown in Fig. 2. A cyclonic eddy is located at the Enshu-nada and accompanied warm water of the Kuroshio approaches to the Kii Peninsula. Therefore, we presents the main results of the observation in this paper.

2. Observation

CTD (Neil Brown Mark IIIB) observations along the observational lines shown in Fig. 3 were made by use of the Training Vessel "Seisui-Maru" of Mie University during 26–31 August 1999. Five observational lines are set to observe the western part of the cyclonic eddy and its influence on the coastal area off Kii Peninsula. CTD observation began at Station 1 of Line 1 and ended at Station 16 of Line 5 along the continuous observational line shown Fig. 3.
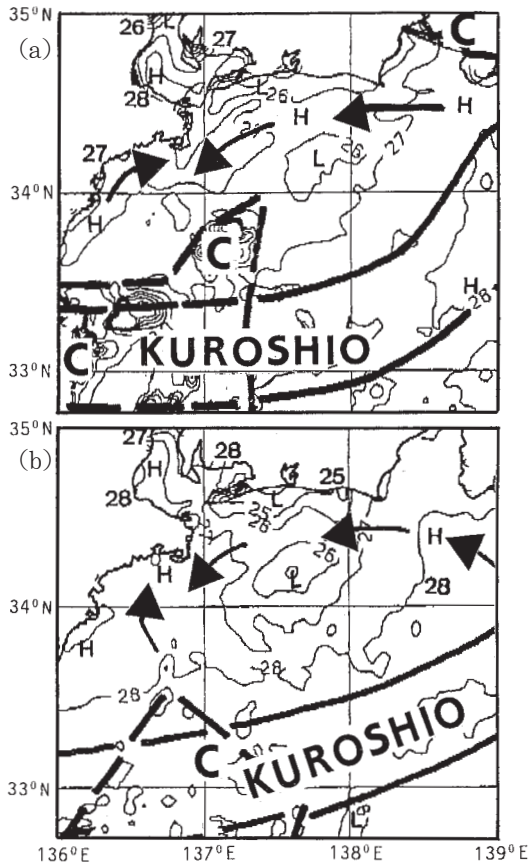
Fig. 2. SST (℃) shown by NOAA 12, 14 and 15
AVHRR composite on August 25 (after, Fisher-
ies Research Institute of Mie, 1999). (a) 2 images
composite from 3:15 to 6:03 (b) 3 images compos-
ite from 14:37 to 18:37. Arrows indicate direction
of the shift of the warm water, estimated by the
comparison of the sequential imagery map of
SST. C shows the cloud area. H and L show the
area with warmer and colder temperature, re-
spectively.

ADCP (CI–30 of Furuno Electric Inc.) obser-
vations at depths of 10 m, 50 m and 100 m were
also carried out along these observational lines.
Checks of the observed CTD data in comparison
with standard salinity water were carried out
at three observational points with about 10 lay-
ers and the worst-case accuracy of the observed
CTD data was found to be 0.02 psu.

3. Results

Observed ADCP velocities are shown in Fig.
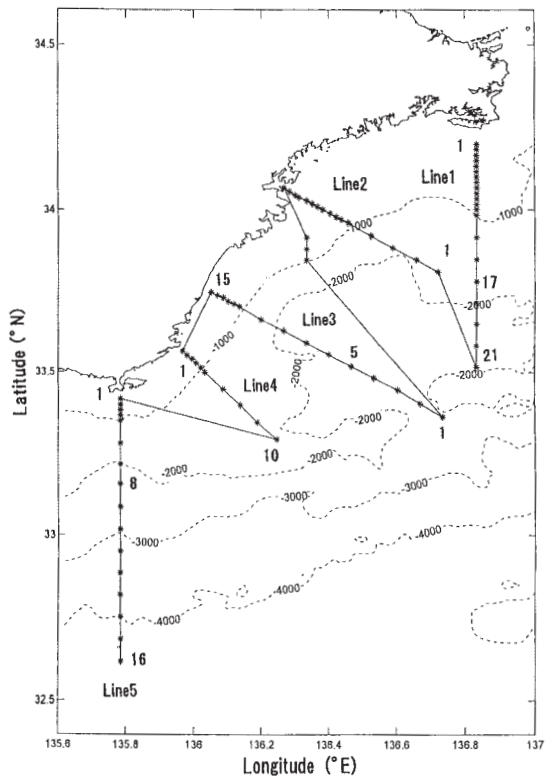4. Because the ADCP velocity observed during

Fig. 3. Observational CTD points and ship track of
the present study during August 26–31, 1999.

CTD observation are omitted and those ob-
served in constant ship velocity are employed,
some downstream shifts of the observational
points of ADCP velocity are recorded in the
Kuroshio region with large eastward velocity.
As indicated in Fig. 2, a southwestward
counter current is observed along the Lines 1
and 2 and coastal sides of Lines 3 and 4, a west-
ern part of the cyclonic eddy is found in a west-
ern region of the Kii Peninsula. A strong
eastward flow of the Kuroshio is observed in
the southeastern area of lines 3 and 4. Further-
more, the eastward Kuroshio flow is dominant
in all the range of Line 5.

Temperature, salinity and density (σ_θ) fields
along five observational lines are shown in
Figs. 5, 6 and 7. As for Line 1 (Fig. 5a), iso-
therms, isohaline and isopycnal lines shift
downward in the coastal region with the depths
from 100 m to 900 m. Because the gradient of
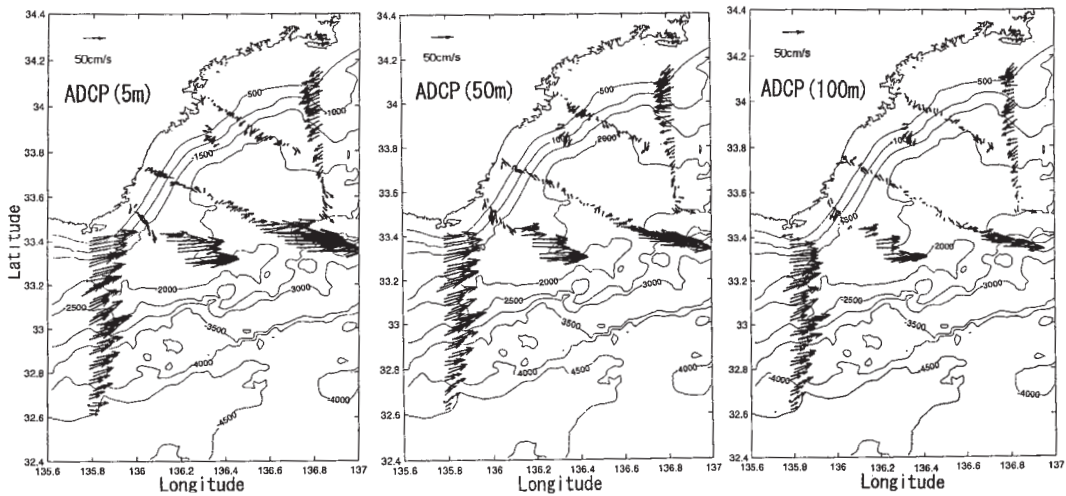which is opposite to that in the region of the

Fig. 4.   Observed ADCP velocities at depths of 5 m (left), 50 m (center) and 100 m (right).

main flow of the Kuroshio, the westward flow is suggested from the geostrophic flow balance, which corresponds to the southwestward ADCP velocity shown in Fig. 4. Less saline water (<34.25 psu) is observed at the offshore stations south of Station 17, while it is not observed at the coastal area.

As the Line 2 is located at nearshore region (Fig. 4), the gradients of isotherms, isohaline and isopycnal lines in the coastal region are weak (Fig. 5b) and less saline water (<34.25 psu) is not observed. This suggests that the less saline water does not exist in the marginal region of the cyclonic eddy. However, the less saline water appears in an eastern offshore part of the Line 3 (Fig. 6a) with Stations of 1–5, which corresponds to the downstream part of the cyclonic eddy observed in the Line 1 shown in Fig. 5a. the Line 2 does not reach to this area. The opposite gradient of the isotherms, isohaline and isopycnal lines are detected at the offshore stations of the Line 3 in the upper layer shallower than 200 m (Fig. 6a) and it corresponds to the eastward strong main Kuroshio flow shown in Fig. 4.

As the offshore southern part of Line 4 is located at the Kuroshio region, the existence of the Kuroshio flow is clearly seen at the offshore stations by the gradient of isotherms, isohaline and isopycnal lines (Fig. 6b). The Subtrocpcal Mode Water (> 34.8 psu) is seen

in the upper layer shallower than 100 m, while it is not observed at the Line 3. Less saline water (< 34.25 psu) is not found in the Line 4.

More significant features of the eastward Kuroshio flow are seen at all the Stations of Line 5 (Fig. 7) by the prominent gradient of isotherms, isohaline and isopycnal lines. The Subtropical Mode Water is seen in the upper layer with depths of 100 m–300 m at Stations 6 –16.

It is suggested from Figs. 2 and 4 that the main Kuroshio flow exists from Station 1 to Station 8 of the Line 5. Less saline water (<34.25 psu) in a lower part of the main thermocline is the NPIW and it occupies the Stations 9–16 (Fig. 7) in a southern area of the main Kurosho flow, which agrees with the fact that the NPIW is essentially confined to the southern offshore side of the main Kuroshio flow pointed out by SEKINE and MIYAMOTO (2002). It is also shown from Fig. 7 that the NPIW south of the main Kuroshio flow has vertically thick structures in comparison with those of the less saline water in the coastal side of the main Kuroshio flow shown in Figs. 5 and 6.

In order to see the water characteristics, T-S diagram of the stations with less saline water (<34.25 psu) of Lines 1,3 and 5 are shown in Fig. 8. The ordinary T-S distribution of the Kuroshio water in the Shikoku Basin is totally
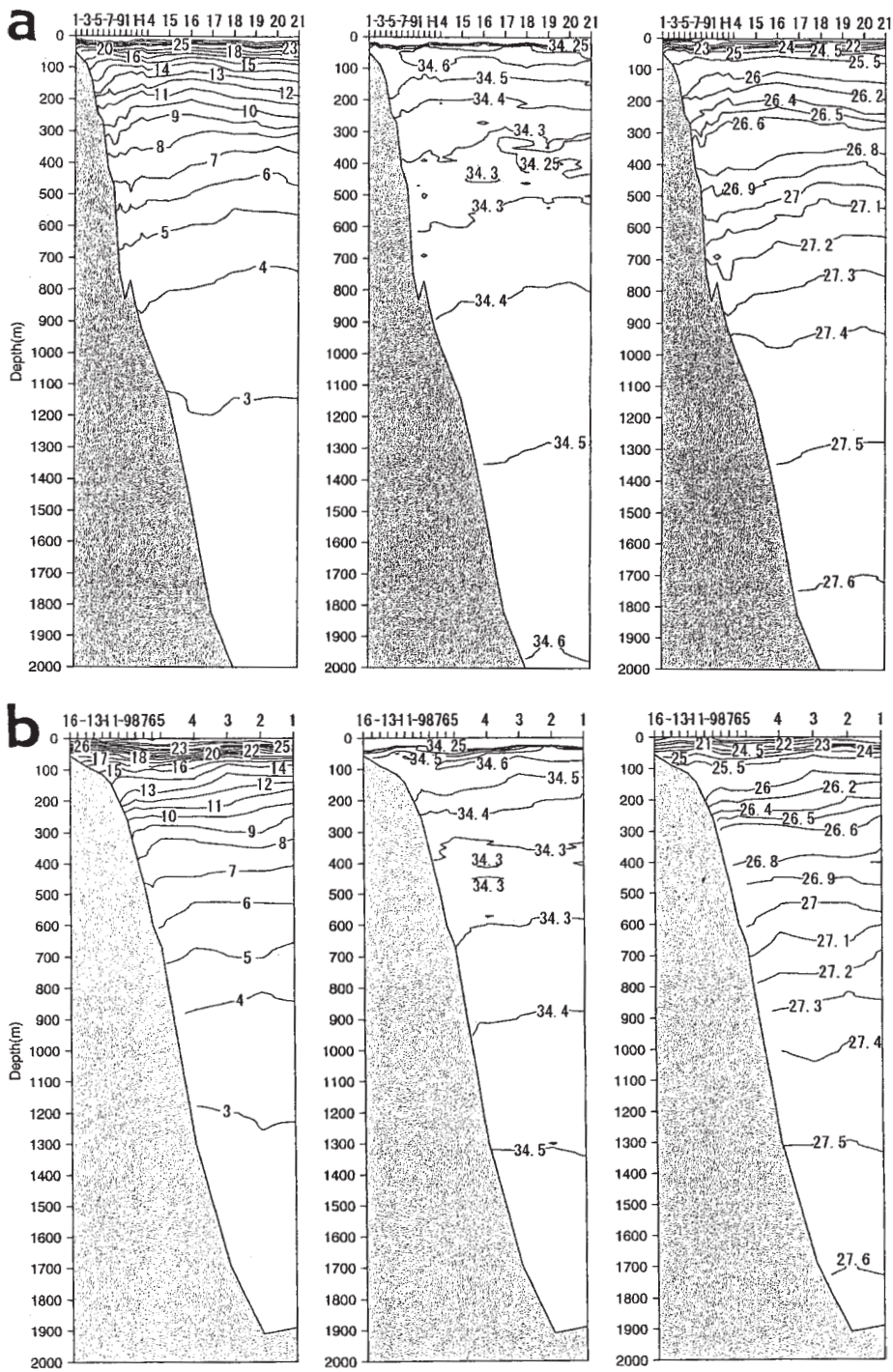
Fig. 5.   Observed temperature (℃) (left), salinity (psu) (center) and density(σ_θ) (right) fields along Line 1
(a) and Line 2 (b). Numerals at the top of each panel show the observational stations shown in Fig. 3.
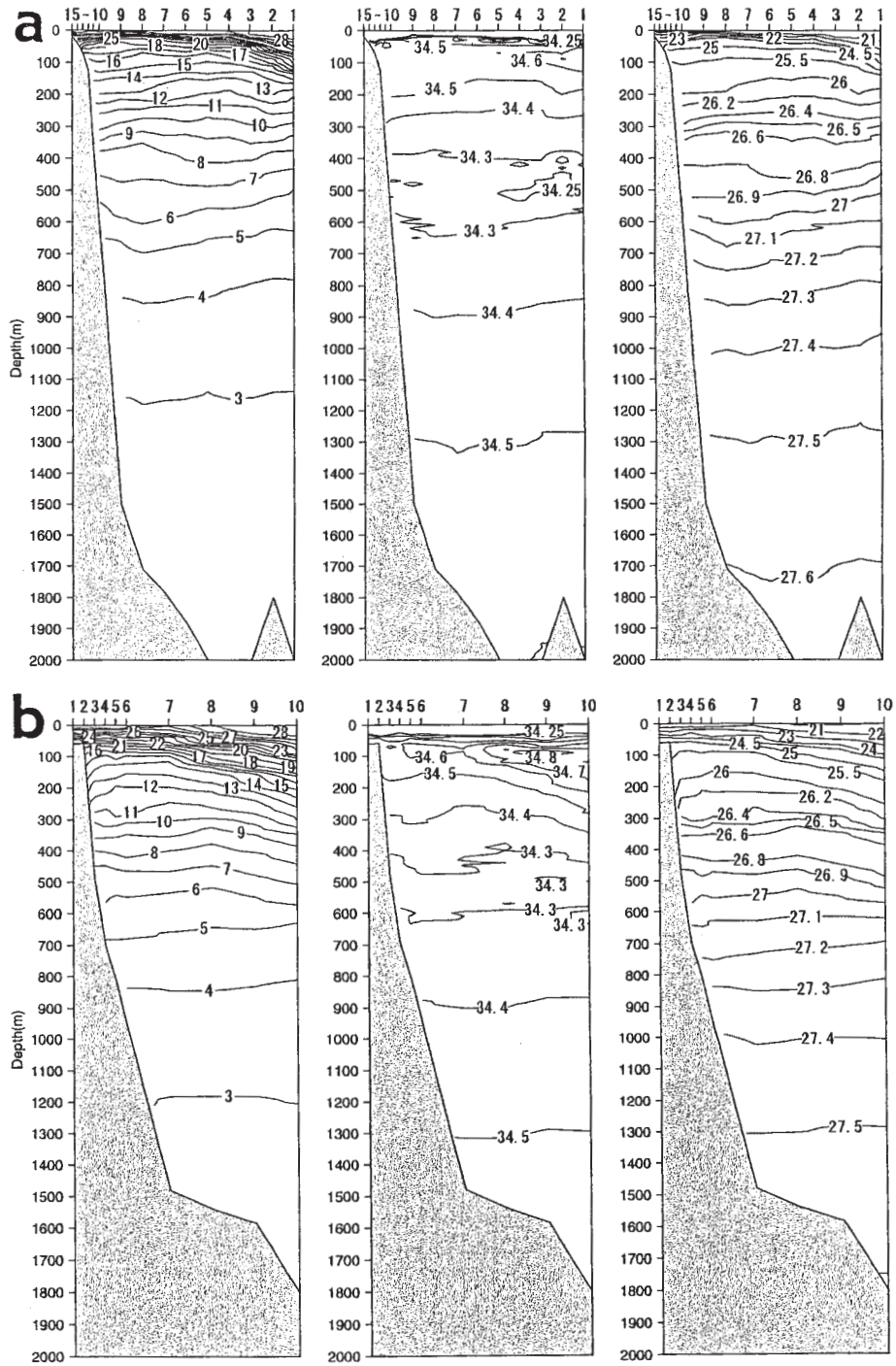
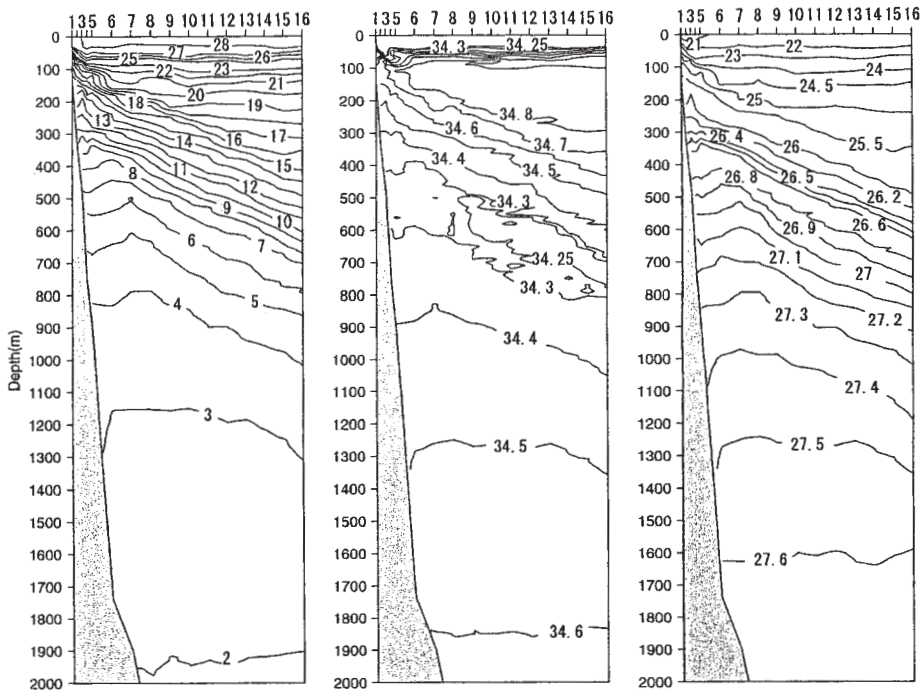Fig. 6.   Same as in Fig. 5 but for the (a) Line 3 and (b) Line 4.

Fig. 7.   Same as in Fig. 5 but for the Line 5.

suggested (ISHII *et al.*, 1983). It is noted that there exists a splitting of the T-S lines near the salinity minimum layer, which suggests the horizontal intrusion of less saline water in this level.

To see this more clearly, salinity distribution on potential density (σ_θ) coordinate is shown in Fig. 9. It is found that the horizontal intrusions are not carried out along an equal σ_θ surface and some minimum peaks of less saline water exist in the salinity minimum layer, which implies the occurrence of various kinds of less saline water intrusion with different σ_θ in the salinity minimum layer. Since almost similar σ_θ range of the intruding salinity minimum layer is found between Station 21 of Line 1 and Station 2 of Line 3, it is suggested that both Stations are commonly located at the western part of the cyclonic eddy. As for Line 3, σ_θ range of the intruding less saline water is relatively narrow and the peak of the salinity minimum becomes weak, if we go to the coastal side (from Station 2 to Station 5). In contrast to this, the horizontal intrusion of the less saline water is significant in all southern stations
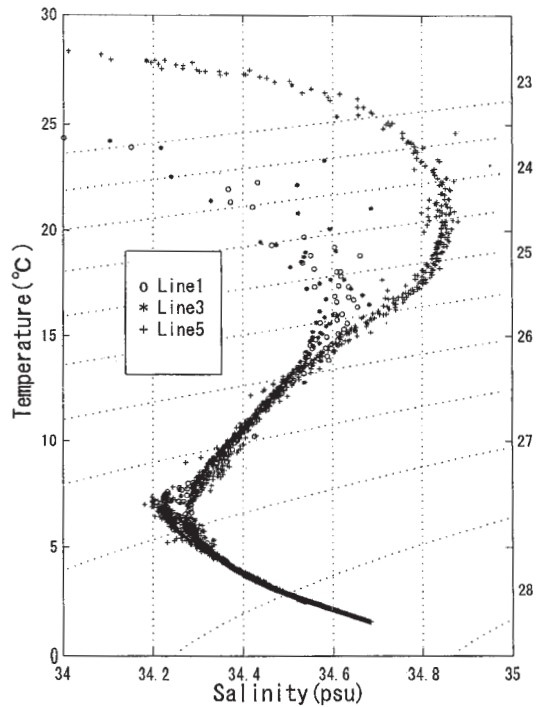
Fig. 8.   T-S diagram of Lines 1, 3 and 5. Here, only data at Stations with less saline water (<34.3 psu) shown in Fig. 9 are plotted.
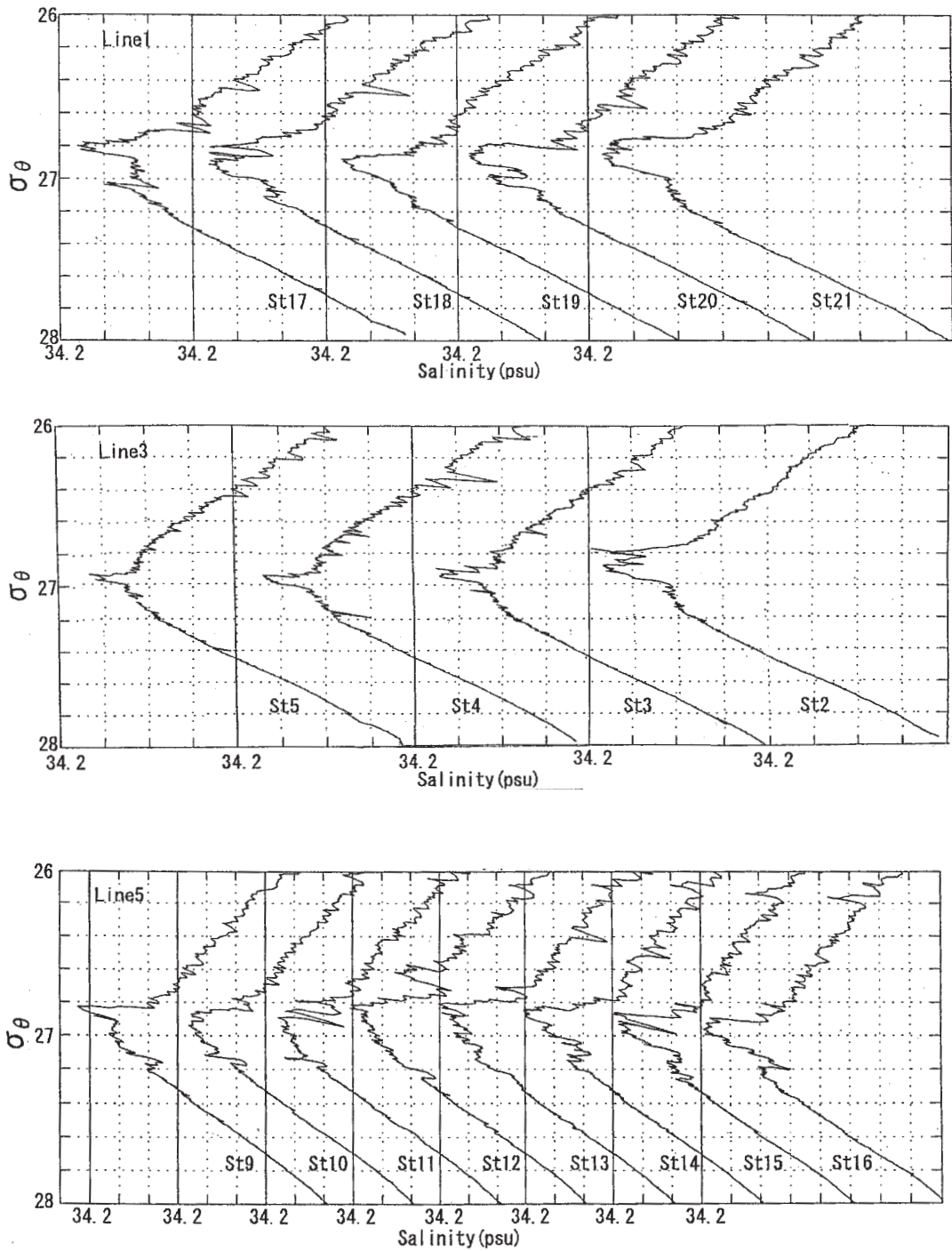
Fig. 9. Salinity distribution on σ_θ coordinates. Line 1 (top), Line 3 (middle) and Line 5 (bottom). One vertical scale mark corresponds to 0.05 psu and the next scale mark to 34.2 psu shown by solid line is 34.25 psu.

of Line 5 and various minimum peaks with wide range of σ_θ are detected.

4. Discussion

We could observed a western part of the cyclonic eddy in the coastal side of the non-large meander path of the Kuroshio by use of training vessel "Seisui-Maru" of Mie University in August of 1999. It is shown that there exist various horizontal intrusions of the less saline water with different potential density (σ_θ) in the salinity minimum layer. Less saline water accompanied by the cyclonic eddy in the coastal side of the main Kuroshio flow is relatively thin and covers a narrow range of σ_θ in the marginal area of the cyclonic eddy. Conversely, in the offshore side of the main Kuroshio flow, the horizontal intrusion of NPIW is thick and covers a wider range of σ_θ.

It is suggested from these results that origin of the less saline water in the coastal side of the main Kuroshio flow is the intermediate Oyashio Water (IOW) that comes from Sagami Bay and/or gate area over the Izu Ridge between Miyake-jima and Hatijou-jima to the Shikoku Basin. Because NPIW in southern offshore side of the main Kuroshio axis has very weak tendency to go northward crossing the Kuroshio flow (SEKINE and MIYAMOTO, 2002), the NPIW has little possibility to be the origin of the less salinity in the northern side of the Kuroshio. No less saline coastal and bay waters have a potential density greater than 26.0 (e.g., SEKINE et al., 1991), they can not be the origin of less salinity water with $\sigma_\theta > 26.7$. Therefore, it is suggested that the less saline water on the coastal side of the main Kuroshio flow is originated from IOW flows out from Sagami Bay and/or the gate area of the Kuroshio over the Izu Ridge. However, these discussion has few quantitative characteristics, to draw firm conclusion, more dense observations are needed for the less saline water on the coastal side of the main Kuroshio flow in the Shikoku Basin.

References

Fisheries Research Institute of Mie (1999): Daily Information on the Ocean Condition from the Satellite. Nos. **97** and **98**. (in Japanese).

ISHII, H., Y. SEKINE and Y. TOBA (1983): Hydrographic structure of the Kuroshio large meander-cold water mass region down to the deeper layers of the ocean. J. Oceanogr. Soc. Japan. **39**, 240–250.

REID, J. L. (1965): Intermediate waters of the Pacific Ocean. Johns Hopkins Oceanogr. Studies, **2**, 85 pp.

SEKINE, Y., Y. SATO and I. SAKAMOTO (1991): Observation of the salinity minimum layer in the Shikoku Basin south of Japan. Bull. Fac. Bio. Mie Univ., **6**, 83–108.

SEKINE, Y., S. WATANABE and F. YAMADA (2000): Topographic effect of the Izu Ridge on the horizontal distribution of the North Pacific Intermediate Water. J. Oceanogr., **56**, 429–438.

SEKINE, Y. and K. UCHIYAMA (2002): Outflow of the Intermediate Oyashio Water from Sagami Bay to the Shikoku Basin. J. Oceanogr., **58**, 531–537.

SEKINE, Y. and S. MIYAMOTO (2002): Influence of the Kuroshio flow on the horizontal distribution of North Pacific Intermediate Water in the Shikoku Basin. J. Oceanogr., **58**, 611–616.

SENJYU, T., N. ASANO, M. MATSUYAMA and T. ISHIMARU (1998): Intrusion events of the intermediate Oyashio Water into Sagami Bay, Japan. J. Oceanogr., **54**, 29–44.

SHOJI, D. (1972): Time variation of the Kuroshio south of Japan. *In* Kuroshio－Its Physical Aspects, ed. by H. Stommel and K. Yoshida, Univ. Tokyo Press, Tokyo. pp. 217–234.

TAFT, B.A. (1972): Characteristics of the flow of the Kuroshio south of Japan. *In* Kuroshio－Its Physical Aspects, ed. by H. Stommel and K. Yoshida, Univ. Tokyo Press, Tokyo. pp. 165–216.

TALLEY, L.D. (1993): Distribution and formation of the North Pacific Inter-mediate Waters. J. Phys. Oceanogr., **23**, 517–537.

YANG, S.K., Y. NAGATA, K. TAIRA and M. KAWABE (1993a): Southward intrusion of the intermediate Oyashio water along the east coast of the Boso Peninsula I. Coastal salinity-minimum-layer water off the Boso Peninsula. J. Oceanogr.,

49, 89–114.

YANG, S.K., Y. NAGATA, K. TAIRA and M. KAWABE (1993b): Southward intrusion of the intermediate Oyashio water along the east coast of the Boso Peninsula, Japan. II. Intrusion events into Sagami Bay. J. Oceanogr., **49**, 173–191.

YASUDA, I., K. OKUDA and Y. SHIMIZU (1996): Distribution and midification of North Pacific Intermediate water in the Kuroshio-Oyashio interfrontal zone. J. Phys. Oceanogr., **26**, 448–465.

The relationship between logPow and molecular weight of polycyclic aromatic hydrocarbons and EC50 values of marine microalgae

Yutaka Okumura,*† Jiro Koayama,‡ and Seiichi Uno‡

Abstract : The effect of five polycyclic aromatic hydrocarbons (dibenzothiophene, phenanthrene, naphthalene, fluorene and hydroxybiphenyl) on the growth of eight marine microalgae (Bacillariophyceae; *Skeletonema costatum, Chaetoceros calcitrans*, Prasinophyceae; *Tetraselmis tetrathele*, Haptophyceae; *Isochrysis galbana, Pavlova lutheri,* Dinophyceae; *Prorocentrum minimum,* Euglenophyceae; *Eutreptiella* sp. and Chlorophyceae; *Dunaliella tertiolecta*) was investigated. *D. tertiolecta* to all polycyclic aromatic hydrocarbons (PAHs) was the most tolerant species of the microalgae tested, EC50 values of dibenzothiophene, phenanthrene and naphthalene on *D. tertiolecta* were higher than the highest concentrations tested and therefore could not be determined in this experiment. On the other hand, the most sensitive microalgae varied with the compounds of PAHs. *Eutreptiella* sp. to dibenzothiophene, *P. lutheri* to phenanthrene, fluorene and naphthalene, *P. minimum* to phenanthrene and C. *calcitrans* to hydroxybiphenyl were the most sensitive species. Linear equation between the octanol/water partition coefficient (logPow) of all PAHs tested and EC50 values (log (1/EC50)) of all microalgae tested was $\log(1/\text{EC50}) = 0.87 \times \log\text{Pow} - 0.76$ ($r^2 = 0.75$). The ranges of the upper and lower 95% confidence limits were more than 1.4, the variation of algal sensitivity was more than twenty-five fold. EC50 values of C. *calcitrans* and *T. tetrathele* tested had a higher correlation to the molecular weight than to the logPow of the PAHs.

Keywords : *Toxicity tests, Marine microalgae, Aromatic hydrocarbons, Octanol/water partition coefficient, Molecular weight*

INTRODUCTION

Toxicity tests of petroleum components have been examined to predict the influence of accidental pollution on aquatic organisms. The toxicity effects on microalgae, primary producers in the aquatic food web, have also been reported (Pulich *et al.,* 1974, Winters *et al.,* 1976, Hsiao, 1978, Bate and Crofford, 1985, Vandermeulen and Lee, 1986, Vandermeulen, 1986, Morales-Loo and Goutx, 1990, El-Dib *et al.,* 1997). Several of these studies report that the toxic concentration for microalgae varied with the origin of crude oil (Winters *et al.,* 1976, Hsiao, 1978), because the components of

†Tohoku National Fisheries Research Institute 3–27–5 Shinhama-cho, Shiogama-shi, Miyagi 985–0001, Japan
‡Kagoshima University 50–20 Shimoarata 4-Chome, Kagoshima 890–0056, Japan
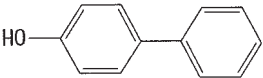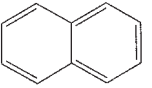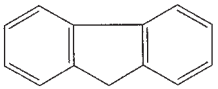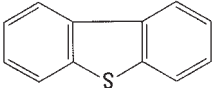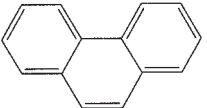
aromatic hydrocarbons in crude oil vary with the source of origin. Therefore, toxicity effects of individual aromatic hydrocarbons which along with paraffin and asphalt from the main components in crude oil, on microalgae should be examined. Although the toxic effects on freshwater microalgae (U.S. EPA, 1980, Herman *et al.,* 1990, Herman *et al.,* 1991, Sheedy *et al.,* 1991), on marine microalgae (Dunstan *et al.,* 1975, Kusk, 1980, 1981a, 1981b) have been investigated, there is little available data on polycyclic aromatic hydrocarbons (PAHs) on marine microalgae.

Recently, predictions of toxicity have led to the examination of relationships between the physicochemical properties of chemicals (water solubility, octanol/water partition coefficient etc.) and the bioconcentration factor, or between the physicochemical properties and toxic effects. Although there are several reports for

Table 1 Structure, molecular weight and logPOW of aromatic hydrocarbons in this study.

Generic name	Structure	Molecular weight	logPOW	Reference of logPOW
Hydroxybiphenyl		170.21	3.20	Hansch et al. (1995)
Naphthalene		128.18	3.30	Hansch et al. (1995)
Fluorene		166.22	4.18	Hansch et al. (1995)
Dibenzothiophene		184.26	4.38	Hansch et al. (1995)
Phenanthrene		178.24	4.46	Hansch et al. (1995)

freshwater microalgae (Geyer et al., 1981, Geyer et al., 1984, Calamari et al., 1983, Wong et al., 1984, Shigeoka et al., 1988, Herman et al., 1991) and several aquatic organisms (Galassi et al., 1988, Ikemoto et al., 1992, Fukushima, 1983), there are few reports which have investigated the relationship between EC50 (Effective Concentration of 50%) values in marine microalgae and octanol/water partition coefficient (Pow) of PAHs, particularly, reports which investigate multiple species of marine microalgae under the same test conditions are limited.

The OECD guidelines (OECD, 1984), one of the manuals for standard methods of toxicity tests, recommends that test species of microalgae are freshwater microalgae; *Selenastrum capricornutum, Scenedesmus subspicatus* and *Chlorella vulgaris*. However, test species of marine microalgae, that are necessary to toxicity estimation of chemicals in the marine environment were not selected. Therefore, it is important for establish methods to select suitable species for algal sensitivity testing.

The purpose of this study is to determine the EC50 values of PAHs on eight species of marine microalgae. Moreover, we compared the sensitivity among test microalgae, or the toxicity among test chemicals. The relationship between EC50 values of microalgae and physicochemical properties (logPow or logM.W.) of PAHs are investigated.

MATERIALS AND METHODS

Test organisms

Eight species of marine microalgae were used in the experiments as test organisms. Bacillariophyceae; *Skeletonema costatum* (NIES-324) was obtained from The Microbial Culture Collection, National Institute for Environmental Studies (NIES-Collection), Ministry of the Environment Japan. Prasinophyceae; *Tetraselmis tetrathele*, Haptophyceae; *Pavlova lutheri* were obtained from Marine Ecology Research Institute, Japan. Haptophyceae; Isochrysis galbana, Dinophyceae; *Prorocentrum minimum*, and Euglenophyceae; *Eutreptiella* sp. were obtained from JANUS Co., Japan. Chlorophyceae, *Dunaliella tertiolecta* and Bacillariophyceae, *Chaetoceros calcitrans* were obtained from Kitasato University, Japan.

Test chemicals

The PAHs used in the experiments were dibenzothiophene ($C_6H_4C_6H_4S$), phenanthrene

Table 2. Estimated EC50 values with slope, y inter-
cept and r² of linear regression.

	esti-mated EC50	Slope	y inter-cept	r² Squared
Dibenzothiophene				
S. costatum	0.20	128.2	139.0	0.99
C. calcitrans	0.14	63.9	103.6	0.98
T. tetrathele	0.14	48.2	91.1	0.97
I. galbana	0.14	53.3	95.4	0.89
P. lutheri	0.12	60.7	105.4	0.98
P. minimum	0.16	270.6	267.5	1.00
Eutreptiella sp.	0.06	78.1	147.7	0.95
D. tertiolecta	>0.49	—	—	—
Phenanthrene				
S. costatum	0.15	60.6	99.7	0.93
C. calcitrans	0.34	153.7	122.8	1.00
T. tetrathele	0.29	156.3	133.7	1.00
I. galbana	0.14	62.4	103.5	0.97
P. lutheri	0.09	63.1	115.0	0.97
P. minimum	0.09	105.4	157.9	0.99
Eutreptiella sp.	0.13	107.1	144.7	1.00
D. tertiolecta	>0.46	—	—	—
Naphthalene				
S. costatum	1.83	196.8	−1.8	1.00
C. calcitrans	3.73	114.4	−15.4	0.97
T. tetrathele	5.39	274.3	−150.7	0.97
I. galbana	0.84	102.5	57.8	1.00
P. lutheri	0.66	120.4	71.9	0.96
P. minimum	1.63	330.5	−20.2	0.79
Eutreptiella sp.	1.14	73.5	45.9	0.98
D. tertiolecta	>13.8	—	—	—
Fluorene				
S. costatum	0.17	64.5	100.2	0.99
C. calcitrans	0.34	79.7	87.3	0.98
T. tetrathele	0.67	81.5	64.0	1.00
I. galbana	0.11	50.7	99.2	0.95
P. lutheri	0.08	44.8	100.0	0.98
P. minimum	0.24	104.4	114.6	0.96
Eutreptiella sp.	0.23	109.0	119.9	0.99
D. tertiolecta	1.07	40.4	48.8	0.98
Hydroxybiphenyl				
S. costatum	1.11	119.5	44.5	0.99
C. calcitrans	0.59	108.9	74.7	1.00
T. tetrathele	0.85	160.3	61.5	1.00
I. galbana	1.54	87.5	33.6	0.92
P. lutheri	0.73	66.7	59.3	0.57
P. minimum	1.06	79.1	48.1	0.90
Eutreptiella sp.	1.27	61.0	43.6	0.94
D. tertiolecta	3.61	50.8	21.7	0.94

(unit of EC50s: mg/l)

$(C_{14}H_{10})$, naphthalene $(C_{10}H_8)$, fluorene $(C_6H_4CH_2$ $C_6H_4)$ and hydroxybiphenyl $(C_6H_5C_6H_4OH)$. All PAHs tested were purchased from Wako Chemicals, Japan. The chemical structure, molecular weight (M.W.) and logPow of the PAHs tested are shown in Table 1. Relationship between logPow and logM.W. of naphthalene, fluorene and phenanthrene showed strong linear relationships (logM.W.$=0.12 \times$ logPow$+$ 1.7, $r^2 = 0.99$), while the correlations of all PAHs contain hydroxybiphenyl and dibenzothiophene (logM.W.$=0.0067 \times$ logPow$+2.0$, $r^2 =0.43$) were weaker than of naphthalene, fluorene and phenanthrene.

Culture conditions

Each alga was cultured in a 300 ml of Erlenmeyer flask containing 200 ml of f/2 medium (GUILLARD and RYTHER, 1962) in stock culture. In toxicity tests, glass test tubes (25×200mm, 64 ml) containing 30 ml of f/2 medium were used to directly measure *in vivo* fluorescence using a fluorescence meter (Turner designs 10–005R). All growth media were autoclaved at 121℃ for 20 minutes. The algae were cultured at a temperature of 20 ± 1℃, under light intensity of 3500 to 4500 lux (38.9 to 50.0 μ mol m^{-2} s^{-1}) and a 14:10 light: dark cycle for the stock cultures and toxicity tests.

Toxicity tests

Firstly, the test concentrations of each PAH were adjusted. The maximum concentration of each PAH was prepared by adding a specific volume to the filtered sterile f/2 medium, shaking in a 1000ml beaker for about 24 hours under dark conditions and filtering using sterile glass fiber filters (Whatman GF/F). Each test concentration was prepared by diluting the maximum concentration medium with filtered sterile f/2 medium.

Secondly, test tubes containing 30ml of the growth medium into which the PAHs were mixed at appropriate concentrations, and 0.6ml of the algal stock solution at exponential growth phase were inoculated into the growth media. The experiments were carried out in triplicate. The growth of the algae was monitored daily by *in vivo* fluorescence using a fluorescence meter (Turner designs 10–005R),

which has been shown to have a strong relation to the Chl *a* concentration (LORENZEN, 1966, STRICKLAND, 1968) and cell numbers (YAMAGUCHI, 1994), and has been used as a measurement of microalgal biomass (LEWIS, 1995). The test period was 4 days.

Thirdly, after each chemical in test medium was extracted using *n*-hexane (Ministry of the Environment, 1998), chemical concentrations were measured by using gas chromatography (Shimadzu GC–14B) coupled with flame-ionization detecter (FID) (Standard methods, 1998).

Data analysis

EC50 values were calculated using modified methods of the OECD guidelines (OECD 1984), as outlined below.

The area under the growth curve of individual test vessels was calculated using the following equation.

$$A = (N_1 - N_0)/2 \times t_1 + (N_1 + N_2 - 2N_0)/$$
$$2 \times (t_2 - t_1) + ... + (N_{n-1} + N_n - 2N_0)/$$
$$2 \times (t_n - t_{n-1})$$

where;
A = area under the growth curve,
N_0 = *in vivo* fluorescence intensity at t_0 (relative units),
N_1 = *in vivo* fluorescence intensity at t_1 (relative units),
Nn = *in vivo* fluorescence at t_n (relative units),
t_1 = time of first measurement after beginning of test,
t_n = time of nth measurement after beginning of test.

Then, the percent inhibition of the growth area of the mean value for individual test concentration to the mean value for controls in each experiments was calculated using the following equation.

$$Ia = (Ac - At)/Ac \times 100.$$

Where;
Ia = percent inhibition of the growth area for an individual test vessel.
At = mean area of each test concentration,

Ac = mean area of the controls in each experiment.

The Ia value was plotted against each test concentration on a semi-logarithmic scale. The growth inhibition rates were calculated by linear regression analysis. EC50 is the concentration showing a $Ia = 50\%$.

After calculating the EC50 values, the mean rank of the toxicity of PAH and the algal sensitivity and PAHs toxicity were determined by using the statistical method; Friedman test using SPSS 10.0J for Windows, SPSS Inc.. 95% confidence limits of the linear relationship between logPow of PAHs and log(1/EC50) of all microalgae except for *D. tertiolecta* were calculated using methods of KAWABATA (1995) and SNEDECOR (1963).

RESULTS
Algal sensitivity

The EC50 values of PAHs on marine microalgae are shown in Table 2. The most sensitive species of microalgae varied with the compounds of PAHs. *Eutreptiella* sp. was most sensitivite to dibenzothiophene. *P. lutheri* was most sensitive to phenanthrene, naphthalene and fluorene. *P. minimum* and *P. lutheri* were of equally the most sensitive to phenanthrene. *C. calcitrans* was the most sensitive to hydroxybiphenyl. On the other hand, *D. tertiolecta* had the lowest sensitivity to all PAHs of all the microalgae. EC50 values of dibenzothiophene, phenanthrene and naphthalene for *D. tertiolecta* were not measured, because the inhibition values on the maximum concentrations used in the toxicity testing were less than 50%, and were approximately 30%, 10%, and 40%, respectively. The EC50 value of fluorene for *D. tertiolecta* was approximately six times as high as *P. lutheri*. The EC50 value of hydroxybiphenyl for *D. tertiolecta* was approximately thirteen times as high as *C. calcitrans*.

The mean rank calculated using the Friedman nonparametric test was *P. lutheri* < *Eutreptiella sp.* < *I. galbana* < *P. minimum* < *C. calcitrans* < *S. costatum* < *T. tetrathele* (The value of the chi-square statistic is 12.906, with a significant of 0.045).

Toxicity of PAHs

In this study, EC50 values for dibenzothio-phene were between 0.06 and >0.49ppm. EC50 values for phenanthrene were between 0.09 and >0.46ppm. Those for naphthalene were between 0.66 and >13.8ppm, and for fluorene between 0.08 and 1.07ppm and for hydroxybiphenyl between 0.59 and 3.6ppm. The mean rank calculated by the Friedman test was dibenzothiophene< fluorene< phenanthrene< hydroxybiphenyl< naphthalene (The value of the chi-square statistic is 22.540, with a significant of 0.000).

Relationship between the EC50 values (mM/l) and the physical properties of PAHs

The square of the regression coefficients between logPow of naphthalene, fluorene and phenanthrene gave a strong linear relationship with the molecular weight, and the log (1/EC50) values of *S. costatum, T. tetrathele, P. lutheri, I. galbana, P. minimum, Eutreptiella* sp. and *C. calcitrans* were 0.97, 0.99, 0.92, 0.91, 0.99, 0.99 and 0.96, respectively. All values for individual microalga except for *D. tertiolecta* , were more than 0.91 (data not shown in figure). The square of the regression coefficient of all microalgae except for *D. tertiolecta* was approximately 0.78 (log(1/EC50) $= 1.05 \times$ log Pow-1.56). The square of regression coefficients between log Pow of all PAHs and log (1/EC50) ranged from 0.57 to 0.95 (Fig. 1). In test microalgae, the square of the regression coefficients of *S. costatum, I. galbana, P. mini−mum, P. lutheri* and *Eutreptiella* sp. were more than 0.91, while for *C. calcitrans* and *T. tetrathele* were less than 0.61. The square of the regression coefficients between the molecular weight of all PAHs and logEC50, except for *D. tertiolecta* ranged from 0.35 to 0.93 (Fig. 2). The square of the regression coefficients of *S. costatum, I. galbana, P. minimum, P. lutheri* and *Eutreptiella* sp. were less than 0.65, while for *C. calcitrans* and *T. tetrathela* approximated 0.93. The linear equation between all PAHs and microalgae tested, except for *D. tertiolecta* , was log(1/EC50) $= 0.87 \times$ logPow-0.76 ($r^2 = 0.75$). The upper and lower ranges of the 95% confidence limits of the linear equation were more than 1.4.

DISCUSSION
Algal sensitivity

In this experiment, *D. tertiolecta* was most tolerant to the PAHs of the microalgae tested and therefore as a test species *D. tertiolecta* should not be use. On the other hand, the most sensitive microalgae varied with the compounds of PAHs, although *P. lutheri* was the most sensitive species to all the PAHs tested (from the results of Friedman test). From these results, it can be conducted that sensitivity testing should be carried out on several species of microalgae. In similar results regarding algal toxicity, *D. tertiolecta* was more tolerant to PCBs and DDT than diatoms (MOSSER *et al.,* 1972, MENZEL *et al.,* 1970), more tolerant to benzene, toluene and xylene than *S. costatum* (DUNSTAN *et al.,* 1975), and was the most tolerant to five organic solvents in nine marine microalgae tested (Y. OKUMURA, personal communication). VANDERMEULEN (1986) reported that the sensitivity of *P. lutheri* to naphthalene was higher than other microalgae. However, algal sensitivities to oils varied with the type of oils (PULICH *et al.,* 1974, WINTERS *et al.,* 1976). Contrary to our results, there is a report that *D. tertiolecta* is the more sensitive to crude oil than *S. costatum* and *P. minimum* (MORALES-LOO and GOUTX, 1990). One factor by which algal sensitivity varies with components of oil is the variation of oil type, or the components of chemicals in the oil, such as the ratio between the aromatic, paraffinic and asphaltic fractions, or the volatile fractions. PULICH *et al.* (1974) reported that the volatile fractions of oils have variable effects on microalgae. BATE *et al.,* (1985) reported that the different oil treatments have different effects on several microalgae. In this study, the slopes of the linear regressions between the EC50 values and the logPow of naphthalene, fluorene and phenanthrene, show strong linear relationships to all microalgae except for *D. tertiolecta* , and ranging from 0.88 to 1.20, with the intercepts of the linear regression ranging from -0.67 to -2.60. The slopes and the intercepts of the linear regressions varied with the algal species. Some of the linear regressions intersected. So, it is possible that the sensitivity of each microalgae

Fig. 1. The linear regression equation relationship between logPow of the five PAHs and log (1/EC50) of the microalgae tested. *1 is the linear equation and upper and lower 95% confidence limits of all microalgae except for *D. tertiolecta* .
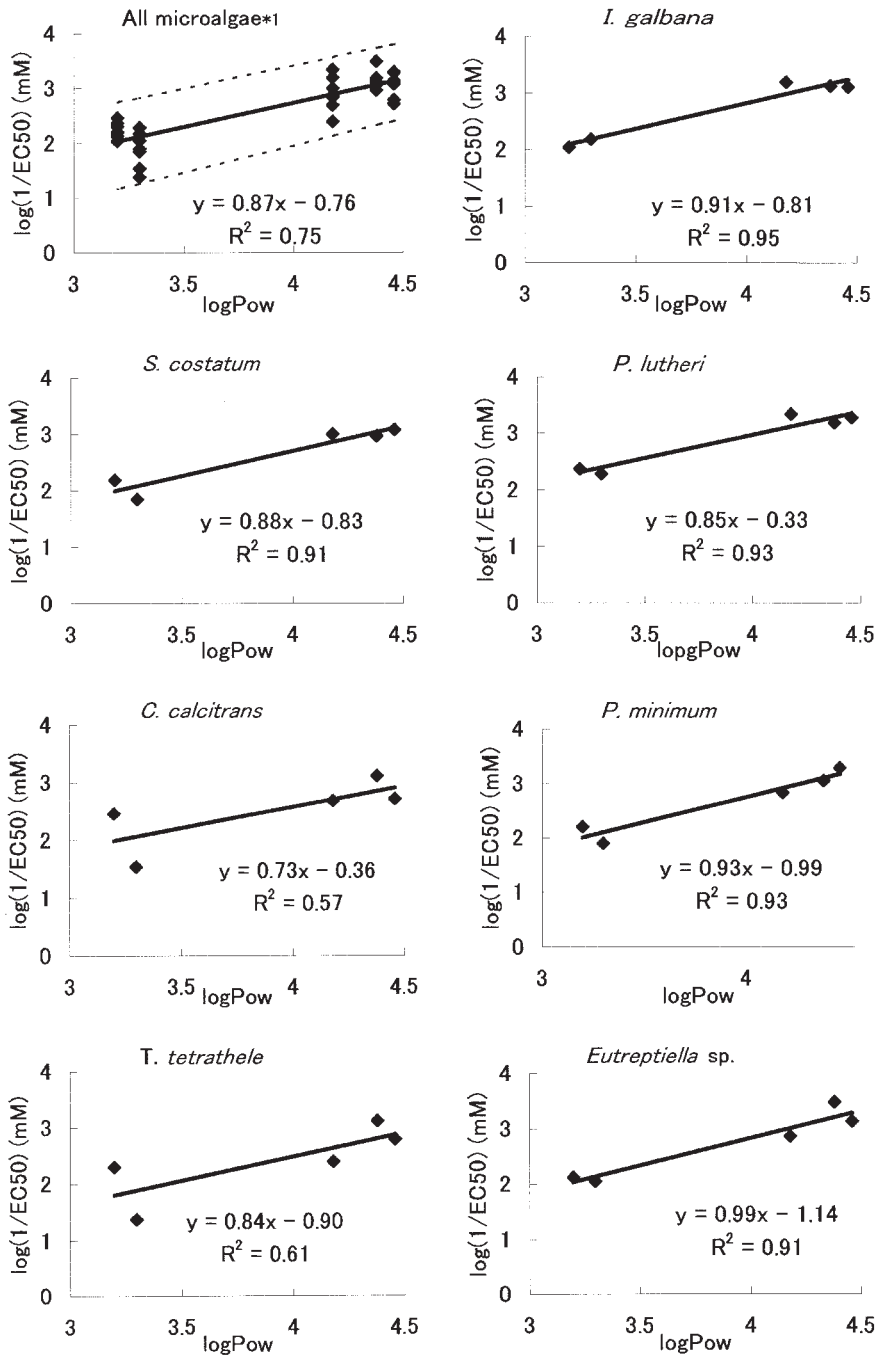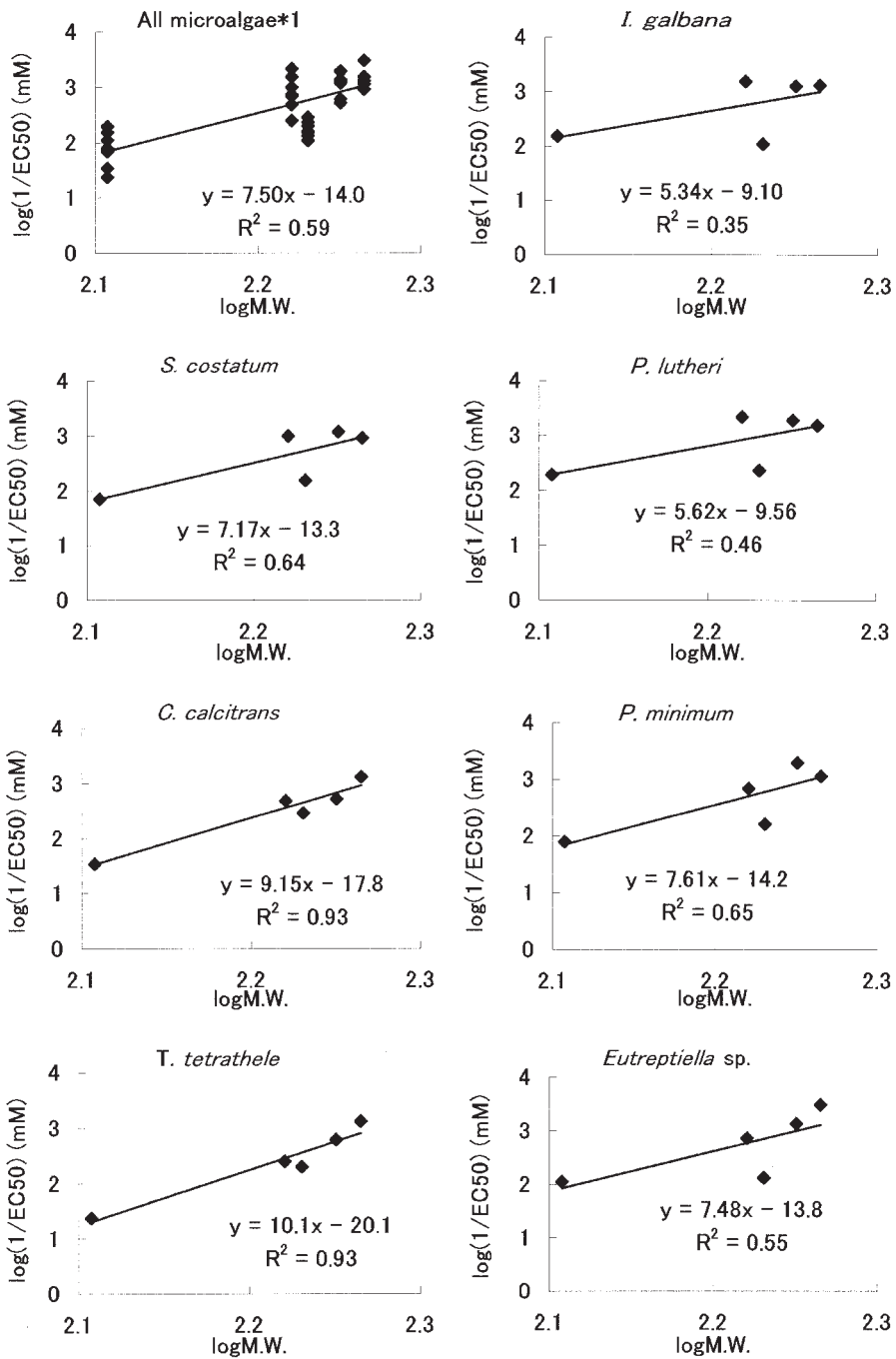
Fig. 2.　The linear regression equation relationship between logM.W. of the five PAHs and log (1/EC50) of the microalgae tested. *1 is the linear equation of all microalgae except for *D. tertiolecta.*

Table 3   The relationship between logPow and EC50

chemicals	habitat of test algae	linear regression equation	corre-lation coeffi-cient r	test periods	unit	reference
polycyclic aromatic hydrocar-bons	marine	log (1/EC50) =0.87×logPow−0.76	0.75	96-h	mM/l	This study
clorobenzenes	freshwater	log (1/EC50) =0.92×logPow−1.4	0.97	96-h	mM/l	CALAMARI et al. 1983
clorobenzenes	freshwater	log (1/EC50) =0.99×logPow−1.8	0.997	3-h	mM/l	CALAMARI et al. 1983
clorobenzenes	freshwater	log (1/EC50) =1.000×logPow−2.676	0.968	4-h	mM/l	WONG et al. 1984
chlorophenols	freshwater	log (1/EC50) =0.887×logPow−1.545	0.98	96-h	mM/l	SHIGEOKA et al. 1988
chlorophenols	freshwater	log (1/EC50) =0.543×logPow−0.909	0.845	96-h	mM/l	SHIGEOKA et al. 1988
volatite aromatic hydrocarbons	freshwater	log (1/EC50) =0.94×logPow−3.59	0.99	12-h	mg/l	HERMAN et al. 1991
aromatic hydrocarbons	freshwater	log (1/EC50) =0.91×logPow−4.45	0.9471	72-h	mM/l	GALASSI et al. 1988
alcohols, benzenes	freshwater	log (1/EC50) =0.935×logPow−3.341	0.964	120-h	mM/l	IKEMOTO et al. 1992

was reversed by logPow of test PAHs. For example, it may be that one microalgae is more sensitive to PAHs of low logPow than the other microalgae, which is less sensitive to PAHs of high logPow than the other microalgae, or that one microalgae is less sensitive to PAHs of low logPow than the other microalgae, is more sensitive to PAHs of high logPow than the other microalgae. Dibenzothiophene and hydroxy-biphenyl for which the ratio of logM.W. to logPow was higher than values of naphthalene, fluorene and phenanthrene for some of the microalgae (*C. calcitrans* and *T. tetrathele*) and tended to have a higher toxicity than the other PAHs. The regression coefficients between logM.W. and log (1/EC50) values of these microalgae tended to be higher than of the other microalgae, and the regression coefficients between logPow and log (1/EC50) values of the microalgae. So, it may be that PAHs are the ratio of logM.W. to logPow are higher, varied with algal sensitivity.

Regarding strains of test microalgae, FISHER *et al.* (1973) and MURPHY *et al.* (1980) reported that algal sensitivity, even if within the same species of microalgae, varied with environmental factors. It may be that the strain influences the algal sensitivity.

SHEEDY *et al.* (1991) reported that the 14day-EC50 value of naphthalene on the freshwater algae, *Selenastrum capricornutum* was 25ppm. US-EPA (1980) reported that the 48hour-EC50 value of naphthalene on *Chlorella vulgaris* was 33ppm. In our study, EC50 values of naphthalene were between 0.66 to >13.8ppm. The sensitivity of marine microalgae to naphthalene tended to be higher than the freshwater microalgae.

Comparison of linear regression equations be−tween logPow and EC50

Several reports regarding the linear regression equation between logPow of chemicals and EC50 values of microalgae have been published (Table 3). The slope of the linear equations ranged from 0.54 to 1.00, the intercept ranged from −4.45 to −0.91. In this study, the slope and intercept of all PAHs tested were 0.87 and −0.76, respectively. The slope and intercept of the linear regression equation to naphthalene, fluorene and phenanthrene were 1.05 and −1.56, respectively. Our equations are approximately in agreement with the equations of given in the references in the Table 3. The ranges of the

upper and lower 95% confidence limits of the linear regression equations were more than 1.4, the variation of algal sensitivity was more than twenty-five fold. Although the species of test chemicals and the range of logPow of chemicals were limited, the upper 95% confidence limit of our equation was highest and in the linear regression equations of given in the references in the Table 3, the upper 95% confidence limit of our equation was the most sensitive compared to other values in the literature.

From our equation, for example it is clear that the toxicity of phenanthrene, for which the logPow is 4.46, is higher in toxicity than naphthalene, which has a logPow of 3.3, while the water solubility of phenanthrene is lower than naphthalene. So, we conclude that the PAHs such as hydroxybiphenyl and dibenzothiophene for which the ratio of molecular weight to Pow is high, have a higher toxicity than naphthalene, fluorene and phenanthrene.

References

BATE, G.C. and S.D. CROFFORD (1985): Inhibition of phytoplankton photosynthesis by the WSF of used lubricating oil. Mar. Pollut. Bull., **16**, 401–404.

CALAMARI, D.,S. GALASSI, F. SETTI and M.VIGH (1983): Toxicity of selected chlorobenzenes to aquatic organisms. Chemosphere, **12**, 253–262.

DUNSTAN, W.M., L.P. ATKINSON and J. NATOLI (1975): Stimulation and inhibition of phytoplankton growth by low molecular weight hydrocarbons. Mar, Biol., **31**, 305–310.

EL-DIB, M.A., H.F. Abou-Waly and A.M.H. El-NABY (1997): Impact of fuel oil on the freshwater alga *Selenastrum capricornutum*. Bull. Environ. Contam. Toxicol., **59**, 438–444.

FISHER, N.S., L.B. GRAHAM and E.J. CARPENTER (1973): Geographic differences in phytoplankton sensitivity to PCBs. Nature, **241**, 548–549.

FUKUSHIMA, M. (1983): Evaluation of water pollution by determining chemicals in plankton. Seitai Kagaku, **6**, 4–15, in Japanese.

GEYER, H., R. VISWANATHAN, D. FREITAG and F. KORTE (1981): Relationship between water solubility of organic chemicals and their bioaccumulation by the alga *Chlorella*. Chemosphere, **10**, 1307–1313.

GEYER, H., G. POLITZKI and D. FREITAG (1984): Prediction of ecotoxicological behaviour of chemicals: relationship between n-octanol / water partition coefficient and bioaccumulation of organic chemicals by alga *Chlorella*. Chemosphere,

13, 269–284.

GALASSI, S., M. MINGAZZINI. L. VIGANO, D. CESAREO and M.L. TOSATO (1988): Approaches to modeling toxic responses of aquatic organisms to aromatic hydrocarbons. Ecotoxicol Environ Safety, **16**, 158–169.

GUILLARD, R.R.L. and J.H. RYTHER (1962): Studies of marine planktonic diatoms. I. Cyclotellanana Hustedt, and *Detonula confervacea* (Cleve) Gran. Can J Microbiol, **62**, 229–239.

HANSCH, C., A. LEO and D. HOEKMAN (1995): Exploring QSAR -Hydrophobic, Electronic, and Steric Constants. ACS Professional Reference Book, American Chemical Society, Washington, DC, 97 –118.

HERMAN, D.C., W. E.INNISS and C.I. MAYFIELD (1990): Impact of volatile aromatic hydrocarbons, alone and in combination, on growth of the freshwater alga *Selenastrum capricornutum*. Aquat. Toxicol., **18**, 87–100.

HERMAN, D.C., W.E. INNISS and C.I. MAYFIELD (1991): Toxicity testing of aromatic hydrocarbons utilizing a measure of their impact on the membrane integrity of the green alga Selenastrum capricornutum. Bull. Environ. Contam. Toxicol., **47**, 874–881.

HERMAN, D.C., C.I. MAYFIELD and W.E. INNISS (1991): The relationship between toxicity and bioconcentration of volatile aromatic hydrocarbons by the alga *Selenastrum capricornutum*. Chemosphere, **22**, 665–676.

HSIAO, S.I.C. (1978): Effects of crude oils on the growth of arctic marine phytoplankton. Environ Pollut., **17**, 93–107.

IKEMOTO, Y. K. MOTOBA T. SUZUKI and M. UCHIDA (1992): Quantitative structure-activity relationships of nonspecific and specific toxicants in several organism species. Environ Toxicol Chem, **11**, 931–939.

KAWABATA, K. (1995): Kaiki to soukan (regression and correlation). *In* Ouyou Toukei Handbook, OKUNO *et al.* (eds) Ouyou Toukei Handbook, Youkendo, Japan, p91–105, in Japanese

KUSK, K.O. (1980): Effects of crude oils and aromatic hydrocarbons on the photosynthesis of three species of *Acrosiphonia* grown in the laboratory. Bot, Mar., **23**, 587–593.

KUSK, K.O. (1981a): Effects of hydrocarbons on respiration, photosynthesis and growth of the diatom *Phaeodactylum tricornutum*. Bot. Mar., **24**, 413–418.

KUSK, K.O. (1981b): Effects of naphthalene on the diatom *Phaeodactylum tricornutum* growth under varied conditions. Bot. Mar., **24**, 485–487.

LEWIS, M.A. (1995): Algae and vascular plant tests. *In* Fundamental of aquatic toxicology. Secnd edition, RAND, G.M. (ed) Fundamental of aquatic

toxicology. Second edition, Taylor and Francis, USA, p144–155

LORENZEN, C.J. (1966): A method for the continuous measurement of *in vivo* chlorophyll concentration. Deep-Sea Res, **13**, 223–227.

MENZEL, D.W. J. ANDERSON and A. RANDTKE (1970): Marine phytoplankton vary in their response to chlorinated hydrocarbons. Science, **167**, 1724–1726.

MINISTRY of the ENVIRONMENT (1998): Benzothiophene, dibenzothiophene. *In* the analytical methods of chemicals. Tokyo, p.176–185.

MORALES-LOO, M.R. and M. GOUTX (1990): Effects of water-soluble fraction of the Mexican crude oil "Isthmus Cactus" on growth, cellular content of chlorophyll *a*, and lipid composition of planktonic microalgae. Mar. Biol., **104**, 503–509.

MOSSER, J.L., N.S. FISHER, T.S. TENG and C.F. WURSTER (1972): Polychlorinated biphenyls: Toxicity to certain phytoplankters. Science, **175**, 191–192.

MURPHY, L.S. and R.A. BELASTOCK (1980): The effect of environmental origin on the response of marine diatoms to chemical stress. Limnol Oceanogr, **25**, 160–165

Organization for Economic Cooperation and Development (1984): Alga growth inhibition test. TG201. *In* OECD Guidelines for Testing of Chemicals. Paris, p. 1–14.

PULICH, W.M., K.WINTERS and C.VAN BAALEN (1974): The effects of a No. 2 fuel oil and two crude oils on the growth and photosynthesis of microalgae. Mar. Biol., **28**, 87–94.

SHEEDY, B.R., J.M. LAZORCHAK, D.J. GRUNWALD Q.H. PICKERING, A. PILLI, D. HALL and R.WEBB (1991): Effects of pollution on freshwater organisms. Res. Jour. WPCF., **63**, 619–696.

SHIGEOKA, T. Y. SATO, Y. TAKEDA, K. YOSHIDA and F. YAMAUCHI (1988): Acute toxicity of chlorophenols to green algae, *Selenastrum capricornutum and Chlorella vulgaris*, and quantitative structure-activity relationships. Environ Toxicol Chem, **7**, 847–854.

SNEDECOR, G.W. (1963): linear regression. *In* Statistical methods. Fifth Edition, HATAMURA, M., T. OKUMO and Y. TSUMURA (translators), Statistical methods. Fifth edition, Iwanami Shoten, Japan, p. 127–131, in Japanese.

Standard methods for the examination of water and wastewater (1998): polynuclear aromatic hydrocarbons. CLESCERI L.S., A.E. GREENBERG and A.D. EATON (eds), p. 6–79–6–84.

STRICKLAND, J.D.H. (1968): Continuous measurement of *in vivo* chlorophyll;a precautionary note. Deep-Sea Res, **15**, 225–227.

U.S. Environmental Protection Agency (1980): Ambient water quality criteria for naphthalene. B–10. EPA440/5–80–059. NTIS/PB81–117707. Washington DC.

VANDERMEULEN, J.H. (1986): Altered grazing patterns in an experimental copepod- alga ecosystem exposed to naphthalene and Kuwait crude oil. Bull. Environ. Contam. Toxicol., **36**, 260–266.

VANDERMEULEN, J.H. and R.W. LEE (1986): Lack of mutagenic activity of crude and refined oils in the unicellular alga *Chlamydomonas reinhardtii*. Bull. Environ. Contam. Toxicol., **36**, 250–253.

WINTERS, K., R. O'DONNELL, J.C. BATTERTON and C. VAN BAALEN (1976): Water-soluble components of four fuel oils: chemical characterization and effects on growth of microalgae. Mar. Biol., **36**, 269–276.

WONG, P.T.S. Y.K. CHAU J.S. RHAMEY and M. DOCKER (1984): Relationship between water solubility of chlorobenzenes and their effects on a freshwater green alga. Chemosphere, **13**, 991–996.

YAMAGUCHI, M. (1994): Physiological ecology of the red tide flagellate *Gymnodinium Nagasakiense* (Dinophyceae) - Mechanism of the red tide occurrence and its prediction -, Bull Nansei Natl Fish Res Inst, **27**, 251–394, in Japanese

Influence of seagrass leaf density and height on recruitment of the cardinalfish *Cheilodipterus quinquelineatus* in tropical seagrass beds: an experimental study using artificial seagrass units

Yohei NAKAMURA*, Masahiro HORINOUCHI** and Mitsuhiko SANO*

Abstract : To clarify the effects of differences in seagrass leaf density and height on the appearance of newly-recruited fishes, a field experiment using artificial seagrass units (ASUs) was undertaken at Iriomote Island, the Ryukyu Islands, Japan. Four types of small-scale, structurally-different ASUs, including (1) long dense leaves (D-units), (2) long leaves thinned to about 40% of D-unit density (T-units), (3) dense leaves shortened to 40% of D-unit height (S-units), and (4) no leaves (control; C-units), were used. Dividing observations were made to count recruited fishes on each ASU daily over 14 consecutive days. A total of 10 species in 7 families were recruited to the ASUs. The cardinalfish, *Cheilodipterus quinquelineatus*, dominated (85% of cumulative total number of fishes). The mean number of *C. quinquelineatus* recruits per replicate on D-units was significantly greater than that on the other unit types, indicating that difference in leaf density and height affected the recruitment of the juvenile of this fish species.

Keywords : recruitment, seagrass leaf density, seagrass leaf height, *Cheilodipterus quinquelineatus*.

1. Introduction

Leaf density and height in seagrass habitats could be important as fish appearance and abundance, because complexity as habitat can provide shelters (HECK and ORTH, 1980; BELL and POLLARD, 1989), microhabitat availability (HECK and ORTH, 1980), and diverse and abundant prey (ORTH *et al*., 1984; CONNOLLY and BUTLER, 1996; JENKINS *et al*., 2002). Such complexity in habitat structured by seagrass leaves strongly affects juvenile growth rates and mortality especially for vulnerable juveniles (HECK and ORTH, 1980; BELL and POLLARD, 1989; LEVIN *et al*., 1997). However, relationships between seagrass structural attributes (leaf density and height) and fish abundance patterns are not fully understood (WILLIAMS and HECK, 2001), in spite of several attempts. While some studies have found that greater leaf density and/or height support larger numbers of fish species and individuals (BELL and WESTOBY, 1986a, b), others have found little or no relationship among these factors (BELL and WESTOBY, 1986c; BELL *et al*., 1987; CONNOLLY, 1994; HORINOUCHI and SANO, 1999, 2001).

Use of artificial seagrass has been effective in manipulative experiments to clarify the relationships between habitat structure and organisms in seagrass habitats (BELL *et al*., 1987; LEE *et al*., 2001; JENKINS *et al*., 2002). BELL *et al*. (1985), for example, found that artificial seagrass effectively attracted juvenile fish and macro-invertebrates typical of natural seagrass. In the present study, artificial seagrass units (ASUs) were used to simulate natural reef-associated seagrass patches so as to clarify the influence of seagrass leaf density and

*Department of Global Agricultural Sciences, Graduate School of Agricultural and Life Sciences, The University of Tokyo, Yayoi, Bunkyo, Tokyo 113–8657, Japan

**Research Center for Coastal Lagoon Environments, Shimane University, 1060 Nishikawatsu-cho, Matsue, Shimane 690–8504, Japan
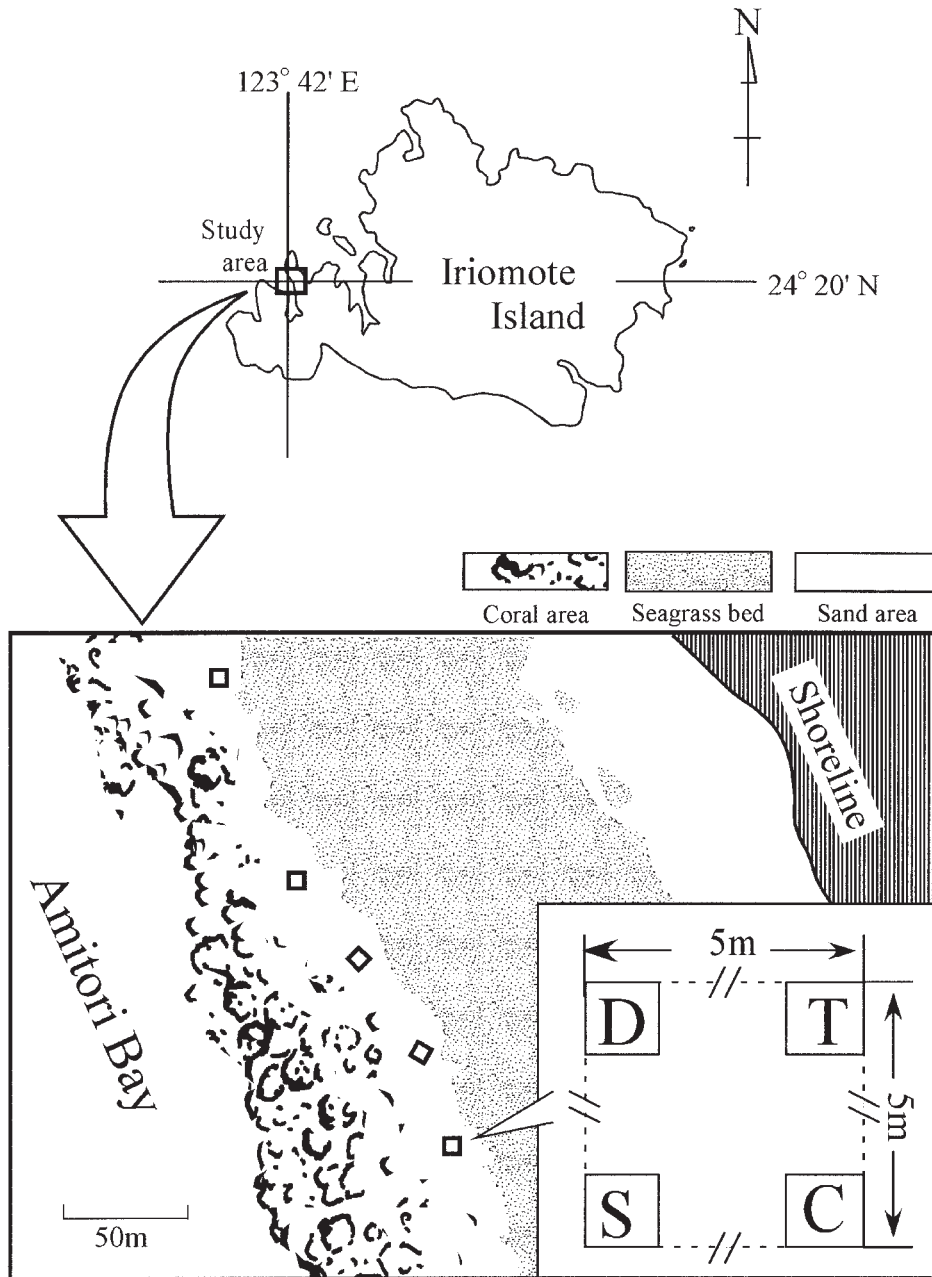
Fig. 1   Map of the study site at Iriomote Island, Ryukyu Islands, Japan, showing the locations of the five experimental square plots. D, T, S and C on each corner of the plot indicate four artificial seagrass treatments. For explanation of each artificial seagrass treatment, see text.

height on the abundance of newly-recruited fishes. Specifically, the recruitment of cardinalfish, *Cheilodipterus quinquelineatus*, which was dominant in the seagrass habitats was examined in ASUs with different seagrass leaf density and height.

Top view

Fig. 2 Design of four different types of artificial seagrass units (D-, T-, S-, and C-units).
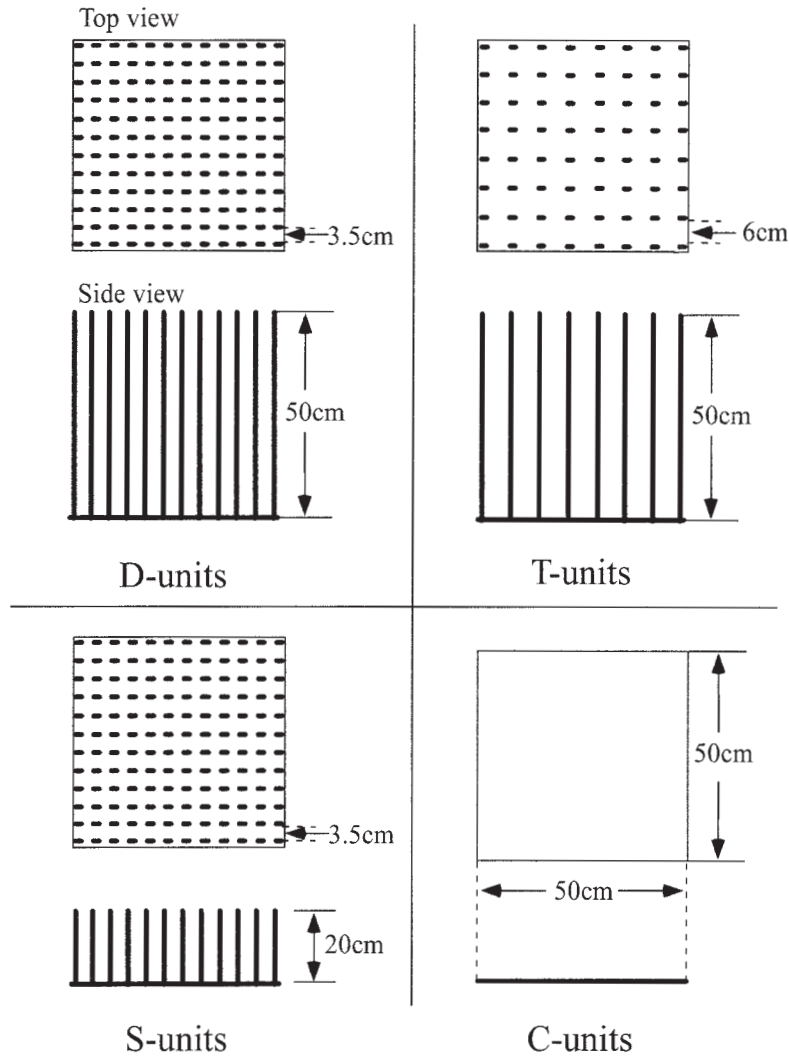
2. Materials and Methods
2.1 Study site

The study was carried out on a fringing coral reef in Amitori Bay (24° 20' N, 123° 42' E), western side of Iriomote Island, the Ryukyu Islands, southern Japan, in May, 2003 (Fig. 1). Next to a coral-dominated area, a seagrass bed formed an extensive belt along the shore. Vegetation in the bed was dominated by *Enhalus acoroides*, having a mean shoot density of 122.4 ±18.9(SD)m^{-2} ($n=6$), and mean height of 50.6 ± 10.4cm ($n=30$). The experiment was conducted in a flat and sandy-rubble area adjacent

to the edge of the seagrass bed. In this area, some coral and seagrass patches occurred at a low-tide depth of about 1 m.

2.2 Experimental design

Each ASU was constructed of green polypropylene leaves (10mm in width and 1mm in thickness) tied to a 50cm square green steel mesh base. The basic experimental design involved five replicates of each of four artificial seagrass treatments (Fig. 2): (1) long dense leaves (50cm in height, 12×12 rows=144 leaves per unit, D-units), (2) long leaves thinned to

about 40% of D-unit density (50cm in height, 8×8 rows$=$64 leaves, T-units), (3) dense leaves shortened to 40% of D-unit height (20cm in height, 12×12 rows$=$144 leaves, S-units) and (4) base without leaves (control, C-units).

At the study site, five 5 m square plots, separated from one another by at least 30 m, were established randomly at least 5 m distant from natural seagrass and coral patches (Fig. 1). Each ASU treatment was randomly assigned to each corner of each plot (i.e. 4 ASU treatments per plot). The ASUs were set on May 14, with deliberate efforts made not to disturb fishes.

2.3 Fish censuses

All individuals of each fish species in the ASUs were visually counted using SCUBA, between 1000 and 1600 h everyday from May 15 to 29. Individuals maintaining a position in open areas close to the outer edge of the units were also regarded as residents of the units and counted. During the underwater observations, the total length (TL) of each individual was estimated to the nearest millimeter with a transparent plastic ruler (SANO, 1997). Such observations were conducted very carefully, in order not to disturb the fishes.

Cheilodipterus quinquelineatus was selected as the target species of the study, because it recruited on the ASUs more abundantly than other species (see Results). We defined recruits as settled juveniles surviving until the final census date (JONES, 1990; LEVIN, 1994). In Amitori Bay, juvenile *C. quinquelineatus* commonly inhabit seagrass beds and coral patches on reef flats, whereas adults are abundant on reef slopes (KAGAWA, 2003). Newly-recruited individuals (<25mm TL; FINN and KINGSFORD, 1996) are found mostly in May and June (KAGAWA, 2003), feeding mainly on calanoid copepods (93 % of total food volume) (NAKAMURA, unpubl. data).

2.4 Data analysis

Cheilodipterus quinquelineatus recruit numbers in the ASUs were compared among the four treatments. Because the fish censuses were repeated without any removal of fish from the ASUs, the number of individuals counted at each census included both new and previously observed recruits. Under this sampling design, the data set obtained on each census date is not independent. Therefore, single-factor repeated-measures analysis of variance (ANOVA) was applied to test whether or not the density of *C. quinquelineatus* recruits differed among ASU types, and a post hoc Student-Newman-Keuls multiple comparison test was conducted to examine the difference in the mean values. Prior to the analyses, data were transformed to $\sqrt{x+0.5}$, owing to fish being absent on some ASUs during the study period (ZAR, 1999). C-units were excluded from this analysis, because no fish were observed on those units throughout the study period.

3. Results

A total of 10 species in 7 families were recorded in the ASUs (Table 1). *Cheilodipterus quinquelineatu*s recruits accounted for 85% of the cumulative total number of all species (Table 1). The size range of this species was 11 to 25mm TL (Table 1).

The repeated-measures ANOVA demonstrated a highly significant difference in the mean number of *C. quinquelineatus* recruits per replicate, among the three types (D-, T-, and S-units) ($F_{2,207} = 21.4$, $P < 0.001$; Fig. 3). The Student-Newman-Keuls multiple comparison test indicated that density of recruits on the D-unit was significantly greater than those on the T- and S-units (D->T-=S-unit, $P < 0.05$). *C. quinquelineatus* recruits were always observed on the D-units, from the first day after setting the ASUs until the last day of the experiment (Fig. 3). Although the mean numbers of recruits in the D-units were low ($0.2 - 1.6$ individuals) during the first to ninth days, many recruits (> 8.8 individuals) were found from the tenth to fourteenth days. In the T- and S-units, on the other hand, the few individuals observed on the second and third days after setting subsequently disappeared (Fig. 3). No recruits were observed in the C-units.

In the D-units, most *C. quinquelineatus* recruits occurred along the outer wall of the units (about 90% of the cumulative total number of fish counted), although some individuals were found inside the units.

Table 1   Cumulative number of individuals and size range (total length) of fish species which occurred on the
ASUs during the study period

Family	Species	No. of individuals	Total length range (mm)
Pomacentridae	*Dischistodus prosopotaenia*	21	15
Labridae	*Coris batuensis*	1	25
	Oxycheilinus bimaculatus	2	40
Scaridae	*Calotomus spinidens*	2	25,40
Apogonidae	*Apogon ishigakiensis*	1	11
	Apogon properuptus	2	12
	Cheilodipterus quinquelineatus	232	11–25
Pinguipedidae	*Parapercis cylindrica*	3	40
Blenniidae	*Meiacanthus grammistes*	9	15–18
Monacanthidae	*Acreichthys tomentosus*	1	20
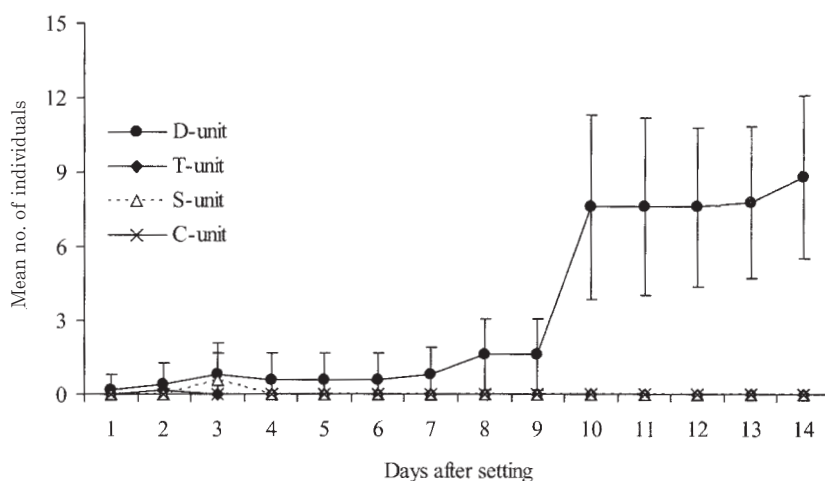
Fig. 3   Mean number ($\pm$ SE) of *Cheilodipterus quinquelineatus* recruits per replicate ($n=5$) on each type of artificial seagrass unit (D-, T-, S-, and C-units) over 2 weeks.

4. Discussion

All of the fish species occurred in the ASUs were observed in adjacent natural seagrass habitats (NAKAMURA *et al.*, 2003; NAKAMURA and SANO, 2004). In addition, a large number of *Cheilodipterus quinquelineatus* recruits appeared in the ASUs simultaneously with their occurrence in adjacent natural seagrass habitats. This indicates that the ASUs in the present study were effective in investigating the effects of seagrass leaf height and density on fish recruitment patterns.

D-units with long dense seagrass leaves supported a number of *C. quinquelineatus* recruits, whereas few or no recruits appeared on the other unit types with shorter or sparser leaves, throughout the study period. This suggests a preference by recruits for some factors associated with long dense seagrass.

Most recruits on the D-units were positioned in open areas close to the outer limit of the reefs. Similarly, recruit abundance of *C. quinquelineatus* at the outer limits of natural seagrass microhabitat is significantly greater than that inside such habitats (NAKAMURA, unpubl. data).

Several possible explanations for such microhabitat use can be offered. Hydrodynamics sometimes plays an important role in affecting the distribution patterns of small fishes. BREITBURG *et al.* (1995), for example, found that larvae of *Gobiosoma bosc* actively selected a low flow microhabitat associated with the downcurrent sides of structures. In the present study, the greater abundance of *C. quinquelineatus* in open areas close to the

"walls" of seagrass leaves indicate their preference for low-flow microhabitats, owing to possible wave attenuation at such sites (GAMBI *et al.* 1990). On the other hand, the occurrence of few recruits inside the units may be due to the oscillation of the leaves with water motion. At the present study site, flapping and undulating movements of seagrass leaves were regularly observed, sometimes having high amplitude. Because such movements can physically disturb small fish among the seagrass leaves, the juveniles would prefer the outer edge (HORINOUCHI and SANO, 1999).

For such small-sized fish such as the *C. quinquelineatus* vulnerable to predation, availability and accessibility of shelters against predators can affect the distribution of recruits. Denser and higher seagrass leaves may provide more effective shelters, compared with sparser or shorter seagrass leaves (HECK and ORTH, 1980; BELL and POLLARD, 1989). Since some predators such as *Caranx sexfasciatus* often observed, it is likely that the recruits preferred the long and dense leaves of the D-units as shelters. Open areas along the outer edge of the D-units in which most recruits appeared can be a safe zone from which they can easily flee to escape from approaching danger.

In conclusion, the appearance patterns of *C. quinquelineatus* recruits reflected their preference for weak flow microhabitats and effective shelters created by long dense seagrass leaves.

References

BELL, J.D. and D.A. POLLARD (1989) : Ecology of fish assemblages and fisheries associated with seagrasses. *In* Biology of seagrasses. LARKUM, A.W.D., A.J. McCOMB and S.A. SHEPHERD (eds.), Elsevier, Amsterdam, p. 565–609.

BELL, J.D., A.S. STEFFE and M. WESTOBY (1985) : Artificial seagrass: how useful is it for field experiments on fish and macroinvertebrates? J. Exp. Mar. Biol. Ecol., **90**, 171–177.

BELL, J.D. and M. WESTOBY (1986a) : Importance of local changes in leaf height and density to fish and decapods associated with seagrasses. J. Exp. Mar. Biol. Ecol., **104**, 249–274.

BELL, J.D. and M. WESTOBY (1986b) : Abundance of macrofauna in dense seagrass is due to habitat preference, not predation. Oecologia, **68**, 205–209.

BELL, J.D. and M. WESTOBY (1986c) : Variation in seagrass height and density over a wide spatial scale: effects on common fish and decapods. J. Exp. Mar. Biol. Ecol., **104**, 275–295.

BELL, J.D., M. WESTOBY and A.S. STEFFE (1987) : Fish larvae setting in seagrass: do they discriminate between beds of different leaf density? J. Exp. Mar. Biol. Ecol., **111**, 133–144.

BREITBURG, D.L., M.A. PALMER and T. LOHER (1995): Larval distributions and the spatial patterns of settlement of an oyster reef fish: responses to flow and structure. Mar. Ecol. Prog. Ser., **125**, 45–60.

CONNOLLY, R.M. (1994) : Removal of seagrass canopy: effects on small fish and their prey. J. Exp. Mar. Biol. Ecol., **184**, 99–110.

CONNOLLY, R.M. and A.J. BUTLER (1996) : The effects of altering seagrass canopy height on small, motile invertebrates of shallow Mediterranean embayments. P.S. Z. N. I: Mar. Ecol., **17**, 637–652.

FINN, M.D. and M.J. KINGSFORD (1996) : Two-phase recruitment of apogonids (Pisces) on the Great Barrier Reef. Mar. Freshwater Res., **47**, 423–432.

GAMBI, M.C., A.R.M. NOWELL and P.A. JUMARS (1990) : Flume observations on flow dynamics in *Zostera marina* (eelgrass) beds. Mar. Ecol. Prog. Ser., **61**, 159–169.

HECK, K.L. JR. and R.J. ORTH (1980) : Seagrass habitats: The roles of habitat complexity, competition and predation in structuring associated fish and motile macroinvertebrate assemblages. *In* Estuarine perspectives. KENNEDY, V.S. (ed), Academic Press, New York, p. 449–464.

HORINOUCHI, M. and M. SANO (1999) : Effects of changes in seagrass shoot density and leaf height on abundances and distribution patterns of juveniles of three gobiid fishes in a *Zostera marina* bed. Mar. Ecol. Prog. Ser., **183**, 87–94.

HORINOUCHI, M. and M. SANO (2001) : Effects of changes in seagrass shoot density and leaf

height on the abundance of juveniles of *Acentrogobius pflaumii* in a *Zostera marina* bed. Ichthyol. Res., **48,** 179–185.

JENKINS, G.P., G.K. WALKER-SMITH and P.A. HAMER (2002) : Elements of habitat complexity that influence harpacticoid copepods associated with seagrass beds in a temperate bay. Oecologia, **131:** 598–605.

JONES, G.P. (1990) : The importance of recruitment to the dynamics of a coral reef fish population. Ecology, **71,** 1691–1698.

KAGAWA, M. (2003) : Breeding behavior, early life history, and ecology of the cardinalfish genus *Cheilodipterus* (Perciformes: Apogonidae). Msc Thesis, Tokai University, Shimizu. 57pp., 6 tables, 67 figs. (in Japanese).

LEE, S.Y., C.W. FONG and R.S.S. WU (2001) : The effects of seagrass (*Zostera japonica*) canopy structure on associated fauna: a study using artificial seagrass units and sampling natural beds. J. Exp. Mar. Biol. Ecol., **259,** 23–50.

LEVIN, P.S. (1994) : Fine-scale temporal variation in recruitment of a temperate demersal fish: the importance of settlement versus post-settlement loss. Oecologia, **97,** 124–133.

LEVIN, P.S., R. PETRIK and J. MALONE (1997) : Interactive effects of habitat selection, food supply and predation on recruitment of an estuarine fish. Oecologia, **112,** 55–63.

NAKAMURA, Y., M. HORINOUCHI, T. NAKAI and M. SANO (2003) : Food habits of fishes in a seagrass bed on a fringing coral reef at Iriomote Island, southern Japan. Ichthyol. Res., **50,** 15–22.

NAKAMURA, Y. and M. SANO (2004) : Comparison between community structures of fishes in *Enhalus acoroides*- and *Thalassia hemprichii*-dominated seagrass beds on fringing coral reefs in the Ryukyu Islands, Japan. Ichthyol. Res., **51,** 38–45.

ORTH, R.J., K.L. HECK JR and J. VAN MONTFRANS (1984) : Faunal communities in seagrass beds: a review of the influence of plant structure and prey characteristics on predator-prey relationships. Estuaries, **7,** 339–350.

SANO, M. (1997) : Temporal variation in density dependence: recruitment and postrecruitment demography of a temperate zone sand goby. J. Exp. Mar. Biol. Ecol., **214,** 67–84.

WILLIAMS, S.L. and K.L. HECK, JR. (2001) : Seagrass community ecology. *In* Marine community ecology. BARTNESS, M.D., S.D. GAINES and M.E. HAY (eds). Sinauer Associates, Sunderland, p.317–337.

ZAR, J.H. (1999) : Biostatistical analysis, 4th edn. Prentice Hall International, London, 663pp.

Seasonal variations in circulation and average residence time of the Bangpakong estuary, Thailand

Anukul Buranapratheprat[1,*] and Tetsuo Yanagi[2]

Abstract : Seasonal variations in 3-dimensional circulation and average residence time of conservative and passive tracer in the Bangpakong estuary were investigated using the Princeton Ocean Model (POM) and the Euler-Largrange method. Observed salinity and temperature, average wind velocity and river discharge, and calculated tidal elevation were significant inputs for computation. The results indicated that all driving forces interacted complicatedly to the seasonal variation of circulation in the estuary. Wind-driven current is predominant and its magnitude is large at the sea surface while tidal prevalence is observed throughout the water column. Influence of river discharges as an outflow and density-driven current is also observed near the river mouth during wet season. The tracer experiment indicated that tidal current played an important role to move particles out of the estuary in a short time and seasonal variation in residence time depended on variations in wind-driven circulation, tide and river discharge. Calculated residence times from the longest to the shortest are 29.1 days, 20.8 days, 10.8 days and 6.0 days in April, June, December and September, respectively, corresponding to those from a box model analysis based on the mass balance of salt using the same salinity and discharge data.

Keywords : circulation, residence time, POM, Bangpakong estuary, Gulf of Thailand

1. Introduction

The Bangpakong estuary is an estuary located in the northeastern corner of the upper Gulf of Thailand (Fig. 1) and is a highly eutrophic area where blooming of phytoplankton frequently occurs. Much nutrients and organic substances from the Bangpakong river are supposed to be the cause of the eutrophication in the estuary and surrounding areas (NRCT-JSPS, 1998, Jintasaeranee *el al.*, 2000 and Buranapratheprat *et al.*, 2002). How-

[1]Present address: Department of Geography, University of Victoria PO Box 3050, STN CSC, Victoria, BC V8W 3P5 Canada
Permanent address: Department of Aquatic Science, Faculty of Science, Burapha University, T. Saensuk, A. Muang, Chonburi 20131 Thailand
*Corresponding author
[2]Research Institute for Applied Mechanics, Kyushu University
Kasuga, Fukuoka, 816–8580 Japan

ever, we have not yet known the mechanism of the eutrophication because of complicated physical characteristics of this estuary. They are due to its shallowness, river discharge, tide and wind which interact intricately under strong seasonal variations. Therefore, if we do not understand well these entire mechanisms, we may not succeed in understanding the phenomena occurring in this estuary.

Takeoka and Hashimoto (1988) noted that transport of matter in coastal waters was an important subject relating to water quality problems, and that of nitrogen, phosphorus or carbon was especially important relating to eutrophication problems, which often spoiled the marine environment or even caused red tides or anoxic water masses. From this reason, circulation in the study area must be investigated because the results can be applied for further specific studies in terms of material transport, which help us to understand the
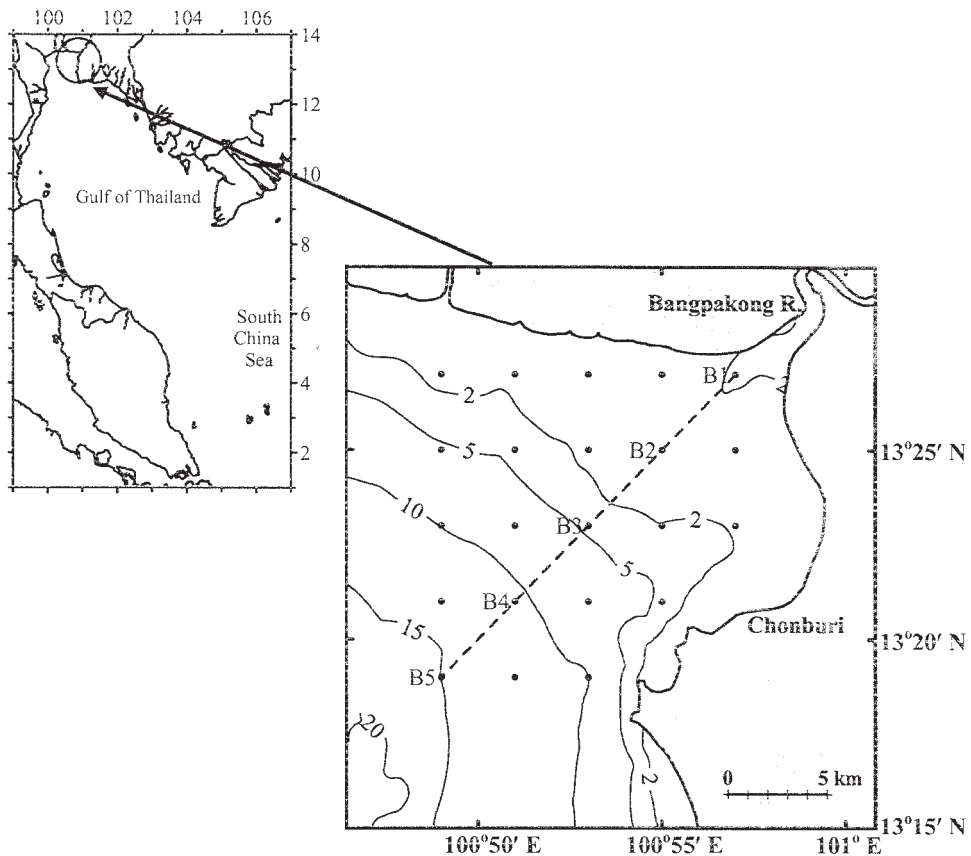
Fig. 1.   The Bangpakong estuary and its bathymetry in meters, dots and a broken line represent
observation points and the B-stations for vertical distributions, respectively.

behavior of materials in an estuary.
BURANAPRATHEPRAT and YANAGI (2000) tried
to calculate vertical circulation of the Bang-
pakong estuary using a vertical 2-dimensional
diagnostic model. Unfortunately, this model
could not reproduce strong horizontal circula-
tion generated by wind and river discharge
that had 3-dimensional structure. They sug-
gested that only 3-dimensional hydrodynamic
model should succeed to reproduce circulation
generated by all significant driving forces.
Therefore, in this study, we will use a 3-
dimensional hydrodynamic model, the Prince-
ton Ocean Model (POM), to investigate the
circulation in the Bangpakong estuary.

Residence time of material in an estuary is a
significant physical characteristic. It depends
on the exchange time of the material in the
area (YANAGI, 1999a). Longer residence time of

any material means more opportunity of the
material to interact physically, chemically or
biologically with surrounding water. For in-
stance, if inorganic nutrients carried by river
water into an estuary have long residence time,
any plants and phytoplanktons living there
will have more chance to use them for their
photosynthesis. BURANAPRATHEPRAT et al.
(2002) used a box model based on the mass bal-
ance of salt to investigate the seasonal varia-
tion in residence time of fresh water in the
Bangpakong estuary. They found that long
residence time appeared during the transition
period between dry and wet seasons, and wet
and dry seasons. Short residence times were ob-
served in mid-seasons, dry and wet seasons.
They suggested that such results occurred
from interaction between river discharge vary-
ing seasonally and tidal force. This hypothesis

needs proofing because the box model in that study can not elucidate in details what is really occurring or what are the actual factors governing the phenomenon. Therefore, we will calculate the residence time of material in the estuary in terms of passive tracer experiment using POM to confirm the results of the previous study and to investigate the mechanism of material transport in the Bangpakong estuary.

2. Field observations

Field observations in the Bangpakong estuary were conducted four times according to seasonal variation in river discharge presented in BURANAPRATHEPRAT *et al.* (2002). They are the dry season (5 and 7 April 2002), the transition period from dry to wet seasons (15–16 June 2002), the wet season (13–14 September 2002), and the transition period from wet to dry seasons (13–14 December 2002). Figure 1 shows sampling stations (dots) covering the entire estuary and a broken line in central part of the area (B-stations) indicates stations for vertical distributions. Salinity and temperature were measured from the sea surface to the bottom every 0.5 meter using a CTD/STD meter (Sensor Data model SD204). These data including calculated density in terms of sigma-t (σ_t) are used to study the horizontal and vertical distributions of these parameters in the estuary. The observed salinity and temperature are also employed in POM as computational inputs for the circulation and the tracer experiment.

Seasonal variations in horizontal distributions of salinity, temperature and density at the sea surface are illustrated in Fig. 2. Temporal changes in salinity and density depended on the river discharge, while that in temperature was not prominent because the area was located in the tropical zone. The lowest sea surface water temperature was around 28℃ and the highest was around 32℃ in December and June, which were wintertime and summertime, respectively. Lowest salinity but highest gradient in sea surface salinity appeared in September while highest salinity but lowest gradient occurred in April. The salinity distributions also showed the penetration of fresh water into the northwest of the area in April and June.

We can observe the plume obviously in April when sea surface salinity is high in almost area but low salinity emerges just in the northwest. In December, the distribution of sea surface salinity showed a plume of fresh water from the Bangpakong river having trend to the west more than to the south of the river mouth.

Seasonal variations in vertical distributions of salinity and temperature along B-stations in Fig. 1 are presented in Fig. 3. Vertical distribution of density is not shown because it varies in the same way as that of salinity (Fig. 2). As a result, the density variation will be discussed from the salinity distribution. Temperature near the river mouth at the sea surface was higher than that near the sea boundary in all seasons except December which was wintertime. It might depend on the difference in temperature between land and sea which was not quite large and fresh water from land was a little colder than outside seawater in wintertime. Vertical distribution of salinity also showed seasonal interaction of river water and seawater. Seawater intruded into the river during the time of low river discharge in April causing high salinity near the river mouth. On the other hand, salinity became much lower in June and September when river discharge was very large. In both seasons, fresh water from the river floated over salty water while going further from the river mouth to the sea which was the major cause of stratification there. Salinity gradient was largest in September due to the largest magnitude of river discharge at this time.

A scene of transition period from wet to dry seasons appeared in the vertical distribution of salinity in December when the river discharge became smaller. Intrusion of fresh water from another source outside the study area was also observed in the vertical distribution of salinity in April. When we consider with the horizontal distributions of surface salinity and surface density in April (Fig. 2), the contour line of 29 psu in Fig.3 suggests the fresh water intrusion from the west.

3. Circulation model

The Princeton Ocean Model (POM) is applied to calculate the 3-dimensional circulation of the
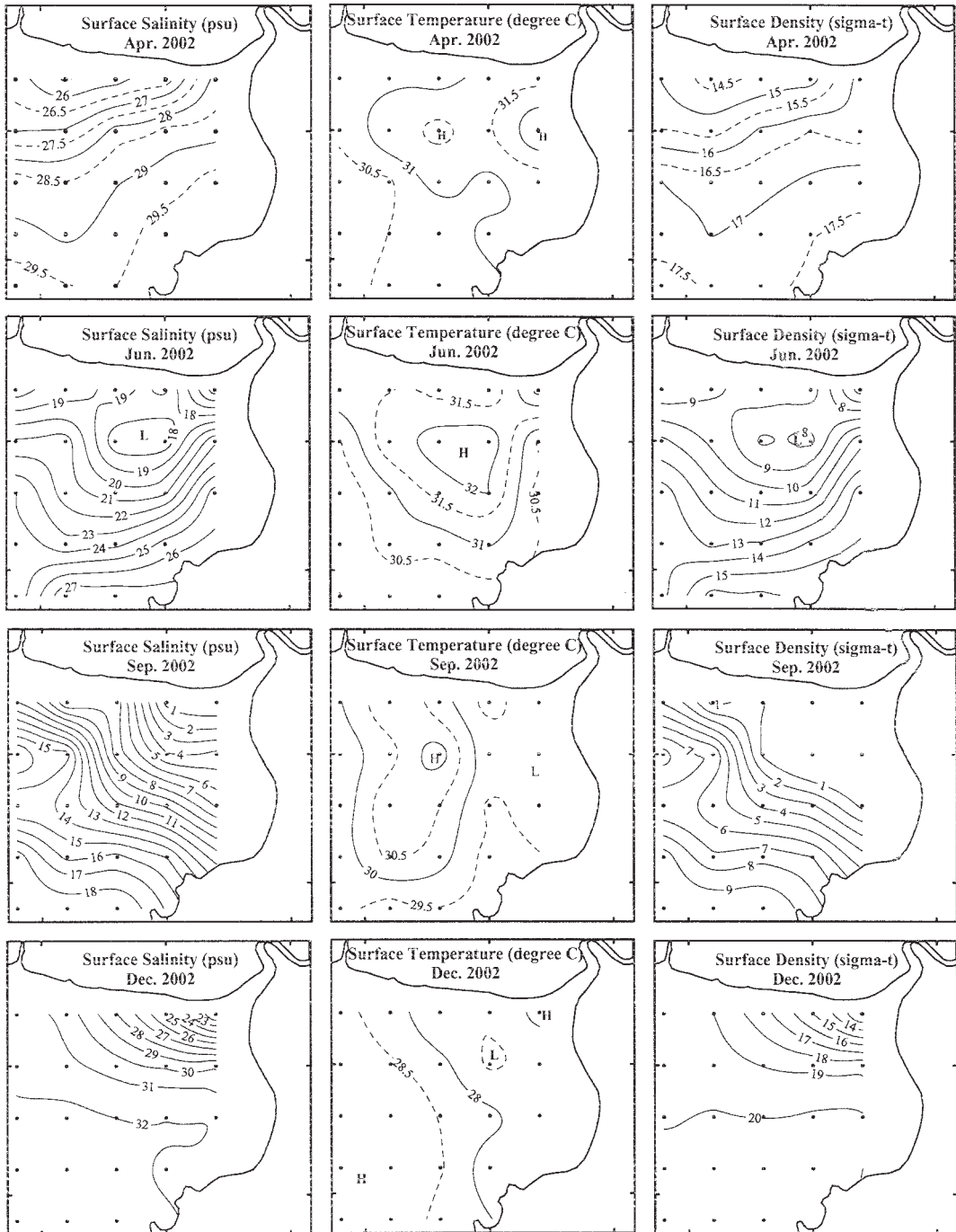
Fig. 2.   Seasonal variations in surface distributions of water temperature, salinity and density (sigma-t).
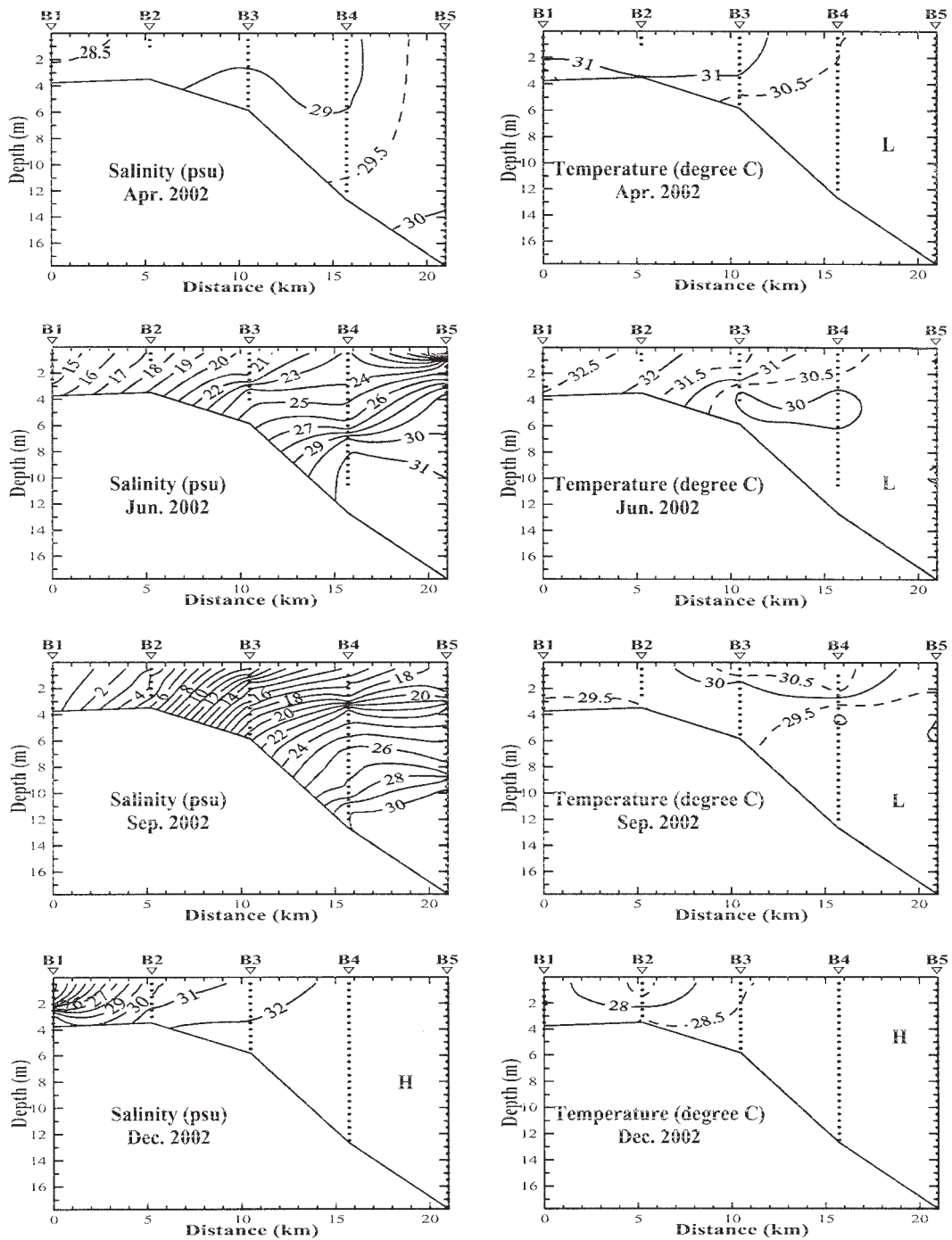   Dots show the observation stations.

Fig. 3. Seasonal variations in vertical distributions of water temperature and salinity along the B-stations. Dots show the observation points.
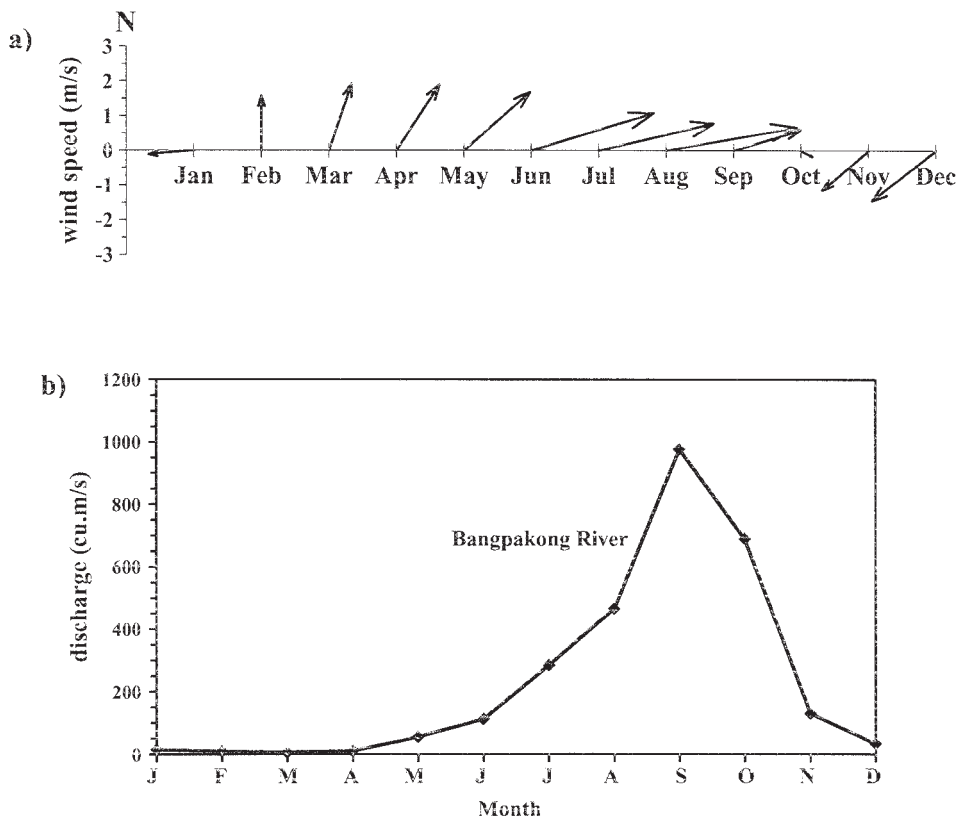
a)

b)

Fig. 4.   Seasonal variations in average wind velocity over the Bangpakong estuary (applied from
BURANAPRATHEPRAT and BUNPAPONG (1998)) (a) and average discharge of the Bangpakong River
(BURANAPRATHEPRAT et al., 2002) (b).

Bangpaking estuary. The governing equations
of the model consist of conservation of mass,
momentum, salinity and temperature under
the hydrostatic and Boussinesq approxima-
tions written in a bottom-following, sigma co-
ordinate system (BALOTRO et al., 2002). The
model has a free surface and a split time step.
The external mode portion of the model is 2-
dimensional and uses a short time step based
on the Courant-Friedrichs-Levi (CFL) condi-
tion and the external wave speed. The internal
mode is 3-dimensional and uses a long time step
based on the CFL condition and the internal
wave speed (MELLOR, 1998). Vertical mixing
coefficient is calculated in an imbedded second
moment turbulence closure sub-model, while
the Smagorinski diffusivity equation is applied
for horizontal diffusivity. POM is a sigma co-
ordinate model in that the vertical coordinate is

scaled on the water column depth. Although
the horizontal grid uses curvilinear orthogonal
coordinates, it is easy for users to apply an-
other horizontal grid system such as orthogo-
nal and spherical coordinates. More details in
POM including mathematical description are
referred to BLUMBERG and MELLOR (1987), and
MELLOR (1998).

The estuary area is divided horizontally into
37×37 grids in the spherical coordinate with
grid spacing 0.5×0.5 minutes in latitude and
longitude, respectively. The vertical domain is
divided into 10 σ-levels with no logarithmic por-
tions. Bathymetry data of the Bangpakong es-
tuary are digitized from the navigation chart
produced by the Royal Thai Navy. Salinity and
temperature data from the observations are in-
terpolated horizontally using Gaussian inter-
polation   and   vertically   using   linear

interpolation to fit all grid spacing of the computational domain. Average discharge of the Bangpakong river (Fig. 4b) conditioned at the river boundary is from the study of BURANAPRATHEPRAT et al. (2002), and the average wind velocity (Fig. 4a) is estimated from that of BURANAPRATHEPRAT and BUNPAPONG (1998), because the river discharge and wind data in 2002 have not been published yet. As the meteorological condition in 2002 was not unusual, the employing average river discharge and wind data will not become a serious problem. Tidal stress calculation from tidal calculation (BURANAPRATHEPRAT et al., 2003) is also included in this model.

Normal components of velocity to land boundary are set to be zero while radiation condition is assigned along open boundary in the internal mode that is also used as boundary condition along the open boundary for salinity and temperature. Tidal force in terms of water elevation along the open boundary is extracted from computational results of a 2-dimensional hydrodynamic model from the study of BURANAPRATHEPRAT et al. (2003), and it is updated in POM every external time step. The model is operated in diagnostic mode called the robust diagnostic mode where a damping term is added to the conservation equations of temperature and salinity. Please see more details in BALOTRO et al. (2002). Seawater state is set at rest at initial time of model operation (t = 0). Time steps are 3 seconds and 45 seconds for the external mode and the internal mode, respectively. The model is forced by wind, tide and river discharge from initial state until reaching a quasi-steady state 30 days after the beginning of calculation. Computed circulations from 30 days to 60 days are averaged to present the residual circulation of the estuary.

Seasonal variations in circulation of the estuary at the sea surface (0.5 m), 5.0 m depth and 8.0 m depth are presented in Fig. 5a and 5b. Wind driven current is predominant at the sea surface and has a strong seasonal change while tide-induced residual current influences over entire water column. Current induced by river discharge could be observed near the river mouth during the time of relatively large discharge especially in September. Surface current

is quite complicated and not so strong with a tendency of flow into the river mouth following wind direction in April. Many small and weak eddies also appear throughout the area. At 5.0 m and 8.0 m depths, two eddies, a clockwise and an anti-clockwise, are generated near west and south boundaries, respectively. Current in these deeper layers inside the area is very weak and tend to flow seaward in southwest direction.

Surface current seems very strong in June (Fig. 5a lower panel) because wind speed is strongest over other seasons during this time. There is a strong flow coming into the area through the north of west boundary being in line with wind direction. This flow is then separated into two parts; one moves directly further into the inner estuary reaching the east coast, while the other bends to the south and flows out of the area through south boundary. A weak outflow by the river discharge is observable at the east coast near the river mouth. This river flow then converges with current coming from the southwest which is supposed to be a part of separated flows coming through the west boundary. There is only an area in the northern coast that current is very weak. A clockwise eddy that used to emerge near west boundary in deeper layers in April seems to spread wider but an anti-clockwise one near south boundary almost disappears and turns to be a flow coming in from the east and going out from the west of south boundary at 5.0 m depth during this time. All eddies are combined and transformed to be a meander starting near the south boundary and ending at west boundary at 8.0 m depth.

Surface current is still strong and moderately complicated during the time of largest river discharge in September (Fig. 5b upper panel). The river outflow is strongest and density driven current could be clearly observed at the river mouth. A strong clockwise gyre appears at the north of west boundary and an anti-clockwise gyre arises at south boundary near the east coast. Over all flowing pattern has a trend of water coming in from west boundary and going out the area from south boundary. Two eddies near both open boundaries like those in April also emerge in deeper
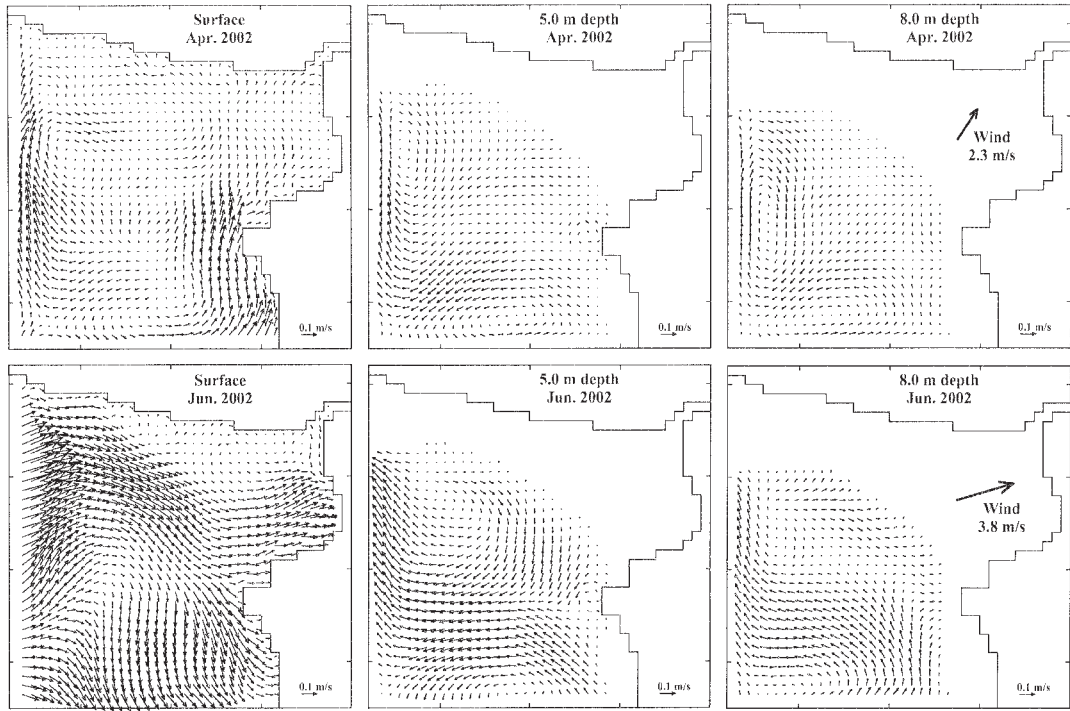
Fig. 5a.   Calculated circulations at surface, 5.0 m depth, and 8.0 m depth in April and June 2002.
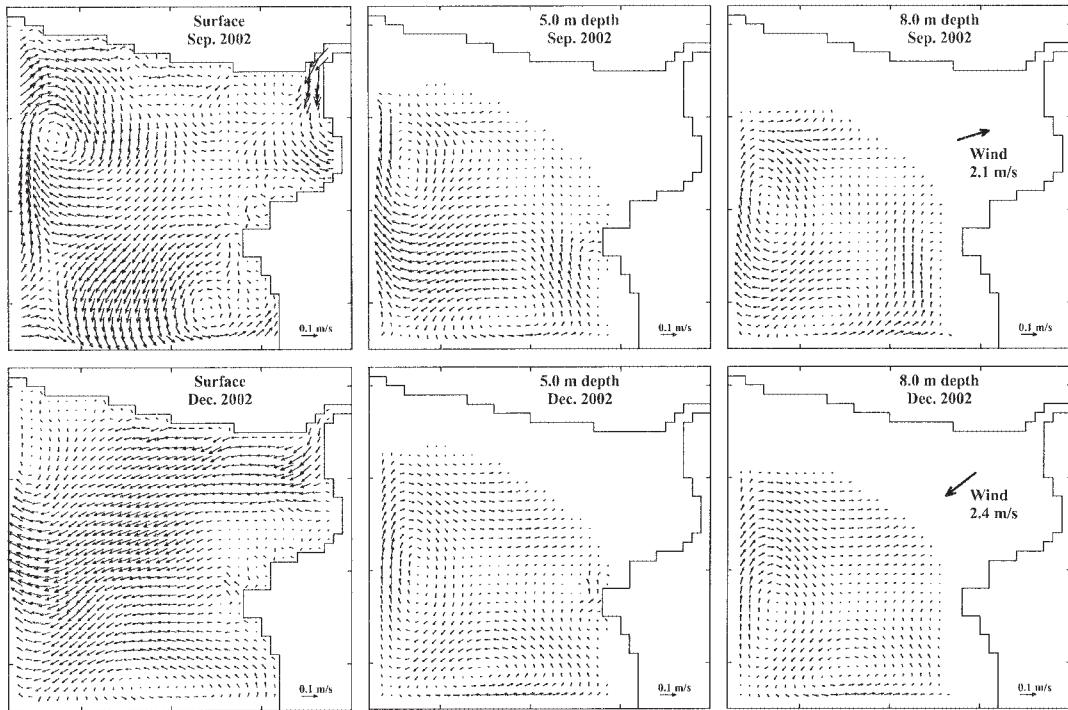

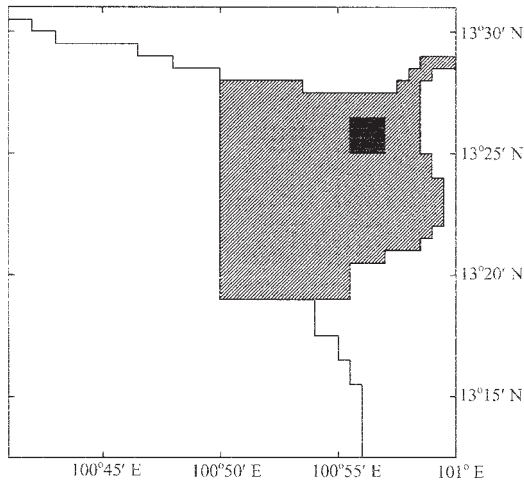Fig. 5b.   Same as Fig. 5a but for September and December 2002.

Fig. 6. Initial position of particles (solid rectangular area) and the boundary for the tracer experiment (screen area)

layers and near bottom water intrusion occurs along the north and east coasts. Current patterns at the sea surface in December (Fig. 5b lower panel) have a trend to flow seaward from the river mouth and move out through the middle of west boundary following the northeast wind that occupies over the area during this time. Eddies still appear along the open boundaries but they are very much weaker than those in September. Current patterns in deeper layers are not so different from the previous season, that is, there are two eddies along both open boundaries and intrusion of near bottom water into the river mouth from mid-area. Occurrence of the intrusion of near bottom water in September is supposed to be a part of density driven current because fresh water discharge is very large during this time while that in December should be occurred from compensation process to the outflow surface water from the river mouth to the sea.

Although the calculated currents are quite strong especially near the open boundary, the tracer experiment is still reliable because we focus our attention to the near field of river mouth shown Fig. 6 where the effect of currents near the open boundaries is very small.

4. Passive tracer experiment

We also apply POM for a material transport

study in terms of the passive tracer experiment using Euler-Largrange method (YANAGI, 1999 a). A passive tracer having no sinking speed is initially spread into the computed current field near the river mouth and then its spatial and temporal distributions are calculated. The position of tracer X_{n+1} (x^{n+1}, y^{n+1}, z^{n+1}) at time $n+1$, which was X_n (x^n, y^n, z^n) at time n, can be calculated by the following equations:

$$X_{n+1}=X_n+V\Delta t+\frac{1}{2}(\nabla V)\, V\Delta t^2,\qquad(1)$$

where V denotes the three-dimensional velocity vector of residual flow, (Δt is the time step, and ∇ is horizontal gradient. The spherical coordinate is used for the horizontal spatial derivatives. Thus those terms in equation (1) are transformed according to equations (2) and (3) as following:

$$\frac{\partial}{\partial x}=\frac{1}{a\cos\varphi}\frac{\partial}{\partial\lambda},\qquad(2)$$

$$\frac{\partial}{\partial y}=\frac{1}{a}\frac{\partial}{\partial\varphi},\qquad(3)$$

where a is average radius of the Earth (6.37×10^6m) ; φ and λ are latitude and longitude, respectively.

A tracer module is added in the internal mode of POM and solved at the same time of the circulation and steps of the model operation are also the same as that of the circulation model. After all forces have been added and the circulation reaches a quasi-steady state about on 30 days, the tracers of 3,600 particles are spread at the sea surface near the river mouth (black square in Fig. 6) and then their movements are tracked until they all move out of a bounded area (screened area in Fig.6) or the computational time is over on 60 days. It should be noted here that computational boundary of the tracer experiment is smaller than that of the circulation as shown in Fig. 6. The reason is that we intend to compare our results with those from the previous study by BURANAPRATHEPRAT *et al.* (2002); therefore, the experimental area is set to close to the area in that study for equality in comparison. Residence time of the tracers will be derived from temporal change in their remaining number in the study area.

In order to find out the seasonal variation in average residence time of tracers in the area, a technique described by TAKEOKA (1984) and YANAGI (1999a), which has been applied in the studies of TAKEOKA and HASHIMOTO (1988), BALOTRO et al. (2002), and BALOTRO et al. (2003), is also applied in this study. We will investigate how the study area responses to the instantaneous input provided in the area in terms of the remnant function $(r(t))$, which is shown below.

$$r(t) = R(t)/R(0), \qquad (4)$$

where $R(t)$ and $R(0)$ are the total number of tracers existing in the study area at any given time, and that in the initial time, respectively. Then the average residence time of the tracer (τ_r) can be calculated by time integrating the results of the remnant function. That is

$$\tau_r = \int_0^\infty r(t)dt. \qquad (5)$$

Seasonal variations in tracer distribution after spreading for 3 days, 5 days and 10 days are illustrated in Fig. 7 in order to see enough snapshots of their movement in the estuary. In April, the tracers are little dispersed and shift to the west of the river mouth on 3 days that they also remain around there by closer to the northern coast on 5 days. Most of them still last near the river mouth but some row in east-west along the north coast from the river mouth to west boundary on 10 days. Different scenes of the distribution are observed in June which is the transition period from dry to wet seasons. The particles move southwestward with a little spreading from the river mouth to mid-area from 3 days to 5 days. Instead of accumulation in a small area like in April, most of them still remain but are spreaded widely in almost entire the area on 10 days. Large river discharge in September makes the tracers widely disseminate and drives them out of the estuary very rapidly. Therefore, the distribution on 3 days in the central area looks not so thick because some particles have been moved out through the sea boundaries already. They are also spread widely but not many of them are still left inside the area on 5 days; however,

rare numbers could be observed at the west of northern coast on 10 days. Particles are lined up in north-south in the mid-area on 3 days after releasing in December. Lower parts of this particle stripe are transported out through west boundary on 5 days and only small numbers with a few patches of them still suspend in the west of the river mouth vicinity on 10 days.

Time series plots of the remnant functions and calculated residence times of the tracers derived from equations (4) and (5) are illustrated in Fig. 8. Residence times are 29.1 days, 20.8 days, 6.0 days and 10.8 days in April, June, September and December, respectively. Longest residence time in April (29.1 days) occurs because of accumulation of the tracer with little spreading at the north coast (Fig. 7) of the estuary for a long time. The remnant function curve in April also shows that all particles still remain in the area until 17 days and then move out very slowly with about 3,000 particles left in the area at the end of calculation. In June, particles are dispersed widely and gradually transported out of the area starting from 5 days resulting in continually reduction in rate of the remnant functions and turns its residence time (20.8 days) to be the second order after that in April. Unlike the two previous seasons, residence time of the tracer is very short in September (6.0 days) because all particles are flooded out very rapidly by large river discharge. This phenomenon agrees to sharply reduction in the remnant function rate of change (Fig. 8) and the value becomes zero just on 15 days. However, although its rate of change reduces very fast at first, the remnant function in December still maintains itself in a narrow range from 0.2 to 0.4 from 5 days until the end of computation. This is the reason why the residence time in this season (10.8 days) is longer than that in September but shorter than those in April and June.

5. Discussions

Influences of wind, tide, and river discharge on circulation in the Bangpakong estuary vary in spatial and temporal scale. Seasonal variations in surface circulations (Fig. 5a and 5b) are mostly affected by wind and river discharge while influence of tide could be observed in
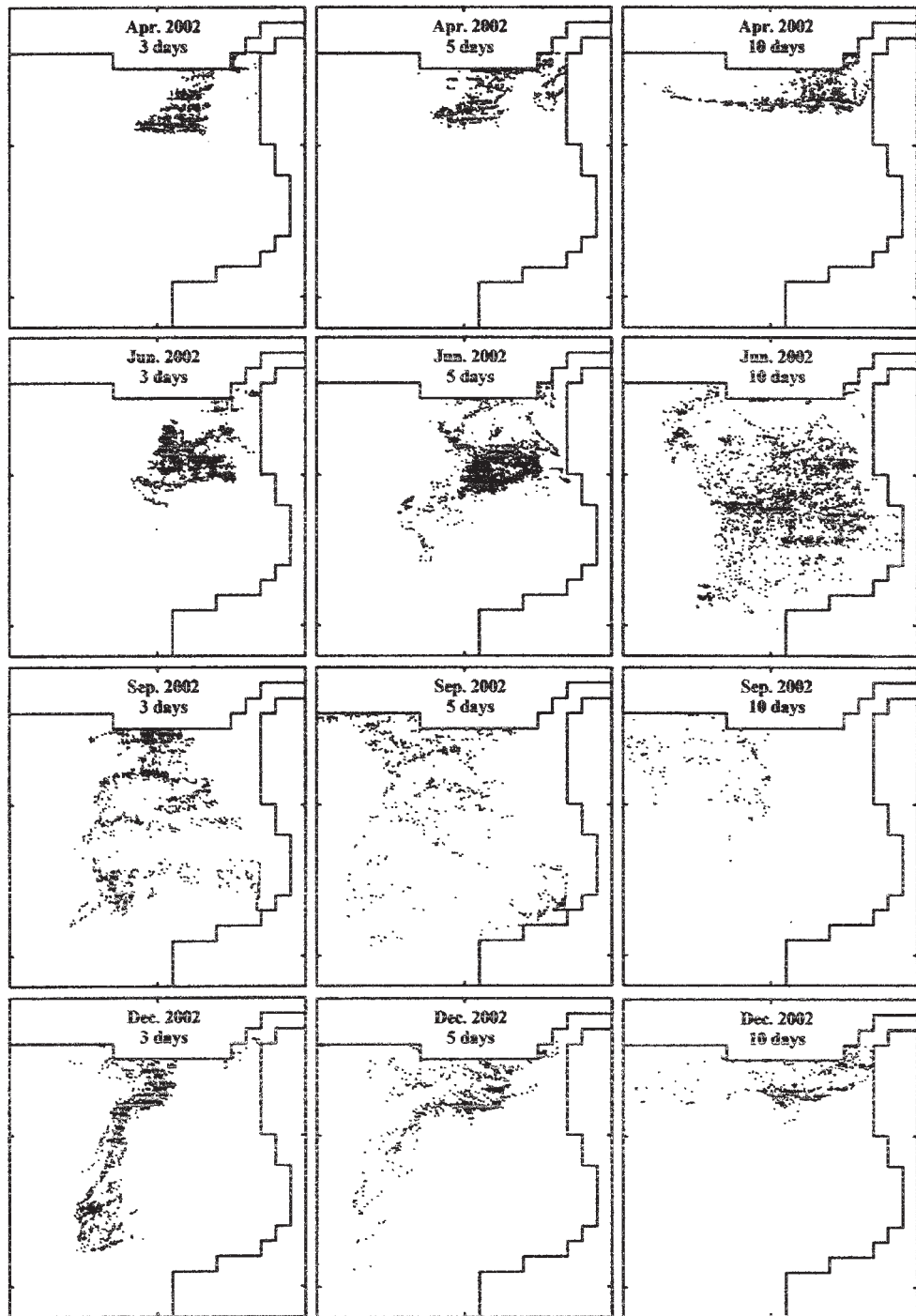
Fig. 7.   Seasonal variation in predicted tracer distribution after 3 days, 5 days and 10 days.

Apr. 2002
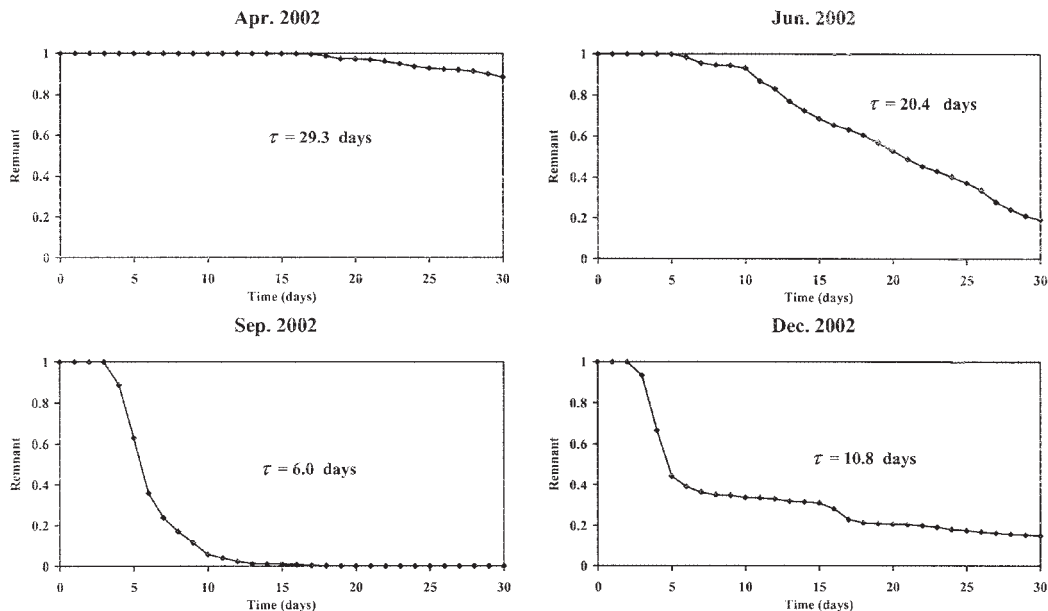
Jun. 2002

Sep. 2002

Dec. 2002

Fig. 8. Seasonal variations in the remnant function and average residence time of tracer.

entire water column. Surface current is quite strong but not so complicated when wind speed has strong power over other forces such as the condition in June. On the other hand, when there is not a force strong enough to govern the entire area, the current patterns would be complicated due to the interaction of all influences such as those in April, September and December. Permanent eddies, a clockwise and an anti-clockwise along west and south boundaries, respectively, in deeper layers are supposed to be generated by tide which is not changed seasonally. These results agree well with the calculated residual current driven by tide and wind in the study of BURANAPRATHEPRAT *et al.* (2003) which shows that the current patterns around that area do not quite change seasonally.

Influences of wind and river discharge are also observed in deeper layers when their influences are relatively strong. In June, for example, the stronger and wider clockwise eddy and the incomplete anti-clockwise one near south boundary at 5.0 m depth, and also transforming from eddies to a meander at 8.0 m depth are supposed to be caused by strong wind during that time. On the other hand, inflows of near bottom water from the mid-area to the river

mouth in September suggest the occurrence of density-driven current because the river discharge is very large during that time. Alternative directions to the surface circulations of near bottom flow when the discharges are small may arise because of compensation process.

Interaction between circulation (Fig. 5a and 5b), material distribution (Fig. 7), and its residence time is discussed. It is quite clear that seasonal variations in wind driven circulation and river discharge have influence to the material distribution and also residence time. Longest residence time of the tracer in April (29.3 days) is controlled by moderate southwest winds which generate landward current to the river mouth at the same time of low river discharges. Therefore, particles will be forced to remain near the river mouth for a long time. In case of June although wind directions are also almost from the southwest, the residence time (20.4 days) becomes shorter than that in April because the discharge during this time is twelve-times larger (10 m^3/s and 120 m^3/s in April and June, respectively) and wind speed is stronger (2.3 m/s and 3.8 m/s in April and June, respectively). Instead of keeping particles inside the area, strong wind driven current will disperse
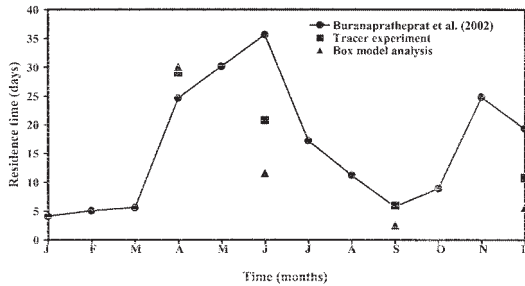
Fig. 9. Comparison of calculated residence times from the tracer experiment (solid rectangular) and box model analysis (solid triangle) with the results from the study of BURANAPRATHEPRAT *et al.*, (2002) (solid circle and solid line).

them widely in a short period (Fig. 7). Consequently, there is more opportunity that the particles are not so difficult to be conveyed by current out of the estuary.

The residence time of material is relatively very short in September (6.0 days) because the river discharge is extremely large even though wind is landward to the river mouth at that time, as a result the particles are flooded out in a very short time. In December, although the river discharge is very small (35 m³/s) but the wind direction is seaward, the residence time (10.8 days) is therefore longer than that in September but shorter than those in April and June. This phenomenon confirms that the river discharge and wind speed play a significant role in controlling residence time of materials in the estuary. The influence of tide is not illustrated but should be noted here. The results of model operation with tidal force suggest the importance of tide that helps the material to move out of the estuary in a short time comparing with the operation without it.

Results from the tracer experiment are compared with those derived from a simple box model based on the mass balance of salt using the same salinity and river discharge data, and from the study of BURANAPRATHEPRAT *et al.* (2002) who also applied such a box model to investigate the residence time of fresh water in the same study area. Boundary for the box model analysis is assigned in the same way as that used in the previous study for equality in comparison. Please see more details of box model calculation in GORDON *et al.* (1996), YANAGI (1999b) or BURANAPRATHEPRAT *et al.*

(2002). All the results are plotted and illustrated in Fig. 9. Results of box model analysis from this study which are 30.1 days, 11.7 days, 2.6 days and 5.7 days in April, June, September and December, respectively, indicate the same trend of seasonal variation in residence time to those from the tracer experiment. This suggests that the residence time of material based on calculated circulation with the use of Euler-Largrange method can reproduce the results derived from the mass balance of salt. However, the results in every seasons from this study also have the same trend as those from the previous study except that in June. In this study, the longest value appears in April while that of the previous study emerges in June. This suggests a possibility of year-to-year variations of river discharge and/or wind. If discharge is smaller and wind speed is weaker in June of some year which is the transition period from dry to wet seasons, the residence time of material can become very long in the same way as that in the previous study. It should be noted here that the distinct characteristics of computed material and fresh water such as diffusion and dispersion properties might result in the difference of calculated residence times from the tracer experiment and the box model analysis.

Importance of the transition period when DIN (dissolved inorganic nitrogen) and chlorophyll-*a* concentration are high, which was discussed in BURANAPRATHEPRAT *et al.* (2002), still remains because not only residence time but also the nutrient loading has to be considered. The rough multiplication of calculated residence times from this study (29.1 days, 20.8 days, 6.0 days and 10.8 days in April, June, September and December, respectively) and DIN load estimated from the results presented in BURANAPRATHEPRAT *et al.* (2002) (10 tons/month, 300 tons/month, 500 tons/month and 30 tons/month in dry season, transition period from dry to wet seasons, wet season and transition period from wet to dry seasons, respectively) also show highest concentrations of DIN during the transition period between dry and wet season. Therefore, the hypothesis that eutrophication in this estuary is promoted during this transition period is still reasonable.

This study has made us to understand clearer in physical processes in terms of water circulation and a material transport. However, we will also use an ecological model which considers not only physical processes but also biogeochemical processes to investigate the mechanism of eutrophication phenomenon in the Bangpakong estuary in the near future.

6.   Conclusions

POM is applied for investigation the seasonal variations in 3-dimensional circulation and residence time of a tracer in the Bangpakong estuary employing observed salinity and temperature, average wind velocity, river discharge, and calculated tidal elevation as significant computational inputs. Wind driven current is predominant and its magnitude is large at the sea surface while tidal prevalence is observed throughout the water column. Influence of river discharges as an outflow and density driven current are also observed near the river mouth during wet season. The tracer experiment indicates that tide plays an important role to move material out of the estuary in a short time. However, seasonal variation in residence time mainly depends on variations in wind driven circulation and river discharge, that is, it is longest in April and shortest in September.

References

BALOTRO, R. S., A. ISOBE and M. SSHIMIZU (2003): Seasonal variability in circulation pattern and residence time of Suo-Nada. J. Oceanogr., **59**, 259–277.

BALOTRO, R. S., A. ISOBE, M. SSHIMIZU, A. KANAEDA, T. TAKEUCHI and H. TAKEOKA (2002): Circulation and material transport in Suo-Nada during spring and summer. J. Oceanogr., **58**, 759–773.

BLUMBERG, A. F. and G. L. MELLOR (1987): A description of a three-dimensional coastal ocean circulation model. p. 1–16. *In* Three-Dimensional Coastal Ocean Models, Coastal and Estuarine Sciences, 4, ed. by N. S. HEAPS, AGU, WASHINGTON, D.C.

BURANAPRATHEPRAT, A. and M. BUNPAPONG (1998): A two dimensional hydrodynamic model for the Gulf of Thailand. Proceedings of The IOC/WESTPAC Fourth International Scientific Symposium, 469–478.

BURANAPRATHEPRAT, A. and T. YANAGI (2000): Hydrodynamical conditions of the Bangpakong estuary in wet and dry seasons. Reports of the Research Institute for Applied Mechanics, Kyushu University, **119**, 83–87.

BURANAPRATHEPRAT, A., T. YANAGI and P. SAWANG-WONG (2003): Seasonal variations in circulation and salinity distributions in the upper Gulf of Thailand: modeling approach. La mer, **40** (3), 141–156.

BURANAPRATHEPRAT, A., T. YANAGI, T. BOONPHAKDEE and P. SAWANGWONG (2002): Seasonal variations in inorganic nutrient budgets of the Bangpakong estuary, Thailand. J. Oceanogr., **58**, 557–564.

GORDON, Jr., D.C., P.R. BOUDREAU, K.H. MANN, J.-E. ONG, W.L. SILVERT, S.V. SMITH, G. WATTAYA-KORN, F. WULFF and T. YANAGI (1996): LOICZ Biogeochemical Modelling Guidelines. LOICZ Reports & Studies No 5, 96 pp.

JINTASAERANEE, P., A. BURANAPRATHEPRAT and P. SAWANGWONG (2000): Dynamics of some water qualities of the Bangpakong estuary, Proceedings of the 11th, Joint Seminar on Marine Science, 9–15.

MELLOR, G. L. (1998): User's guide for a three-dimensional, primitive equation, numerical ocean model. Program in Atmospheric and Oceanographic Sciences Report, Princeton University, Princeton, N.J., 41 pp.

NRCT-JSPS (1998): An integrated study on physical, chemical and biological characteristics of The Bangpakong estuary. Final Report Cooperative Research NRCT-JSPS, the National Research Council of Thailand (NRCT) and the Japan Society for the Promotion of Science (JSPS), 127 pp.

TAKEOKA, H. (1984): Fundamental concepts of exchange and transport time scales in a costal sea. Cont. Shelf Res., **3**, 311–326.

TAKEOKA, H. and T. HASHIMOTO (1988): Average residence time of matter in coastal waters in a transport system including biochemical processes. Cont. Shelf Res., **8**, 1247–1256.

YANAGI, T. (1999a): Coastal Oceanography. Terra Scientific Publishing, Tokyo, 162 pp.

YANAGI, T. (1999b): Seasonal variation in nutrient budgets of Hakata Bay, Japan. J. Oceanogr., **55**, 439–448.

Chlorophyll *a* and primary production in the northwestern Pacific Ocean, July 1997

Akihiro Shiomoto*, Shinji Hashimoto** and Takahiko Kameda***

Abstract : Chlorophyll *a* (Chl *a*) concentration and primary production were measured within the euphotic zone which was defined as from the surface to a depth corresponding to 1% of the surface light intensity (1% light depth), in the northwestern Pacific, July 1997. Stations were divided into the Western Subarctic Gyre (WSG) and the Transition Domain (TD). The Chl *a* concentrations ranged from 0.42 to 2.61 mg m^{-3} in the WSG (mean $\pm$ standard error: 1.86 ± 0.16 mg m^{-3}, n=16) and from 0.33 to 0.57 mg m^{-3} in the TD (0.42 ± 0.01 mg m^{-3}, n=24). The daily primary production integrated in the upper 1% light depth ranged from 910 to 2886 mgC m^{-2} d^{-1} in the WSG (1744 ± 459 mgC m^{-2} d^{-1}, n=4), and from 738 to 1629 mgC m^{-2} d^{-1} in the TD (1094 ± 152 mgC m^{-2} d^{-1}, n=6). The WSG in this study was on the relatively high side of Chl *a* concentrations compared to previous studies in the western subarctic North Pacific during summer season. Moreover, the relatively high Chl *a*-specific primary production (79.4 and 62.4 mgC (mgChl *a*)$^{-1}$ d^{-1}) was also observed compared with the values reported previously in the western subarctic North Pacific in summer (<55 mgC (mgChl *a*)$^{-1}$ d^{-1}). Therefore phytoplankton bloom may occur in the WSG in summer. It is possible that the rise in temperature in early summer is one of the factors for the occurrence of phytoplankton bloom in the summertime WSG. While in the TD, the Chl *a* standing stocks integrated in the upper 1% light depth were nearly equal between stations. However, the daily primary production tended to increase in the southward direction. This trend could be attributed to an increase of the phytoplankton growth rate due to the rise in temperature.

Keywords : *chlorophyll a, primary production, Western Subarctic Gyre, summertime bloom*

1. Introduction

The Alaskan Gyre (AG) is in the eastern subarctic North Pacific and the Western Subarctic Gyre (WSG) is in the west (e.g. Favorite *et al.*, 1976; Fig. 1). Many studies regarding chlorophyll *a* (Chl *a*) and primary production have been carried out in the AG, principally at or in the vicinity of station P (50° N and 145° W) (e.g. Parsons and Lalli, 1988; Welschmeyer *et al.*, 1993; Wong

*National Research Institute of Fisheries Science, 2–12–4, Fukuura, Kanazawa-ku, Yokohama, Kanagawa, 236–8648 Japan
**Japan Science and Technology Corporation, c/o Hydrospheric Atmospheric Research Center, Nagoya University, Chikusa-ku, Furo-cho, Nagoya, Aichi, 464–8601 Japan
***National Research Institute of Far Seas Fisheries, 5–7–1 Shimizu-Orido, Shizuoka, Shizuoka, 424–8633 Japan

et al., 1995; Boyd and Harrison, 1999). In contrast, there has been very little information regarding Chl *a* concentration and primary production in the WSG. Hence, Shiomoto *et al.* (1998) measured Chl *a* concentration and primary production in July 1993 and 1994. They observed summer phytoplankton bloom in 1993 (Chl *a* concentration: 6.95 mg m^{-3}; primary production: 1050 mgC m^{-2} d^{-1}) for the first time, but at only one station.

On the other hand, Banse and English (1994, 1999) showed that phytoplankton pigment levels are low during spring and summer, and that autumn blooms occur in the WSG, based on the Coastal Zone Color Scanner (CZCS) data during 1978 through 1986. In contrast, recently Sasaoka *et al.* (2002) observed an increase in Chl *a* concentration from summer in the WSG and maximum values in autumn, based on Sea-viewing Wide Field-of-
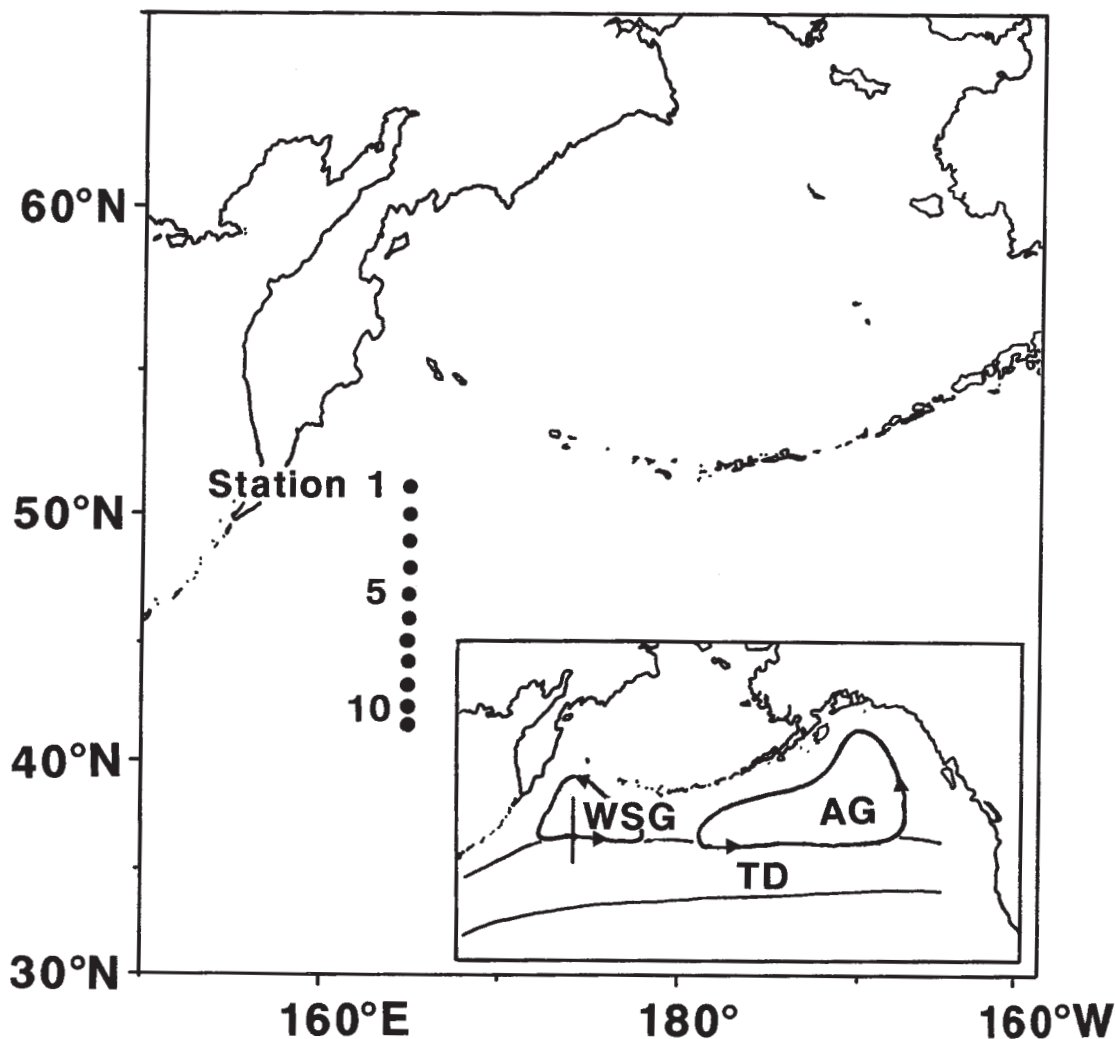
Fig. 1.   Location of sampling stations in the northwestern subarctic Pacific in July 1997. Stations 1–4 and 5–11 were divided between the Western Subarctic Gyre and the Transition Domain, respectively. The vertical line in the superimposed figure indicates the observation line in the present study.

view Sensor (SeaWiFS) data. This implies that phytoplankton in the WSG set about blooming in early summer.

Hence, to ascertain whether or not phytoplankton bloom occurs in the summertime WSG, we measured Chl *a* concentration and primary production in July 1997 at the same stations as the observation stations of SHIOMOTO *et al.* (1998). In this paper, we suggest that phytoplankton in the WSG set to their bloom in summer. We, furthermore, refer to the characteristics of Chl *a* and primary

production in the Transition Domain (TD) located just south of the WSG (e.g. FAVORITE *et al.*, 1976; Fig. 1).

2. Materials and methods

This study was conducted during cruises of the R/V Hokko Maru belonging to the Hokkaido National Fisheries Institute in July1997. Stations were located every 1° between 41° N and 51° N along 165° E (Fig. 1).

Seawater samples were collected at 2 a.m. from four depths corresponding to 100, 30, 10

and 1% of the surface light intensity (hereinafter e.g. 30% light depth) except 45° N (station 7), using acid-cleaned 30-l Niskin PVC samplers with Teflon-coated steel springs hung on a stainless-steel wire. Determination of the four light depths was done past noon the day before the collection of seawater samples with a 2π quantum sensor (LI-COR 192SA). The water samples were immediately sieved through a 200 μm mesh plankton net to remove large-sized zooplankton, and transferred into acid-cleaned 1-l polycarbonate bottles. The seawater in the bottles was spiked with $NaH^{13}CO^3$ (Shoko Co., Ltd., Tokyo). The ^{13}C enrichment was about 10% of the total inorganic carbon in the ambient water. Two light bottles were used for each light depth. Dark bottle uptake is similar to the zero-time blank for the ^{13}C technique and thus dark uptake was not measured (SHIOMOTO *et al.*, 1998). Incubation experiments were begun within 1 hr of sample collection. Bottles with seawater samples inoculated with ^{13}C were held in a deck incubator during about 24-hr incubations in a range of irradiances corresponding to the depths at which the samples were taken, using black mesh screens. Constant temperature was maintained with continuous flowing surface seawater. The experiments were terminated by filtering the samples onto precombusted (450 ℃ for 4 hr) 47 mm Whatman GF/F filters. The filters were rinsed with prefiltered seawater and then immediately frozen at −20 ℃ and stored until isotope analysis later on land. After the filters were treated with HCl fumes for 4 hr to remove inorganic carbon, they were completely dried in a vacuum desiccator. The isotopic ratios of ^{13}C to ^{12}C and particulate organic carbon were determined using a mass spectrometer (ANCA SL, PDZ Europa). The total carbonate in the seawater was measured with a Shimadzu TOC 5000 infrared analyzer. Primary production was calculated according to the equation described by HAMA *et al.* (1983). The primary production values obtained in the two bottles were averaged.

We used on-deck incubations and neutral density filters (black mesh screen) to attenuate the light intensity. The discrepancy between the primary production obtained by the simulated *in situ* method using the black mesh screen and that obtained by the *in situ* method at the 100, 30, 10 and 2% light depths was determined, by using samples collected in the springtime western subarctic North Pacific (SHIOMOTO *et al.*, 1998). The primary production obtained was multiplied by factors of 1.3 at the 30% light depth and 2.4 at the 10% light depth. The value at the 1% light depth was multiplied by a factor of 2.3 which was obtained at the 2% light depth. The primary production values given in the present study are therefore considered net daily primary production by the *in situ* method.

Daily primary production in the subarctic North Pacific was estimated by integrating from the surface to the 0.2–1.7% light depth (WELSCHMEYER *et al.*, 1993; WONG *et al.*, 1995; SHIOMOTO *et al.*, 1998). Hence, the daily primary production integrated from the surface to the 0.2% light depth was calculated by extrapolation, assuming that primary production decreases exponentially with depth (see SHIOMOTO *et al.*, 1998 for detail).

Chl *a* concentrations were measured by fluorometry (PARSONS *et al.*, 1984). Chl *a* was determined in samples (0.5 l) filtered through 47 mm Whatman GF/F filters. The filters were then stored frozen at −20 ℃ until analysis ashore. Pigments were extracted in 90% acetone and the fluorescence was measured with a Hitachi F−2000 fluorophotometer. Calibration of the fluorophotometer was performed with commercially prepared Chl *a* from Wako Pure Chemical Industries, Ltd. (Tokyo).

Nitrite + nitrate, silicate and phosphate concentrations were measured with a Bran and Luebbe Auto Analyzer Traacs 800 after storage at −20 ℃. Surface temperature and salinity were measured with a thermometer and an Auto Lab salinometer, respectively. Subsurface temperature and salinity were measured with a Neil Brown Mark IIIB CTD.

3. Results
3.1 Physical and chemical description
The WSG is located just north of the TD in the northwestern Pacific Ocean (FAVORITE *et al.*, 1976). The southern and northern boundaries of the TD are bordered by the Subarctic
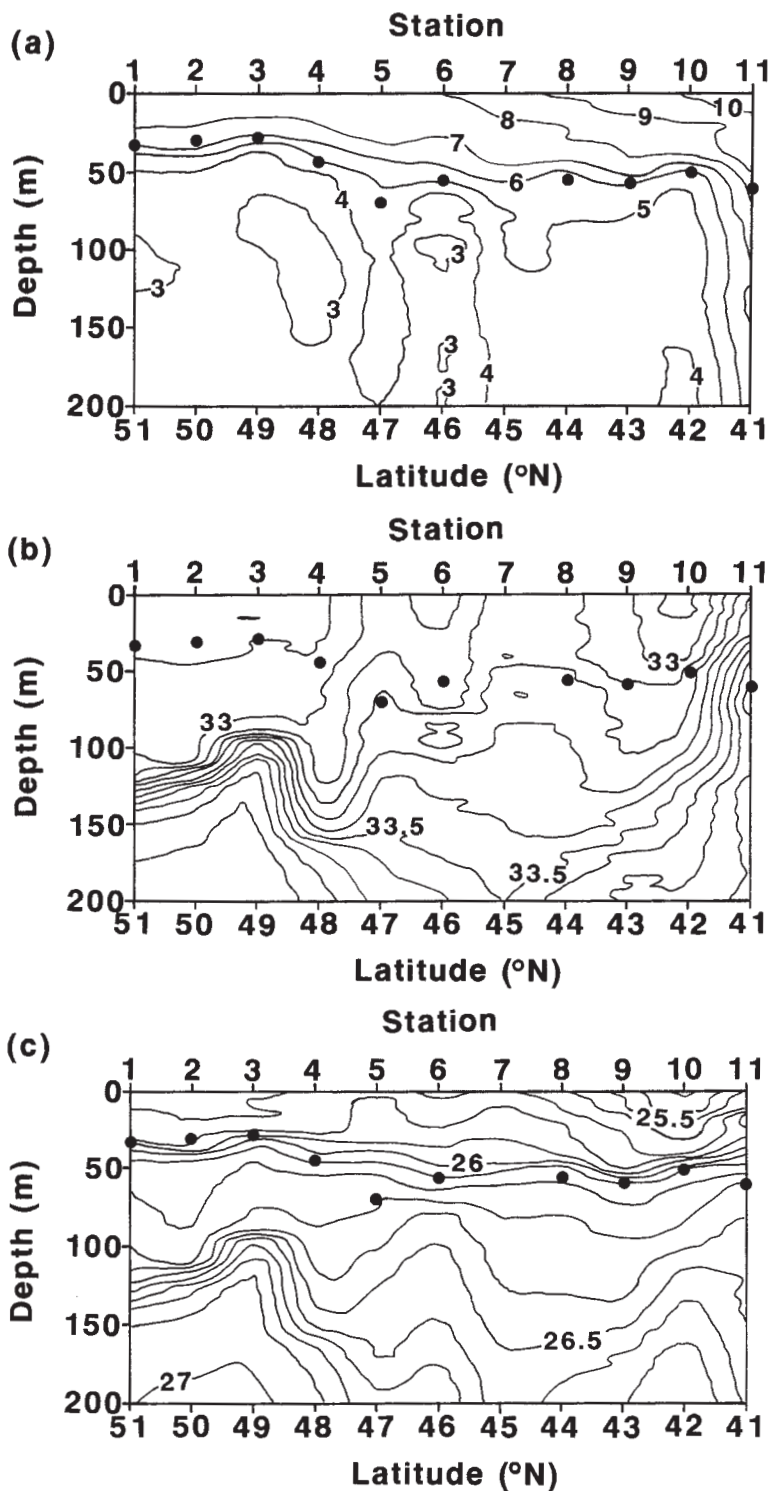
Fig. 2 . Vertical sections of (a) temperature, (b) salinity and (c) sigma-t shallower than 200 m. Solid circles indicate the depths of the euphotic zone(1% light depth).
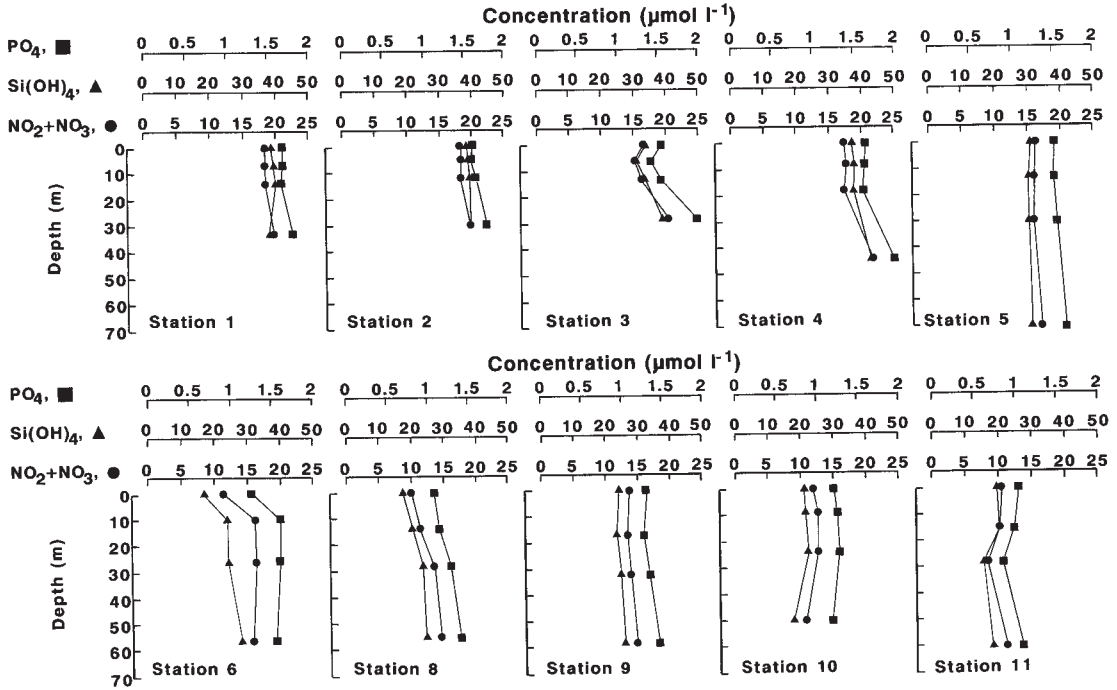
Concentration (µmol l⁻¹)

Fig. 3.   Vertical profiles of nitrite + nitrate (NO$_2$ + NO$_3$), silicate (Si(OH)$_4$) and phosphate (PO$_4$) concentrations within the euphotic zone. Samples were collected at 100, 30, 10 and 1% light depths. Stations 1–4 and 5–11 were located in the Western Subarctic Gyre and the Transition Domain, respectively.

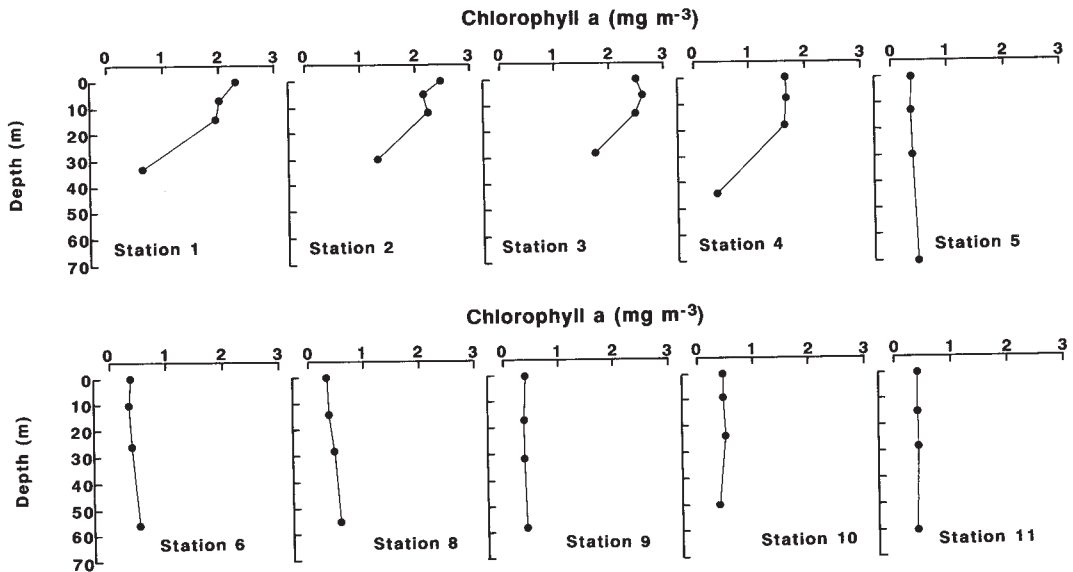## Chlorophyll a (mg m⁻³)

Fig. 4.   Vertical profiles of chlorophyll a concentration within the euphotic zone. Samples were collected at 100, 30, 10 and 1% light depths. Stations 1–4 and 5–11 were located in the Western Subarctic Gyre and the Transition Domain, respectively.

Boundary, denoted as a vertical 34.0 psu isohaline in the upper layer, and by cold water of less than 4℃ below 100 m, respectively (FAVORITE *et al.*, 1976). In this study, salinity of 34.0 psu was not observed in the upper 200 m (Fig. 2 (b)). The salinity in the upper layer increases southward and salinity of 34.0 psu is observed around 40° N (e.g. FAVORITE *et al.*, 1976). The latitude of station 11 was 41° N, and the salinity within the euphotic zone was 33.2–33.9 psu at the stations (Fig. 2 (b)). Salinity of 34.0 psu (the Subarctic Boundary) should have been to the south of station 11. Based on the vertical sections of temperature and salinity (Fig. 2 (a), (b)) and the definition for the WSG and TD, stations 1–4 and 5–11 were thus divided into the WSG and the TD, respectively. Cold water of <4℃ at around 100 m was observed even at station 6 (Fig. 2 (a)). The TD is also characterized by a lower Chl *a* concentration compared with its northern and southern regions (SHIOMOTO *et al.*, 1999). The Chl *a* concentrations in the upper 1% light depth at station 6 were lower than most of the Chl *a* concentrations at stations 1–4, and almost equal to the Chl *a* concentrations at stations 5 and 8–11 (Fig. 4). Accordingly, stations 6 was divided into the TD.

The euphotic zone (1% light depth) was 30–45 m deep in the WSG and 50–70 m deep in the TD. The temperatures and salinity within the euphotic zone were mostly in the 6 to 7℃ level and in the 32.8 psu level, respectively, at every station in the WSG (Fig. 2 (a), (b)). The temperature and salinity within the euphotic zone were nearly uniform throughout the WSG. The values of the temperature and salinity were within the range of those (temperature: 3–8℃; salinity 32.8–33.2 psu) in the upper layers of the summertime WSG reported by FAVORITE *et al.* (1976). In the TD, the temperatures within the euphotic zone increased southward rapidly at or near the surface, whereas the temperature increased slowly from stations 5 to 10 and rapidly at station 11 around the bottom of the euphotic zone. The salinity within the euphotic zone was nearly uniform at each station except station 11 where the salinity increased markedly with depth. The depths of the euphotic zone were nearly equal to the depths of the

pycnocline at all stations (Fig. 2 (c)).

Nutrient concentrations were mostly nearly uniform within the euphotic zone (Fig. 3). The concentrations were 15–20 μ mol l^{-1} for nitrite + nitrate, 30–43 μ mol l^{-1} for silicate and 1.5–2.0 μ mol l^{-1} for phosphate in the WSG, and 8–17 μ mol l^{-1} for nitrite + nitrate, 15–32 μ mol l^{-1} for silicate and 0.8–1.7 μ mol l^{-1} for phosphate in the TD. The result indicates that these nutrients were not limited for phytoplankton within the euphotic zone.

3.2 Chlorophyll *a*

Chl *a* concentrations in the upper 1% light depth ranged from 0.42 to 2.61 mg m^{-3} in the WSG and from 0.33 to 0.57 mg m^{-3} in the TD (Fig. 4). The Chl *a* concentrations were nearly equal in the upper 10% light depth and rapidly decreased at the 1% light depth at every station in the WSG. In contrast, the Chl *a* concentrations were nearly uniform within the euphotic zone at every station in the TD. The mean $\pm$ standard error (SE) was 1.86 $\pm$ 0.16 mg m^{-3} (n=16) in the WSG and 0.42 $\pm$ 0.01 mg m^{-3} (n=24) in the TD. The mean value in the WSG was 4.4 times higher than that in the TD.

The Chl *a* standing stock, calculated by trapezoidal integration from the surface to the 1% light depth, was in the range of 54 and 65 mg m^{-2} in the WSG and in the range of 23 and 28 mg m^{-2} in the TD (Table 1). The mean $\pm$ SE of Chl *a* standing stock was 58 $\pm$ 3 mg m^{-2} (n=4) in the WSG and 25 $\pm$ 1 mg m^{-2} (n=6) in the TD. The mean value in the WSG was 2.3 times higher than that in the TD.

3.3 Primary production

Primary production in the upper 1% light depth ranged from 0.3 to 155.6 mgC m^{-3} d^{-1} in the WSG and from 0.1 to 78.5 mgC m^{-3} d^{-1} in the TD (Fig. 5). In the WSG, the primary production was maximum at the 10% light depth at stations 1 and 2, and at the 30% light depth at station 3, whereas primary production was nearly equal in the upper 10% light depth and rapidly decreased at the 1% light depth at station 4. In the TD, primary production tended to decrease with depth, though the maximum value was observed at the 30% light depth at stations 5 and 6. In general, the vertical profiles

Primary production (mgC m⁻² d⁻¹)

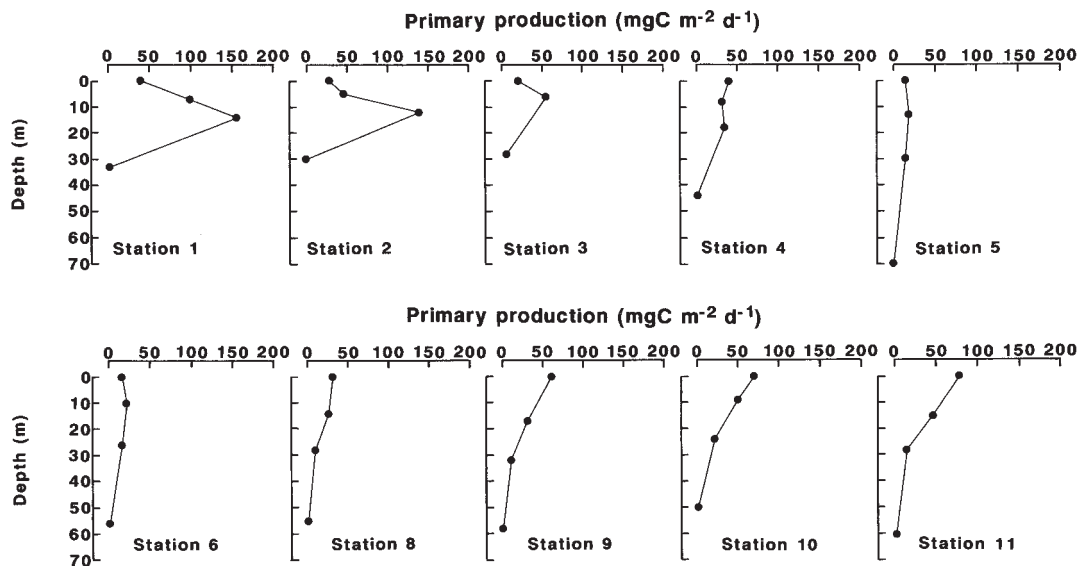**Primary production (mgC m⁻² d⁻¹)**

Fig. 5. Vertical profiles of primary production within the euphotic zone. Samples were collected at 100, 30, 10 and 1% light depths. The data at the 10% light depth at station 3 was missed. Stations 1–4 and 5–11 were located in the Western Subarctic Gyre and the Transition Domain, respectively.

of primary production were not the same as those of Chl a concentration. The mean $\pm$ SE was 46.7 $\pm$ 12.4 mgC m^{-3} d^{-1} (n=15) in the WSG and 23.3 $\pm$ 4.6 mgC m^{-3} d^{-1} (n=24) in the TD. The mean value in the WSG was 2 times higher than that in the TD.

The daily primary production, calculated by trapezoidal integration from the surface to the 1% light depth, was in the range of 910 and 2886 mgC m^{-2} d^{-1} in the WSG and in the range of 738 and 1629 mgC m^{-2} d^{-1} in the TD (Table 1). The mean $\pm$ SE of daily primary production was 1744 $\pm$ 459 mgC m^{-2} d^{-1} (n=4) in the WSG and 1094 $\pm$ 152 mgC m^{-2} d^{-1} (n=6) in the TD. The mean value in the WSG was 1.6 times higher than that in the TD. In addition, the daily primary production integrated in the upper 0.2% light depth was estimated. The values were in the range of 936 and 2901 mgC m^{-2} d^{-1} in the WSG and the range of 751 and 1689 mgC m^{-2} d^{-1} in the TD (Table 1). The mean $\pm$ SE of daily primary production was 1759 $\pm$ 456 mgC m^{-2} d^{-1} in the WSG and 1111 $\pm$ 157 mgC m^{-2} d^{-1} in the TD.

3.4 Chl a-specific primary production

Chl a-specific primary production in the upper 1% light depth ranged from 0.3 to 79.4 mgC (mgChl a)$^{-1}$ d^{-1} in the WSG and from 0.3 to 187.0 mgC (mgChl a)$^{-1}$ d^{-1} in the TD (Fig. 6). The vertical profiles of Chl a-specific primary production were the same as those of primary production. The mean $\pm$ SE was 23.2 $\pm$ 6.0 mgC (mgChl a)$^{-1}$ d^{-1} (n=15) in the WSG and 57.9 $\pm$ 10.8 mgC (mgChl a)$^{-1}$ d^{-1} (n=24) in the TD. The mean value in the WSG was 2.5 times lower than that in the TD.

4. Discussion
4.1 Bloom in the WSG

The Chl a-specific primary production at the 10% light depth of stations 1 and 2 (79.4 and 62.4 mgC (mgChl a)$^{-1}$ d^{-1}; Fig. 6) where relatively high daily primary production was observed was greater than the remaining values in the present study and the values reported in 1993 and 1994 in the WSG (less than 50 mgC (mgChl a)$^{-1}$ d^{-1}; SHIOMOTO et $al.$, 1998). Moreover, the relatively high Chl a-specific primary production in this study exceeded the summer values in the western subarctic North

Chl a-specific primary production (mgC (mgChl a)$^{-1}$ d^{-1})

Chl a-specific primary production (mgC (mgChl a)$^{-1}$ d^{-1})
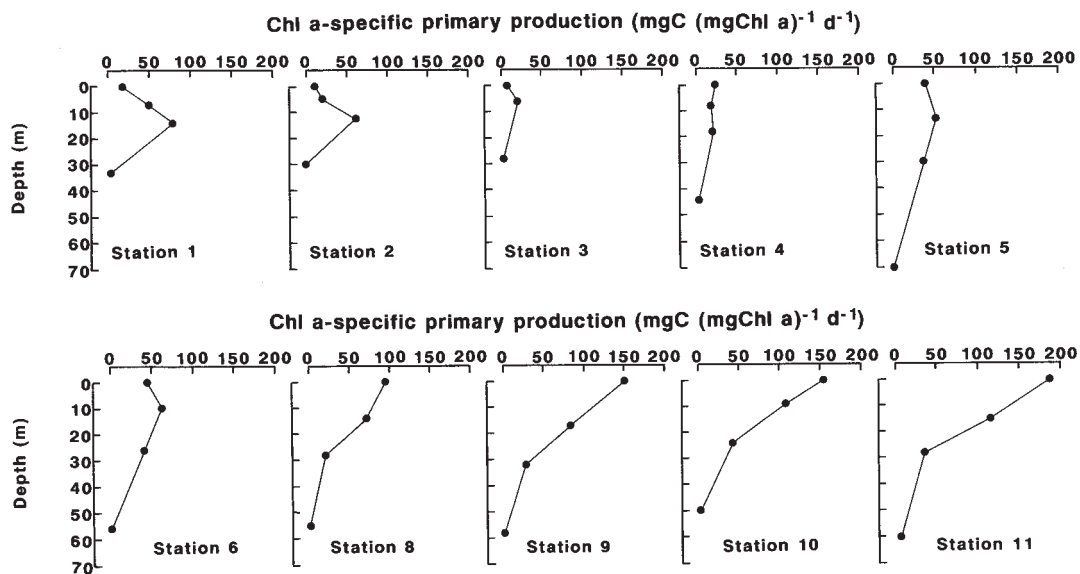

Fig. 6. Vertical profiles of Chl *a*-specific primary production within the euphotic zone. Samples were collected at 100, 30, 10 and 1% light depths. The data at the 10% light depth at station 3 was missed. Stations 1–4 and 5–11 were located in the Western Subarctic Gyre and the Transition Domain, respectively.

Pacific in other studies (maximum: 55 mgC (mgChl *a*)$^{-1}$ d^{-1}; TANIGUCHI and KAWAMURA, 1972; KASAI *et al.*, 1998; SHIOMOTO, 2000; IMAI *et al.*, 2002). Chl *a*-specific primary production is an index of the phytoplankton growth rate (e.g. LALLI and PARSONS, 1995). Thus, relatively high Chl *a*-specific primary production means an increase in the phytoplankton growth rate. On the other hand, the Chl *a* concentrations within the euphotic zone were mostly more than 1 mg m^{-3} in the WSG (Fig. 4). In the summer season, the Chl *a* concentrations more than 1 mg m^{-3} have been observed rarely in the oceanic region of western subarctic North Pacific on shipboard (ANDERSON and MUNSON, 1972; ODATE and FURUYA, 1995; ODATE, 1996; SHIOMOTO *et al.*, 1998; OBAYASHI *et al.*, 2001; IMAI *et al.*, 2002) and satellite observations (BANSE and ENGLISH, 1994, 1999; SASAOKA *et al.*, 2002). Thus, the Chl *a* concentrations in the WSG in this study are on the relatively high side of Chl *a* concentrations in the summertime western subarctic North Pacific. An increase in the phytoplankton growth rate precedes an increase in the phytoplankton biomass in the

process of phytoplankton proliferation (e.g. SPENCER, 1954). Accordingly, phytoplankton at the subsurface at stations 1 and 2 were considered to be in the early stage of bloom.

The relatively high Chl *a* concentration and an increase in Chl *a* concentration were observed in the summertime WSG (SHIOMOTO *et al.*, 1998; SASAOKA *et al.*, 2002). Based on the results in this study and the previous studies, phytoplankton bloom may occur in the WSG in summer.

SASAOKA *et al.* (2002) suggest that the rise in temperature is one in the factors causing an increase in Chl *a* concentration from summer and maximum values in autumn in the WSG, because, in the WSG, the sea surface temperature rises remarkably in early summer, reaching the maximum in late summer and autumn (DODIMEAD *et al.*, 1963; ANONYMOUS, 1993; SASAOKA *et al.*, 2002), and an increase of temperature causes an increase of the phytoplankton growth rate (e.g. EPPLEY, 1972). The relatively high Chl *a*-specific primary production obtained in this study supports their idea regarding the increase in phytoplankton from summer. It is possible

Table 1. Primary production (production) and chlorophyll *a* (chl *a*) integrated in the upper 1% light depth and 0.2% light depth in the Western Subarctic Gyre (WSG) and the Transition Domain (TD) in July 1997.

Region	Station	Integration (%)	depth (m)	Production (mgCm^{-2} d^{-1})		Chl a (mg m^{-2})
WSG	1	1	33	2886		54
		0.2	44	2901	(n=2)	
	2	1	30	2079		55
		0.2	41	2081	(n=2)	
	3	1	28	910[a]		65
		0.2	33	936	(n=2)[b]	
	4	1	44	1102		57
		0.2	60	1117	(n=2)	
TD	5	1	70	782		28
		0.2	91	785	(r^2=0.95, n=3)	
	6	1	56	738		23
		0.2	81	751	(r^2=0.93, n=3)	
	8	1	55	801		25
		0.2	68	812	(r^2=0.95, n=4)	
	9	1	58	1239		23
		0.2	86	1253	(r^2=0.97, n=4)	
	10	1	50	1374		23
		0.2	73	1394	(r^2=0.97, n=4)	
	11	1	60	1629		25
		0.2	81	1669	(r^2=0.99, n=4)	

The values were estimated by trapezoidal integration. r^2: the coefficient of determination when primary production(mgCm^{-3} d^{-1})at the 100, 30, 10 and 1% light depths is applied to the exponential equation for extimation of the primary production at the 0.2% light depth. n: the number of data when the primary production in the upper 1% light depth is applied to the exponential equation. The exponential equation was adjusted by using the values at the 10 and 1% light depths in case of n=2, those at the 30, 10 and 1% light depths in case of n=3 and those at the 100, 30, 10 and 1% light depths in case of n=4. [a]Primary production integrated in the upper 1% light depth was calculated by using the primary production at the 100, 30 and 1% light depths. [b]Fitting of the exponential equation was done by using the primary production at the 30 and 1% light depths.

that the rise in temperature in early summer is one of the factors for the occurrence of phytoplankton bloom in the summertime WSG.

The temperatures in the upper layer were almost equal at stations 1–4 (Fig. 2 (a)). Accordingly, the relatively high Chl *a*- specific primary production should have also been observed at stations 3 and 4. However, relatively high values were not obtained at those stations. The Chl *a* concentrations at station 3 were nearly equal to those at stations 1 and 2, and the Chl *a* concentrations at station 4 were somewhat lower than those at stations 1 and 2 (Fig. 4). The nutrient concentrations in the upper 10% light depth, where relatively active primary production was observed (Fig. 5), were somewhat lower at stations 3 and 4 than at stations 1 and 2 (Fig. 3). These facts imply that the phytoplankton at stations 3 and 4 were in the late stage of bloom when the growth rate of phytoplankton is considered to diminish.

Relatively high Chl *a*-specific primary production was observed at the subsurface a stations 1 and 2 (Fig. 6). In the subarctic North Pacific, solar radiation increases from spring and is maximum in summer (e.g. CAMPBELL and AARUP, 1989; WELSCHMEYER *et al.*, 1995). It is well known that the phytoplankton community suffers from photoinhibition at high light intensity (e.g. ARUGA and MONSI, 1962; PLATT *et al.*, 1980; WELSCHMEYER *et al.*, 1993). These imply a high frequency of photoinhibition in the surface waters during spring and summer. The relatively high Chl *a*-specific primary production at the subsurface can be thus attributed to photoinhibition at the surface. The phytoplankton bloom in the WSG possibly develops at the subsurface, because of avoidance of photoinhibition.

4.2 Characteristics in the TD

The daily primary production in the WSG was roughly equal to that in the TD in the summer season, whereas the Chl *a* concentration and standing stock tended to be higher in the WSG than in the TD (SHIOMOTO *et al.*, 1998). In this study, the daily primary production was higher at stations 1 and 2 in the WSG than in those in the TD, whereas the values at stations 3 and 4 were within the range of the values in the TD (Table 1). The Chl *a* concentration and standing stock were substantially higher in the WSG than in the TD (Fig. 5; Table 1). Stations 1 and 2 were considered to be in the early stage of bloom, and stations 3 and 4 in the late stage of it. Accordingly, primary production and phytoplankton biomass in the TD are possibly characterized by the following in the summer season. Ordinarily, there is no substantial difference between the daily primary production in the TD and in the WSG, whereas the value is lower in the TD than in the WSG in the early stage of the WSG bloom. In contrast, phytoplankton biomass always has a tendency to be lower in the TD than in the WSG. SHIOMOTO *et al.* (1999) suggested an intense grazing effect by zooplankton to explain the low Chl *a* concentration in the TD.

The Chl *a* standing stocks were nearly equal between stations in the TD, whereas the daily primary production tended to increase southward (Table 1). The southward increase of the daily primary production can thus be attributed to an increase of Chl *a*-specific primary production, i.e., the phytoplankton growth rate. Southward increasing trends can be also found for the daily primary production and Chl *a*-specific primary production in the previous shipboard observation in 1994 (SHIOMOTO *et al.,* 1998). According to EPPLEY (1972), the phytoplankton growth rate increases in proportion to temperature. Southward increase in the temperature in the upper mixed layer, i.e., within the euphotic zone, is evident in the TD in all seasons (DODIMEAD *et al.*, 1963; FAVORITE *et al.*, 1976). Accordingly, a southward increasing trend in the phytoplankton growth rate and hence daily primary production are necessarily expected throughout the four seasons in the TD.

References

ANDERSON, G. C. and R. E. MUNSON (1972): Primary productivity studies using merchant vessels in the North Pacific Ocean. *In* Biological Oceanography of the Northern North Pacific Ocean, TAKENOUCHI, A. Y. *et al.* (eds.), Idemitsu Shoten, Tokyo, p. 245–251.

ANONYMOUS (1993): Climatological Charts of the North Pacific Ocean for 30 year period (1961–1990). Marine Department, Japan Meteorological Agency.

ARUGA, Y. and M. MONSI (1962): Primary production in the northwestern part of the Pacific off Honshu, Japan. J. Oceanogr. Soc. Japan, **18**, 37–46.

BANSE, K. and D. C. ENGLISH (1994): Seasonality of coastal zone color scanner phytoplankton pigment in the offshore oceans. J. Geophys. Res., **99**, 7323–7345.

BANSE, K. and D. C. ENGLISH (1999): Comparing phytoplankton seasonality in the eastern and western subarctic Pacific and the western Bering Sea. Prog. Oceanogr., **43**, 235–288.

BOYD, P.W. and P. J. HARISON (1999): Phytoplankton dynamics in the NE subarctic Pacific. Deep-Sea Res. II, **46**, 2405–2432.

CAMPBELL, J. W. and T. AARUP (1989): Photosynthetically available radiation at high latitudes. Limnol. Oceanogr., **34**, 1490–1494.

DODIMEAD, A. J., F. FAVORITE and T. HIRANO (1963): Review of oceanography of the subarctic region. Bull. Int. North Pac. Fish. Comm., **13**, 1–195.

EPPLEY, R. W. (1972): Temperature and phytoplankton growth in the sea. Fish. Bull., **70**, 1063–1085.

FAVORITE, F., A. J. DODIMEAD and K. NASU (1976): Oceanography of the subarctic Pacific region, 1960–71. Bull. Int. North Pac. Fish. Comm-**33**, 1–187.

HAMA, T., T. MIYAZAKI, Y. OGAWA, T. IWAKUMA, M. TAKAHASHI, A. OTSUKI and S. ICHIMURA (1983): Measurement of photosynthetic production of a marine phytoplankton population using a stable ^{13}C isotope. Mar. Biol., **73**, 31–36.

IMAI, K., Y. NOJIRI, N. TSURUSHIMA and T. SAINO (2002): Time series of seasonal variation of primary productivity at Station KNOT (44° N, 155° E) in the sub-arctic western North Pacific.

Deep-Sea Res. II, **49**, 5395–5408.

KASAI, H., H. SAITO and A. TSUDA (1998): Estimation of standing stock of chlorophyll *a* and primary production from remote-sensed ocean color in the Oyashio region, western subarctic Pacific, during the spring bloom in 1997. J. Oceanogr., **54**, 527–537.

LALLI, C. M. and T. R. PARSONS (1995): Biological Oceanography: An Introduction. Butterworth-Heinemann, Oxford, 301pp.

OBAYASHI, Y., E. TANOUE, K. SUZUKI, N. HANDA, Y. NOJIRI and C. S. WONG (2001): Spatial and temporal variabilities of phytoplankton community structure in the northern North Pacific as determined by phytoplankton pigments. Deep-Sea Res. I, **48**, 439–469.

ODATE, T. (1996): Abundance and size composition of the summer phytoplankton communities in the western North Pacific Ocean, the Bering Sea, and the Gulf of Alaska. J. Oceanogr., **52**, 335–351.

ODATE, T. and K. FURUYA (1995): Primary production and community respiration in the subarctic water of the western North Pacific. *In* Biogeochemical Processes and Ocean Flux in the Western Pacific, SAKAI, H. and Y. NOZAKI (eds.), TERRAPUB, Tokyo, p. 239–253.

PARSONS, T. R. and C. M. LALLI (1988): Comparative oceanic ecology of the plankton communities of the subarctic Atlantic and Pacific Oceans. Oceanogr. Mar. Biol. Annu. Rev., **26**, 317–359.

PARSONS, T. R., Y. MAITA and C. M. LALLI (1984): A Manual of Chemical and Biological Methods for Seawater Analysis. Pergamon Press, Oxford, 173pp.

PLATT, T., C. L. GALLEGOS and W. G. HARRISON (1980): Photoinhibition of photosynthesis in natural assemblages of marine phytoplankton. J. Mar. Res., **38**, 687–701.

SASAOKA, K., S. SAITOH, I. ASANUMA, K. IMAI, M. HONDA, Y. NOJIRI and T. SAINO (2002): Temporal and spatial variability of chlorophyll-*a* in ther western subarctic Pacific determined from satellite and ship observations from 1997 to 1999. Deep-Sea Res. II, **49**, 5557–5576.

SHIOMOTO, A. (2000) Chlorophyll-*a* and primary production during spring in the oceanic region of the Oyashio Water, the north-western Pacific. J. Mar. Biol. Ass. U.K., **80**, 343–354.

SHIOMOTO, A., Y. ISHIDA, K. NAGASAWA, K. TADOKORO, M. TAKAHASHI and K. MONAKA (1999): Distribution of chlorophyll-a concentration in the Transition Domain and adjacent regions of the central North Pacific in summer. Plankton Biol. Ecol., **46**, 30–36.

SHIOMOTO, A., Y. ISHIDA, M. TAMAKI and Y. YAMANAKA (1998): Primary production and chlorophyll *a* in the northwestern Pacific Ocean in summer. J. Geophys. Res., **103**, 24651–24661.

SPENCER, C.P. (1954): Studies on the culture of a marine diatom. J. Mar. Biol. Ass. U.K., **33**, 265–290.

TANIGUCHI, A. and T. KAWAMURA (1972) Primary production in the Oyashio region with special reference to the subsurface chlorophyll maximum layer and phytoplankton-zooplankton relationship. *In* Biological Oceanography of the Northern North Pacific Ocean, TAKENOUCHI, A. Y. *et al.* (eds.), Idemitsu Shoten, Tokyo, p. 231–243.

WELSCHMEYER, N. A., S. STROM, R. GOERICKE, G. DITULLIO, M. BELVIN and W. PETERSEN (1993) Primary production in the subarctic Pacific Ocean: Project SUPER. Prog. Oceanogr., **32**, 101–135.

WONG, C. S., F. A. WHITNEY, K. ISEKI, J. S. PAGE and J. ZENG (1995): Analysis of trends in primary productivity and chlorophyll-*a* over two decades at Ocean Station P (50° N, 145° E) in the Subarctic Northeast Pacific Ocean. *In* Climate Change and Northern Fish Populations, BEAMISH, R. J. (ed.), Can. Spec. Publ. Fish. Aquat. Sci., **121**, 107–117.

[Short communication]

Size-fractionated chlorophyll *a* concentration at the surface in the offshore subarctic North Pacific in summer 2000

Akihiro Shiomoto[*], Shinji Hashimoto[**], Kosei Sasaoka[***] and
Mitsuhiro Toratani[****]

Abstract : Small-sized phytoplankton, <2 or 2-10 μm fraction, significantly contributed to the total chlorophyll *a* (chl *a*) concentration at all stations. Each fraction accounted for 35-71% of the total, and the sum of both fractions accounted for 67–93% of the total. Nevertheless, large-sized phytoplankton, >10 μm fraction, as well as the small-sized phytoplankton contributed to the relatively high total chl *a* concentration of $\geq$ 1 mg m^{-3}, accounting for about 30% of the total, in case of much influence of near-shore water.

Keywords : *size$-$fractionated chlorophyll a , large$-$sized phytoplankton, offshore subarctic North Pacific, summer*

1. Introduction

From studies of size-fractionated chlorophyll *a* (chl *a*) in the subarctic North Pacific (Odate and Maita, 1988/89; Yamamoto and Taniguchi, 1993; Odate, 1996; Shiomoto *et al.*, 1999; Boyd and Harrison, 1999; Hashimoto and Shiomoto, 2002; Imai *et al.*, 2002), it gradually emerged that ordinarily small-sized phytoplankton ($<$5 μm fraction) contribute to total chl *a* concentration, whereas in case of total chl *a* concentrations exceeding 1 mg m^{-3}, large-sized phytoplankton ($>$10 μm fraction) contribute to total chl *a* concentration. However, information regarding the circumstances of the contribution of large-sized and small-sized phytoplankton in the subarctic North Pa-

[*]National Research Institute of Fisheries Science, Fisheries Research Agency, 2-12-4, Fukuura, Kanazawa-ku, Yokohama 236-8648, Japan

[**]Japan Science and Technology Corporation, c/o Hydrosphere Atmospheric Research Center, Nagoya University, Chikusa-ku, Furo-cho, Nagoya 464-8601, Japan

[***]Earth Observation Research and Application Center, Japan Aerospace Exploration Agency, Office Tower X, Triton Square, Harumi-Islands, 1-8-10, Harumi, Chuo-ku, Tokyo 104-6023, Japan

[****]Tokai University, 317 Nishino, Numazu 410-0395, Japan

cific Ocean is currently far from sufficient. Hence, we investigated size-fractionated chl *a* concentrations in the offshore subarctic North Pacific in late summer 2000.

2. Materials and methods

This study was conducted during a cruise of the R/V Kurosaki (450t) between 30 August and 9 September 2000. Stations were located between 165°E and 145°W along 48°N (Fig. 1). Seawater samples were collected from the surface by acid-cleaned plastic bucket. Separate surface seawater samples (1 liter) were filtered through Nuclepore filters with pore sizes of 10 μm ($>$10 μm fraction) and 2 μm ($>$2 μm fraction), and a Whatman GF/F (ca. 0.7 μm pore size: total), in order to determine chl *a* concentrations of the $>$10 μm, 2–10 μm and $<$2 μm fractions as well as total. The filters were stored frozen at $-$20℃ until analysis on land. Chl *a* concentrations were determined with a Hitachi F-2000 fluoro-photometer according to Parsons *et al.* (1984) for samples extracted with 90% acetone. Calibration of the fluoro-photometer was performed with a commercially prepared chl *a* standard obtained from Wako Pure Chemical Industries, Ltd. (Tokyo).
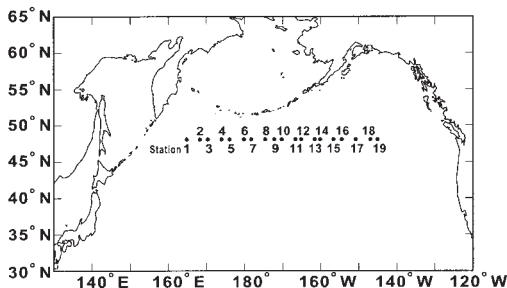
Fig. 1 Location of sampling stations in the subarctic North Pacific between 30 August and 9 September 2000.
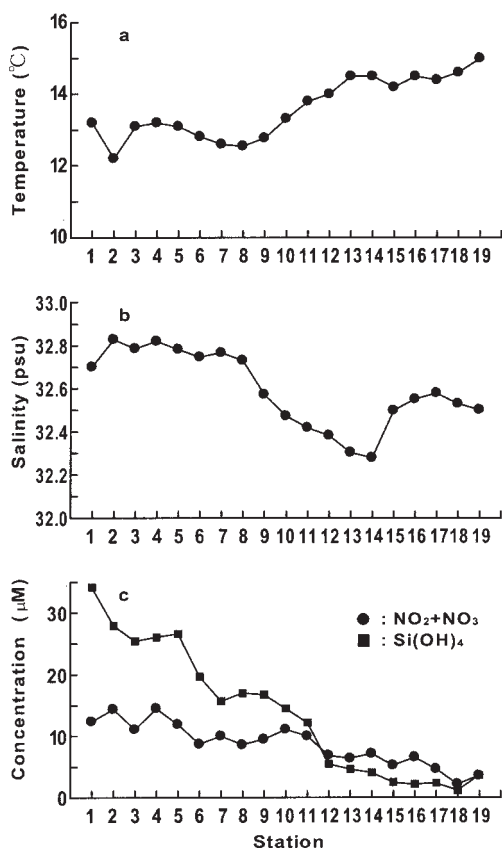

Fig. 2 Variations of (a) temperature (℃), (b) salinity (psu), (c) nitrite + nitrate (NO$_2$ +NO$_3$) and silicate (Si(OH)$_4$) concentrations (μ M) at the surface.

Temperature and salinity were measured with a thermometer and a Guildline

AUTOSAL, respectively. Nitrite + nitrate and silicate concentrations were measured with a Bran and Luebbe Auto Analyser Traacs 800 after storage at -20℃.

3. Results and discussion

Surface temperatures were nearly uniform between Stations 1 and 9, and tended to increase after Station 10 (Fig. 2a). Surface salinity was nearly uniform between Stations 1 and 8, and decreased markedly after Station 9 (Fig. 2b). Salinity increased again at Station 15 and was nearly uniform after that station. Less saline water with salinity of <32.5 psu was observed between Stations 10 and 14, and a minimum value of 32.28 psu was observed at Station 14.

Both nitrite + nitrate and silicate concentrations tended to decrease from Stations 1 to 19 (Fig. 2c). However, the decrease in the concentration was steeper in silicate than in nitrite + nitrate between Stations 1 and 12. The silicate concentrations were lower than the nitrite + nitrate concentrations between Stations 12 and 18.

Total chl a concentrations ranged from 0.32 to 1.32 mg m^{-3} (Fig. 3a). Concentrations of $\geqq$ 1 mg m^{-3} were observed at Stations 1, 9, 11, 12 and 14. Although the percentage contribution of the <2 or 2–10 μ m fraction (small-sized phytoplankton) to the biomass of the phytoplankton community was highest at all five stations, the contribution of the $>10 \mu$ m fraction (large-sized phytoplankton) to the biomass differed between the five stations (Fig. 3b). The contribution of large-sized phytoplankton was relatively high at Stations 11, 12 and 14, and low at Station 1. The chl a concentrations of the total, the $<2 \mu$ m fraction and the 2–10 μ m fraction showed 1.3-fold, 1.6-fold and 1.4-fold changes, respectively, between the five stations, whereas the concentration of the $>10 \mu$ m fraction showed 5.5-fold change. The different contributions of large-sized phytoplankton between the five stations can be thus attributed to different chl a concentrations of large-sized phytoplankton. Consequently, for phytoplankton communities with the relatively high chl a concentration, even if the total phytoplankton biomass is equal, the
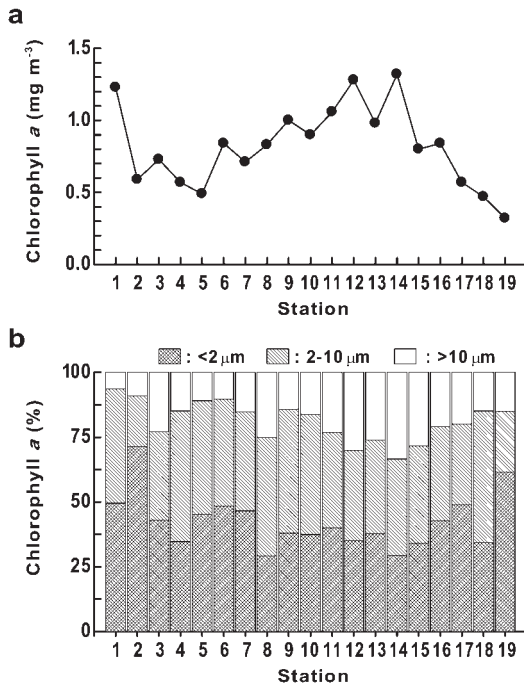
Fig. 3 Variations of (a) total chlorophyll *a* concentration (mg m^{-3}) and (b) percentage contribution of the $>10\,\mu$ m, 2–10 μ m and $<2\,\mu$ m fractions to total chlorophyll *a* concentration at the surface.

Fig. 4 Relationships between salinity (psu) and chlorophyll *a* concentrations (mg m^{-3}) of the $>10\,\mu$ m, 2–10 μ m and $<2\,\mu$ m fractions at the surface. The Spearman rank correlation coefficient (rs) is -0.66 (p$<$0.01) for the $>10\,\mu$ m fraction, -0.49 (p$<$0.05) for the 2–10 μ m fraction and -0.23 (p$>$0.3) for the $<2\,\mu$ m fraction.

contribution of various-sized phytoplankton, especially the large-sized, may differ between the communities, implying a different species composition of phytoplankton between the communities.

Stations 11, 12 and 14 with relatively high chl *a* concentrations of the $>10\,\mu$ m cell size coincided with the less saline water (Figs 2b and 3). A significant negative relationship was observed between chl *a* concentrations of the $>10\,\mu$ m and 2–10 μ m fractions and salinity, but not for the $<2\,\mu$ m fraction (Fig. 4). This means that the near-shore water has an effect in particular on large-sized phytoplankton in the offshore area, but little effect on small-sized phytoplankton.

In the North Pacific, the Subarctic Current flows eastward between 40°N and 50°N east of 165°E, and the Alaskan Stream flows westward north of the Subarctic Current along the Aleutian Islands (e.g., FAVORITE *et al.*, 1976).
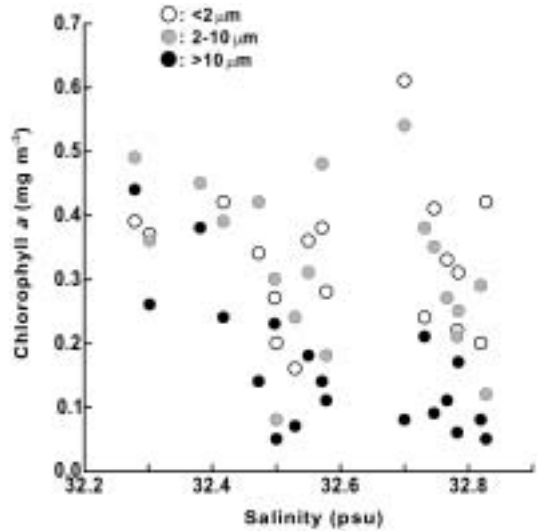
Southward branches from the Alaskan Stream have been observed to flow into the Subarctic Current west of 155°W (THOMSON, 1972; REED, 1984; REED and STABENO, 1994; BOGRAD *et al.*, 1999). Salinity in the upper waters decreases from the offshore area to the near-shore area in the subarctic North Pacific (DODIMEAD *et al.*, 1963; FAVORITE *et al.*, 1976). The low saline water between Stations 10–14 can be thus attributed to the southward branches of the Alaskan Stream. Consequently, large-sized phytoplankton in the less saline water can be generated in the near-shore area and carried into the offshore area by the southward branches of the Alaskan Stream.

Concentrations of nitrite + nitrate and silicate in the less saline water (Stations 10–14) were mostly less than 10 μ M and 5 μ M, respectively (Fig. 2c). The concentration ratios of nitrite + nitrate to silicate of less than 1 were observed in the less saline water (Stations 12-14). In contrast, concentrations of nitrite + nitrate and silicate were 10–15 μ M and 20–30 μ M at the surface in the Alaskan Stream in

summer 2000 (data between 50–51°N along 180° and 165°W in June 2000; ANONYMOUS, 2001). Concentration ratios at the surface were within the range of 1 and 2 (ANONYMOUS, 2001). The concentrations and ratios are judged to be lower in the less saline water than in the source water (the Alaskan Stream). The low concentration ratios as well as the low concentrations in the less saline water are considered to be a result of the active uptake of nutrients, especially silicate, implying abundant diatoms. Relatively high chl *a* concentrations of large-sized phytoplankton at Stations 11, 12 and 14 can thus be attributed to diatoms in the near-shore area.

Acknowledgments

References

ANONYMOUS (2001) : Data Record of Oceanographic Observations and Exploratory Fishing, No. 44. Hokkaido University, Hakodate, 95 pp.

BOGRAD, S. J., R.E. THOMSON, A.B. RABINOVICH and P. H. LEBLOND (1999) : Near-surface circulation of the northeast Pacific Ocean derived from WOCE-SVP satellite-tracked drifters. Deep-Sea Res. II , **46**, 2371–2403.

BOYD, P. and P.J. HARRISON (1999) : Phytoplankton dynamics in the NE subarctic Pacific. Deep-Sea Res. II, **46**, 2405–2432.

DODIMEAD, A.J., F. FAVORITE and T. HIRANO (1963) : Salmon of the North Pacific Ocean-Part II. Review of oceanography of the subarctic Pacific Region. Bull. Int. North Pacific Fish. Comm., **20**, 1–195.

FAVORITE, F., A.J. DODIMEAD and K. NASU (1976) : Oceanography of the subarctic Pacific region, 1960–71. Bull. Int. North Pacific Fish. Comm., **33**, 1–187.

HASHIMOTO, S. and A. SHIOMOTO (2000) : Regional distribution of size-fractionated chlorophyll *a* concentration at sea surface water adjacent to Japan in May-June 2000. Bull. Jpn. Soc. Fish. Oceanogr., **66**, 148–154 (in Japanese with English abstract).

IMAI, K., Y. NOJIRI, N. TSURUSHIMA and T. SAINO (2002) : Time series seasonal variation of primary productivity at station KNOT (44°N, 155°E) in the subarctic western North Pacific. Deep-Sea Res. II, **49**, 5395–5408.

ODATE, T. (1996) : Abundance and size composition of the summer phytoplankton communities in the western North Pacific Ocean, the Bering Sea, and the Gulf of Alaska. J. Oceanogr., **52**, 335–351.

ODATE, T. and Y. MAITA (1988/89) : Regional variation in the size composition of phytoplankton communities in the western North Pacific Ocean, spring 1985. Biol. Oceanogr., **6**, 65–77.

PARSONS, T. R., Y. MAITA and C.M. LALLI (1984) : A Manual of Chemical and Biological Methods for Seawater Analysis. Pergamon Press, Oxford, 173 pp.

REED, R. K. (1984) : Flow of the Alaskan Stream and its variations. Deep-Sea Res., **31**, 369–386.

REED, R. K. and P.J. STABENO (1994) : Flow along and across the Aleutian Ridge. J. Mar. Res., **52**, 639–648.

SHIOMOTO, A., Y. ISHIDA, K. NAGASAWA, K. TADOKORO, M. TAKAHASHI and K. MONAKA (1999) : Distribution of chlorophyll-*a* concentration in the Transition Domain and adjacent regions of the central North Pacific in summer. Plankton Biol. Ecol., **46**, 30–36.

THOMSON, R. E. (1972) : On the Alaskan Stream. J. Phys. Oceanogr., **2**, 363–371.

YAMAMOTO, T. and A. TANIGUCHI (1993) : Spring and summer phytoplankton chlorophyll *a* size fraction ($>10\,\mu$m and $<10\,\mu$m) in the offshore waters around Japan. J. Fac. Appl. Biol. Sci. Hiroshima Univ., **32**, 1–6.

資　料

第 41 巻第 4 号掲載欧文論文要旨

和田明[*]**・落合実：Hybrid box modelによる北極海域（カラ海，バレンツ海）での流動解析**

　本論文の目的は海洋汚染に関連して北極海域（カラ海，バレンツ海）での流動特性を検討することにある。最近，旧ソビエト連邦による北極海（特にカラ海，バレンツ海）への放射性廃棄物の投棄の状況が明らかにされつつある。この海域は狭く，浅く，かつ陸地に近いという特徴を有している。当該海域の海水循環を求め放射性核種の拡散解析，被爆線量評価を行うためには，海洋の流動特性を把握する必要がある。放射性廃棄物の北極海への影響を検討する第一段階として，バレンツ海，カラ海の局所海域を対象として，水平方向に 4°×1°の分割，鉛直方向は 6 層（0〜50 m，50〜100m，100〜200m，200〜500m，500〜900mおよび900〜2500m）に分割した。本論文で用いた解析法は各ボックスで観測されている水温と塩分を再現するような流れを求める方式である。この方法によって得られた流動は，既往の知見による流れと一致した。この流れの解析結果とバレンツ海でのタラの卵稚仔の動きとの関連についても検討を加えた。
（[*]〒275-8875　千葉県習志野市泉町1-2-1　日本大学生産工学部）

和田明[*]**・高野泰隆・落合実：北極海全域の海水循環の解析**

　北極海への放射性廃棄物の投棄による影響を評価するには北極海の局所域（カラ海，バレンツ海）ならびに北極海全域の影響を予測しうる安全評価方法を確立する必要がある。放射性廃棄物の北極海への影響を検討する第一段階として，バレンツ海，カラ海の局所海域を対象として，水平方向に 4°×1°の分割，鉛直方向に 6 層分割し，hybrid box model を用いて流れを解析した。解析より求められた流動は既往の知見による流れと一致した（WADA and OCHIAI, 2004）。研究の第 2 段階として北極海全域を対象として球座標系において場所により異なるが，4°×1°の水平方向のボックスを考え，鉛直方向は 5 層（0〜50m，50〜100m，100〜200m，200〜500m，および500〜4250m）に分割した。流動解析については研究の第 1 段階で採用したhybrid box model を採用した。北極海全域を対象とした流動解析結果は多くの点で既存知見と一致した。特に，ノルウエー海，バレンツ海，カラ海における流れは既存知見とほぼ同じであった。北極海中心部での表層では時計回り，中・深層の流動場は反時計回りの循環が認められた。本文で得られた流動解析結果と局所域モデル（カラ海，バレンツ海）の結果を比較した結果，両者の整合性は良好であった。
（[*]〒275-8875　千葉県習志野市泉町1-2-1　日本大学生産工学部）

関根義彦[*]**・田中俊輔：直進する黒潮の岸側に存在する低気圧渦の観測**

　大冷水塊を持つ大きな低気圧渦は黒潮大蛇行流路に伴われるが，非大蛇行期にも弱い低気圧渦が存在する。1999年8 月に非大蛇行期間の低気圧渦の西側を観測することができたので，その観測結果をまとめた。観測はCTDとADCPにより行われ，幾つかのポテンシャル密度（σ_θ）の異なる低塩分水の水平貫入が塩分極小層に存在することが観測された。黒潮の北側にある低気圧渦の低塩分水層は渦の周辺では薄くなり，σ_θの幅も狭いのに対して，黒潮の南側にある北太平洋中層水の水平貫入は厚く，σ_θの幅も相対的に広いことが観測された。黒潮の北側にある低塩分層の水の起源について議論した。
（〒514-8507 津市上浜町1515　三重大学生物資源学部海洋気候学講座）

奥村裕[*]**・小山次朗**[**]**・宇野誠一：芳香族炭化水素の植物プランクトンに対するEC50とlogPow，分子量との関係**

　芳香族炭化水素 5 種類の海産植物プランクトン8 種類に対する生長阻害試験を行った。緑藻のドナリエラは他の藻類に比べ，実験したすべての芳香族炭化水素について最も耐性が高かった。特にジベンゾチオフェン，フェナントレン，ナフタレンのドナリエラに対するEC50は試験した最高濃度区以上であり，EC50 を決定できなかった。一方，最も感受性の高い植物プランクトンの種類は芳香族炭化水素によって異なった。ユーグレナ藻のユートレプテイラはジベンゾチオフェンに対し，ハプト藻のパブロバはフェナントレン，フルオレン，ナフタレンに対し，渦鞭毛藻のプロロセントラムはフェナントレンに対し，珪藻のキートセロスはヒドロキシビフェニルに対し感受性が高く，藻類の感受性は種類により20 倍以上異なった。

　オクタノール/水分配係数とEC50 の回帰式は，log（1/EC50）＝0.87×logPow−0.76 であり，r$_2$は0.76と高く，両者の間に有意な相関関係が確認された。一方，キートセロスとテトラセルミスのEC50 は，logPow より分子量と相関が高かった。

(*〒985−0001 宮城県塩釜市新浜町3−27−5　独立行政法人水産総合研究センター東北区水産研究所海区水産業研究部海区産業研究室　**〒890−0056 鹿児島県下荒田4−50−20 鹿児島大学水産学部海洋資源環境教育センター）

中村洋平*・堀之内正博**・佐野光彦*：熱帯の海草帯におけるヤライイシモチ *Cheilodipterus quinquelineatus* **の加入に及ぼす海草の草丈と密度の影響：人工海草魚礁を用いた実験的研究**

　琉球諸島西表島において海草の草丈や密度が違うと，稚魚の加入量が変化するかどうかを人工海草魚礁を用いて検証した．実験に用いた人工礁は，①草丈と密度が高いもの（Dユニット），②草丈はDユニットと同じだが，密度を40％減らしたもの，③密度はDユニットと同じだが，草丈を40％減らしたもの，および④葉がなく，基盤だけのものの4タイプである．これらの人工礁をアマモ場に隣接する砂礫底にそれぞれ5基設置し，各礁に加入する稚魚を潜水観察によって14日間毎日記録したところ，合計7科10種が人工礁に加入した．

　すべての魚種の個体数を累積し，各種の割合を算出したところ，ヤライイシモチが最も多く，全体の約85％を占めた．実験期間を通して，人工礁のタイプ間でヤライイシモチ稚魚の個体数を比較したところ，その個体数は草丈と密度が高いDユニットに有意に多かった．この結果は，海草の草丈や密度の違いは，ヤライイシモチ稚魚の加入量に影響を及ぼすことを示唆する．

(*〒113−8657 東京都文京区弥生1−1−1　東京大学大学院農学生命科学研究科農学国際専攻　**〒690−8504　島根県松江市西河津市　島根大学汽水センター）

アヌクル・ブラナプラスプラット*，柳　哲雄**：タイ・バンパコン河口域における循環と平均滞留時間の季節変動

　バンパコン河口域における3次元循環流と保存物質の平均滞留時間の季節変動をPOMとオイラー・ラグランジュ法により計算した。水温・塩分・河川流量・風・潮位が計算への主な入力である。計算結果によると，これらの入力が複雑にからみあって3次元循環流の季節変動を決めている。風の影響は海面近くで大きいが，潮汐の影響は全水深に及んでいる。また河川の影響は雨季の河口近くで著しい。粒子追跡実験の結果は潮流が短期間に粒子を輸送するのに重要な役割を果たしていることを示し，平均滞留時間の季節変化は風，河川流量，潮汐のすべての影響を受けていることを示した。粒子追跡実験による平均滞留時間は4月に29日，6月に21日，12月に11日，9月に6日となったが，それらは塩分収支から推定された平均滞留時間とよく一致した。

(*Department of Geography, University of Victoria, PO. Box 3050, STN CSC, Victoria, BC V8W 3P5 Canada　**福岡県春日市春日公園6−1　九州大学応用力学研究所）

塩本明弘*，橋本慎治**，亀田卓彦***：1997年7月の北西太平洋におけるクロロフィル *a* **と基礎生産力**

　1997年7月の北西太平洋における有光層内のクロロフィル *a* 濃度と基礎生産力を測定した。観測点は西部亜寒帯循環と移行領域に分けられた。クロロフィル *a* の濃度は西部亜寒帯循環で0.42−2.61 mg・m^{-3}（平均値±標準誤差：1.86±0.16 mg・m^{-3}，データ数：16），移行領域で0.33−0.57 mg・m^{-3}（0.42±0.01 mg・m^{-3}，24）であった。1％光深度から表面までを積算した1日あたりの基礎生産量は西部亜寒帯循環で910−2886 mgC・m^{-2}・d^{-1}（1744±459 mgC・m^{-2}・d^{-1}，4），移行領域で738−1629 mgC m^{-2}・d^{-1}（1094±152 mgC・m^{-2}・d^{-1}，6）であった。西部亜寒帯循環でのクロロフィル *a* 濃度はこれまでに夏季の北太平洋亜寒帯域西部で報告されたクロロフィル *a* 濃度中では比較的高い方に位置していた。さらに，西部亜寒帯循環において79.4，62.4 mgC(mgChl *a*)$^{-1}$・d^{-1}という比較的高い単位クロロフィル *a* 当たりの基礎生産量も得られた。これらの値は夏季北太平洋亜寒帯域西部で報告された値（<55 mgC(mgChl *a*)$^{-1}$ d^{-1}）に比べて高かった。以上のことから，西部亜寒帯循環において植物プランクトンは夏季にブルームを起こすと考えられる。初夏における水温の上昇が植物プランクトンのブルームを引き起こす要因のひとつとして挙げられる。一方，移行領域において，各観測点での1％光深度までのクロロフィル *a* の積算量はほぼ等しかったが，1日あたりの基礎生産量は南下に伴い増加する傾向が見られた。この傾向は水温上昇に伴う植物プランクトンの成長速度の増加によるものと考えられる。

(*独立行政法人水産総合研究センター中央水産研究所　〒236−8648　神奈川県横浜市金沢区福浦2−12−4．**日本科学技術事業団，(現住所)愛知県名古屋大学地球水循環研究センター　〒464−8601　名古屋市千種区不老町．***独立行政法人水産総合研究センター遠洋水産研究所　〒424−8633　静岡県静岡市清水折戸5−7−1）

学 会 記 事

1. 2003年 9 月 9 日（火）　東京水産大学海洋環境棟会議室において幹事による会計改革についての検討会を開催した。

2. 2003年10月14日（火）　東京水産大学海洋環境棟会議室において幹事会が開かれた。
　　主な審議事項は下記の通りである。
　　　正会員会費の改定
　　　名簿作成
　　　寄付図書・交換図書の見直し
　　　各試験場・書店への講読価格
　　　ケルゲレン島学術調査計画

3. 2003年11月18日（火）　東京水産大学海洋環境棟会議室において幹事会が開かれた。
　　前回の幹事原案を再度検討した。

4. 2004年 1 月20日（火）　平成16，17年度　評議員選出結果。
　　青木三郎　荒川久幸　有賀祐勝　石丸　隆　磯田　豊
　　市川　香　今脇資郎　岩田静夫　内海真生　奥田邦明
　　神田穣太　河野　博　岸野元彰　北出裕二郎
　　黒田一紀　小池　隆　小池康之　小池義夫　小松輝久
　　斎藤誠一　佐藤博雄　須藤英雄　関根義彦　千手智晴
　　平　啓介　多田邦尚　高橋正征　隆島史夫　谷口　旭
　　田中祐志　寺崎　誠　内藤靖彦　永田　豊
　　中田喜三郎　中田英昭　長島秀樹　平野敏行
　　前田明夫　前田昌調　前田　勝　松生　洽　松山優治
　　村野正昭　門谷　茂　森永　勤　和田　明　八木宏樹
　　山口征矢　柳　哲雄　山崎秀勝　吉田次郎　渡邊精一

5. 2004年 3 月15日（月）　平成16，17年度　会長選出結果。
　　会長には　須藤英雄会員が再選された。

6. 新入会員

氏名	所属	紹介者
佐野光彦	〒113-8657東京都文京区弥生1-1-1 東京大学大学院農学生命科学研究室	河野　博

7. 退会（逝去者含）
　　藤田亀太郎　本座栄一　梶浦欣二郎　杉原滋彦
　　木村　茂

8. 受贈図書
　　養殖研ニュース　No. 51，52
　　なつしま　No. 209〜214
　　しおさい　No. 19
　　東海大学紀要　Vol. 14(1)
　　農業工学研究所ニュース(26，27，28)
　　勇魚　No. 28
　　国立科学博物館専報　35号
　　Nll News　No. 17，18
　　Bulltin of the National Science Museum　Vol. 27
　　　(1)，28(3, 4)，29(2)
　　Journal of the Korean Society of Oceanography
　　　Vol. 28(2, 3)
　　海洋水産研究　Vol. 24(2, 3)
　　中国海洋大学学報　Vol. 2(2)

日仏海洋学会誌「うみ」投稿規定

1．「うみ」（欧文誌名 La mer）は日仏海洋学会の機関誌として，和文または欧文により，海洋学および水産学ならびにそれらの関連分野の研究成果を発表する学術雑誌であり，同時に研究者間の情報交換の役割をもつことを目的としている。

2．「うみ」は，原則として年 4 回発行され，投稿（依頼原稿を含む）による原著論文，原著短報，総説，学術資料，書評その他を，編集委員会の審査により掲載する。これらの著作権は日仏海洋学会に帰属する。

3．投稿は日仏海洋学会会員，および日仏海洋学会正会員に準ずる非会員からとする。共著者に会員を含む場合は会員からの投稿とみなす。

4．用語は日，仏，英 3 ヵ国語のいずれかとする。ただし，表および図の説明の用語は仏文または英文に限る。原著論文には約200語の英文または仏文の要旨を別紙として必ず添える。なお，欧文論文には約500字の和文要旨も添える。ただし，日本語圏外からの投稿の和文要旨については編集委員会の責任とする。

5．原稿はすべてワードプロセッサを用いて作成し，本文・原図とも 2 通（正，副各 1 通）ずつとする。副本は複写でよい。本文原稿はすべてA4判とし，白紙にダブル・スペース（和文ワープロでは相当間隔）で記入する。表原稿および図の説明原稿は本文原稿とは別紙とする。

6．投稿原稿の体裁形式は「うみ」最近号掲載論文のそれに従う。著者名は略記しない。記号略号の表記は編集委員会の基準に従う。引用文献の表示形式は，雑誌論文，単行本分載論文（単行本の一部引用も含む），単行本などの別による基準に従う。

7．原図は版下用として鮮明で，縮尺（版幅または1/2版幅）に耐えられるものとする。

8．初稿に限り著者の校正を受ける。

9．すべての投稿原稿について，1 編あたり 5 万円の論文掲載料を申し受けます。

10．会員に対しては10印刷ページまでの掲載を無料とする。会員の投稿で上記限度を超える分および非会員投稿（依頼原稿を除く）の印刷実費はすべて著者負担（1 万円/ページ）とする。ただし，カラー印刷を含む場合には，別に所定の費用（1 ページあたり9万円）を著者（会員，非会員とも）負担とする。

11．すべての投稿原稿について，1 編あたり別刷り50部を無料で請求できる。50部を超える分は請求により50部単位で有料で作製される。別刷り請求用紙は初稿校正と同時に送付される。

12．原稿の送り先は下記の通りとする。なお著者（共著の場合は代表者）連絡先のe-mailアドレス並びにFAX番号を付けることとする。

〒108–8477　東京都港区港南4-5-7
　　　　　　東京海洋大学海洋科学部海洋環境学科（吉田　次郎気付）
　　　　　　日仏海洋学会編集委員会
　　　　　　e-mail：jiroy@s.kaiyodai.ac.jp

執　筆　要　領

1．原稿

⑴　和文原稿の場合：ワードプロセッサを使用し，A4版の用紙におよそ横30字，縦25行を目安に作成すること。

⑵　欧文原稿の場合：ワードプロセッサを使用し，A4版の用紙にダブルスペース25行でタイプし，十分な英文添削または仏文添削を経て提出すること。

⑶　和文原稿，欧文原稿いずれの場合も，要旨，表原稿および図版説明原稿はそれぞれ本文原稿とは別紙とする。

⑷　最終原稿提出の際に，印刷原稿とともに原稿，表，図版が保存されたフロッピーディスク，CD-R/RW，MO等での提出を依頼する。この場合，原稿はMicrosoft WORD，Just System 一太郎，PDFの原稿のみに限る。また，表，図版はこれら原稿ファイルの中に取り込むか，bmp，jpg等の一般的な画像ファイルに保存したものに限る。なお，電子媒体は返却しない。

2. 原稿記載の順序

(1) 原著（和文原稿）：原稿の第 1 ページ目に表題，著者名，研究の行われた所属機関，所在地，郵便番号を和文と英文で記載する。研究終了後所属機関が変わった場合は現所属機関も記載する。連絡先（共著の場合は連絡先とする著者を明示する）の住所，電話番号，ファックス番号，E-mail アドレスも記す。最後にキーワード（4 語以内），ランニングヘッドを英文で記載すること。第 2 ページ目に欧文要旨（欧文表題，著者名を含む）を200語以内で記す。本文は第 3 ページ目から，「緒言」「資料」「結果」「考察」「謝辞」「文献」「図版の説明」などの章立てあるいは項目で順に記載する。基本的には最近号掲載論文の体裁形式を参考にして投稿原稿を作成すること。原稿には通しのページ番号を記入すること。

(2) 原著（欧文原稿）：原稿の第 1 ページ目に表題，著者名，研究の行われた所属機関，所在地，郵便番号を記載する。研究終了後所属機関が変わった場合は現所属機関も記載する。最後にキーワード（4 語以内），ランニングヘッドを記載すること。第2ページ目に欧文要旨（欧文表題，著者名を含む）を200語以内で記す。本文は第 3 ページ目からとする。「Introduction」「Data」「Results」「Discussion」「Acknowledgement」「References」「Figure Caption」などの章立てで順に記載する。基本的には投稿原稿の体裁形式は最近号掲載論文を参考にして作成すること。最終ページに和文の表題，著者名，連絡先著者住所，電話番号，ファックス番号，E-mail アドレスおよび約500字以内の和文要旨を添える。原稿には通しのページ番号を記入すること。

(3) 原著短報，総説：和文ならびに欧文原稿とも原著論文に準ずる。

(4) 学術資料，書評：特に記載に関する規定はないが，すでに掲載されたものを参考にすること。

3. 活字の指定

原稿での活字は10.5pt〜12ptを目安に設定し，英数字は半角フォントを用いること。学名はイタリック，和文原稿での動植物名はカタカナとすること。句読点は（。）および（，）とするが，文献リストでは（.）および（,）を用いること。章節の題目，謝辞，文献などの項目はボールドまたはゴシックとする。

4. 文献

文献は本文および図表に引用されたもののすべてを記載しなければならない。和文論文，欧文論文共に筆頭著者のアルファベット順（同一著者については，単著，共著の順とし，それぞれ発表年の古い順）にまとめ，以下の例に従って記載する。

(1) 論文の場合

有賀祐勝,前川行幸,横浜康継（1996）：下田湾におけるアラメ群落構造の経年変化.うみ, **34**, 45–52.

YANAGI, T. T. TAKAO and A. MORIMOTO (1997): Co-tidal and co-range charts in the South China Sea derived from satellite altimetry data. La mer, **35**, 85–93.

(2) 単行本分載論文（単行本の一部引用の場合）

村野正昭（1974）：あみ類と近底層プランクトン.海洋学講座10　海洋プランクトン（丸茂隆三編），東京大学出版会，東京, p.111–128.

WYNNE, M. J. (1981): Pheaophyta: Morphology and classification. *In* the Biology of Seaweeds. LOBBAN, C. S. and M. J. WYNNE (eds.), Blackwell Science, Oxford, p.52–85.

(3) 単行本の場合

柳　哲雄（1989）：岸海洋学―海の中でものはどう動くか―. 恒星社厚生閣, 東京, 154pp.

SVERDRUP, H. U., M. W. JOHNSON and R. H. FLEMING (1942): The Oceans: Their Physics, Chemistry and General Biology. Prentice-Hall, Englewood Cliffs, New York, 1087pp.

(4) 本文中での文献の引用

本文中での文献の引用方法はすでに発行された雑誌を参考にするが，基本的には次の形式に従う。

①GREVE and PARSONS(1977)

②（AVIAN and SANDRIN, 1988），

③YANAGI *et al.* （1997）は……（3 名以上の共著の場合）

④……示されている（例えば，YANAGI *et al.*, 1997）（3 名以上の共著の場合）

5. 図，表および写真

(1) 図，表および写真とその説明はすべて英文または仏文を用いる。

(2) 図，表はそのまま写真製版用の草稿となるような明瞭なもので，A4版の上質紙に作製したもの（写真は，正原稿についてもオリジナルとは別にA4版の用紙にコピーしておくことが望ましい）のみを受け付ける。カラー図を希望する場合はその旨明記する。この場合，別に所定の費用を著者負担とする。

(3) 写真は光沢平滑印画紙に鮮明に焼き付けたものを受け付ける。カラー写真の印刷を希望する場合はその旨明記する。この場合，別に所定の費用を著者負担とする。

(4) 図，表および写真は刷り上がり時に最大横が14cm，縦が20cm（説明文を含む）以内であることを考慮して作製すること。

(5) 図（写真を含む）には，Fig. 1, Fig. 2, ……のように通し番号をつけ，一つの図中に複数の図を含む場合はFig. 3（a），Fig. 3（b），……のように指定する。本文中での引用は和文原稿の場合も 「Fig. 1にみられるように……」のようにすること。

(6) 表には，表題の次（表の上のスペース）に説明をつけ，表ごとに別紙とし，Table 1, Table 2,.....のように通し番号をつけること。

(7) 図，表および写真は1枚ごとに著者名，通し番号をつけること。また，本文中での挿入箇所を最終提出原稿の該当箇所右欄外に朱書きすること。

(8) 図，写真の説明は別紙にまとめること。

(9) 地図にはかならず方位と縮尺または緯度，経度を入れること。

6. 単位系

　原則としてSI単位を用いること。塩分は実用塩分単位（Practical Salinity Unit： psuまたは PSU）を用いる場合は単位なしとする。

Information for Contributors

1. The scientific journal,"La mer," the official organ of Japanese-French Oceanographic Society (JFOS), is published quarterly. "La mer" is open to all researchers in oceanography, fisheries and related sciences in the world. The journal is devoted to the publication of original articles, short contributions, reviews, book reviews, and information in oceanography, fisheries and related fields. Submission of a manuscript will imply that it has not been published or accepted for publication elsewhere. The editorial board decides the acceptance of the manuscript on the basis of peer-reviews and is responsible for its final editing. The Society reserves the copyright of all articles in the Journal.

2. *Submission*: Manuscripts must be written in French, English or Japanese. Authors are requested to submit their original manuscript and figures with one copy to the Editor in chief.

3. *Publication charges*: Each accepted article is charged 50,000 yen for publication. For members, there will be no page charge for less than ten printed pages, and 10,000 yen will be charged per page for the excess, except for color pages. For nonmembers there is a publication charge of 10,000 yen per printed page except for color pages. Color illustrations will be provided at cost.

4. *Proofs and reprints*: Fifty reprints of each article will be provided free of charge. Additional reprints can be provided in blocks of 50 copies. Proofs will be sent to the corresponding author. A reprint order form will be sent with the proofs.

5. Manuscripts should be sent to

> Editor in Chief of "La mer"
>> Jiro Yoshida
>> Department of Ocean Sciences
>> Tokyo University of Marine Science and Technology
>> Konan, Minato-Ku, Tokyo, Japan 108–8477.
>> jiroy@s.kaiyodai.ac.jp

Manuscript Preparation

1. General
   1) Manuscripts must be typed with double-spacing on one side of A4 size white paper with wide margins.
   2) Figures, tables, and figure captions should be prepared separate from the main text.
   3) Authors should submit an electronic copy of their paper with the final version of the manuscript. The electronic copy should match the hardcopy exactly and should be stored in CD-R/W or FD. MS-WORD (Windows) and PDF formats are accepted.

2. Details
   1) The first page of the manuscript should include the title, author's full names and affiliations including Fax numbers and E-mail addresses. The corresponding author should be designated. Key words (up to four words) and running head should be written at the bottom of the page.
   2) An abstract of 200 words or less in English or French should be on the second page.
   3) The main text should start on the third page. Please adhere to the following order of presentation: main text, acknowledgements, appendices, references, figure captions, tables. All pages except the first page must be numbered in sequence.
   4) Mathematical formulae should be written with a wide space above and below each line. Syst e me International (SI) units and symbols are preferred.
   5) All references quoted in the text should be listed separately in alphabetical order according to the first author's last name. Citations must be complete according to the following examples:

   Article: YANAGI, T. T. TAKAO and A.MORIMOTO (1997): Co-tidal and co-range charts in the South China Sea

derived from satellite altimetry data. La mer, **35**, 85–93.

Chapter: WYNNE, M.J. (1981): Pheaophyta: Morphology and classification. *In* the Biology of Seaweeds. LOBBAN, C.S. and M. J. WYNNE (eds.), Blackwell Science, Oxford, p. 52–85.

Book: SVERDRUP, H. U., M. W. JOHNSON and R. H. FLEMING (1942): The Oceans: Their Physics, Chemistry and General Biology. Prentice-Hall, Englewood Cliffs, New York, 1087pp.
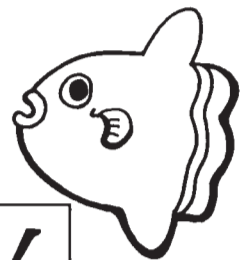
6) *Illustrations*: All illustrations should be provided in camera-ready form, suitable for reproduction (which may include reduction) without retouching. Photographs, charts and diagrams are all to be referred to as "Fig(s)." and should be numbered consecutively in the order to which they are referred. They should accompany the manuscript, but should not be included within the text. All figures should be clearly marked on the back with the figure number and the author's name. All figures are to have a caption. Captions should be supplied on a separate sheet.

7) *Photographs*: Original photographs must be supplied as they are to be reproduced (e.g. black and white or color). If necessary, a scale should be marked on the photograph. Please note that photocopies of photographs are not acceptable. Half-tone illustrations should be kept to a minimum.

8) *Color illustrations*: The printing cost of color illustrations must be borne by authors or their institution. Authors will receive information about the cost on acceptance of the manuscript.

9) *Tables*: Tables should be numbered consecutively and given a suitable caption on top and each table typed on a separate sheet.

賛 助 会 員

日仏海洋学会入会申込書

（正会員・学生会員）

	年度より入会	年　　月　　日申込
氏　名 ローマ字		年　　月　　日　生
勤務先　住所〒 　　　　機関名 　　　　電話		
自宅　住所〒 　　　　電話		
紹介会員氏名		
送付金額　　　　　　　　円	送金方法	
会誌の送り先（希望する方に〇をつける）	勤務先　　　　自宅	

（以下は学会事務局用）

受付	名簿 原簿	会費 原簿	あて名 カード	学会 記事

入会申込書送付先：〒150-0013 東京都渋谷区恵比寿 3-9-25

（財）日仏会館内

日　仏　海　洋　学　会

郵便振替番号：00150-7-96503